

Kinetic and Catalytic Aspects in Propene Oxide Production

Vincenzo Russo



*N. I. C. L.: Naples Industrial Chemistry Laboratory
Chemical Sciences Department
University of Naples "Federico II"
Naples 2014*

Supervised by

Professor Martino Di Serio
N. I. C. L.: Naples Industrial Chemistry Laboratory
Chemical Sciences Department
University of Naples "Federico II"

Professor Elio Santacesaria
N. I. C. L.: Naples Industrial Chemistry Laboratory
Chemical Sciences Department
University of Naples "Federico II"

Tutor

Professor Vincenzo Busico
Chemical Sciences Department
University of Naples "Federico II"

To my grandfather, who didn't live enough to enjoy my goals.

Preface

The present work has been performed between 2011 to 2014 at the Naples Industrial Chemistry Laboratory (N.I.C.L.), heading to the University of Naples “Federico II”. The study has been funded by CONSER S.p.A.

I would like to thank the squad of professors that supervised and advised me during these three years of hard work. My sincerest gratitude goes to Professor Elio Santacesaria for giving me the possibility to work in the laboratory. I consider Professor Santacesaria a mentor of knowledge and science, an indispensable figure of endless experience that taught me how to become a careful scientist with sense of criticism. He is acknowledged also for all the interesting discussions had in this period, sharing with me his experience, opening my mind to always new aspects of the industrial chemistry. My sincerest thanks go to Professor Martino Di Serio, a person of commendable passion in treating the industrial chemistry problems, who thought me that science has to be loved to get even the smallest results. I have appreciated all the time invested together in starting this project, solving problems related to analytical and technical aspects. Moreover, I thank him to have opened my mind to mechanism investigation and understanding. My endless gratitude go to Professor Riccardo Tesser, for all his brilliant knowledge and evaluable experience dealing with numerical and practical problems. He is acknowledged also for giving me support even in the most difficult period of this thesis. Without the involvement and advices of my professors, both in science and in life, this work would have been of course much harder. Professor Tapio Salmi of Åbo Akademi is acknowledged for his brilliant knowledge dealing with industrial chemistry problems, who taught me how to treat them with rigor.

I would like to thank all the friends of our laboratory, because thanks to their friendship the laboratory was fulfilled of a warm and relaxing atmosphere. I acknowledge my co-authors Rosa Turco and Rosa Vitiello, friends of endless passion in dealing with experimental and life problems, thanking them for their support and friendship.

Last, but not least, my special thanks go to both my friends and family. My deepest gratitude goes to the friend of a life, Mirko, who always gave me support in the hardest moments. I would like to express my deepest respect for my family, who supported me in everything and in every case. Especially I would like to acknowledge my parents who believed in me and invested in my studies. My brother, Gianluca, to be always present even when there was nobody left to faith in. On the top of that, my warmest thanks go to my girlfriend, Miriam, for her love and endless patience.

Naples, February 2014

Vincenzo Russo

Abstract

Propene oxide synthesis has a relative long history. Many processes have already been developed and some of them even applied at the industrial scale. By comparing them, one of the most promising is the HPPO process (Hydrogen Peroxide Propene Oxide), because hydrogen peroxide is used as direct oxidant in propene oxidation and only water is obtained as theoretical byproduct. The reaction is catalyzed by TS-1, a titanium silicalite MFI zeolite, it is carried out under mild conditions of temperature and propene pressure (40°C, 20 bars). Methanol is used as solvent. Since 25 years now, this process is under development and recently some industrial plants, based on this technology, are already running. Despite the industrial interest, only few papers have been published till now dealing with the kinetics of the reactions involved in the process, paying attention only on the main reaction and without taking into account the mechanism proposed by other authors.



HPPO Process – From batch to the continuous scale

The first part of this thesis is devoted to the kinetic investigation of the overall reaction network of the HPPO process, considering both the main and the side reactions, taking care on the mechanism suggestions reported in the literature. The study has been performed in a fed-batch reactor. The collected runs have been interpreted by adopting a reliable mechanism and reaction scheme. By taking into account also the mass transfer phenomena, it has been possible to investigate the kinetics of the reaction system and to obtain the kinetic rate laws with related kinetic parameters.

The second part of the work is devoted to the design and realization of a continuous lab-scale pilot plant, that includes the possibility to work with several continuous reactors such as continuous stirred tank reactor (CSTR), adiabatic tubular reactor and jacketed tubular reactor. In this way, by using a CSTR, the kinetic model found in the previous step of this thesis has been validated and the correct strategy to enhance the hydrogen peroxide conversion and propene oxide selectivity has been evaluated.

Finally, the third part of this work is strictly related to the waste water effluents treatment coming from the HPPO plant, that contain unreacted hydrogen peroxide. A detailed catalytic investigation has been performed on the hydrogen peroxide decomposition and the best catalysts tested in continuous too, paying attention to the intensification of this last step of the HPPO process.

List of Publications

The thesis consists of the following publications, which are referred to, in the text, by their Roman numerals.

- I. **V. Russo**, R. Tesser, E. Santacesaria, M. Di Serio. Chemical and Technical Aspects of Propene Oxide Production via Hydrogen Peroxide (HPPO Process). *Industrial & Engineering Chemistry Research* **2013**, 52 (3), 1168–1178.
- II. **V. Russo**, R. Tesser, E. Santacesaria, M. Di Serio. Kinetics of Propene Oxide Production via Hydrogen Peroxide with TS-1. Accepted for publication on *Industrial & Engineering Chemistry Research* **2014**.
- III. **V. Russo**, L. Protasova, R. Turco, M. H. J. M. de Croon, V. Hessel, E. Santacesaria. Hydrogen Peroxide Decomposition on Manganese Oxide Supported Catalyst: From Batch Reactor to Continuous Microreactor. *Industrial & Engineering Chemistry Research* **2013**, 52 (23), 7668–7676.
- IV. R. Turco, J. Haber, I. Yuranov, **V. Russo**, E. Santacesaria, L. Kiwi-Minsker. Sintered metal fibers coated with transition metal oxides as structured catalysts for hydrogen peroxide decomposition. *Chemical Engineering and Processing: Process Intensification* **2013**, 73, 16-22.

List of other Publications

- A. **V. Russo**, T. Kilpio, M. Di Serio, R. Tesser, E. Santacesaria, D. Y. Murzin, T. Salmi. Dynamic non-isothermal trickle bed reactor with both internal diffusion and heat conduction: arabinose hydrogenation as a case study. Submitted to *Industrial & Engineering Chemistry Research* **2014**.
- B. E. Santacesaria, R. Vitiello, R. Tesser, **V. Russo**, R. Turco, M. Di Serio. Chemical and Technical Aspects of the Synthesis of Chlorohydrins from Glycerol. *Industrial & Engineering Chemistry Research* **2013**, doi 10.1021/ie403268b.
- C. R. Turco, R. Vitiello, **V. Russo**, R. Tesser, E. Santacesaria, M. Di Serio. Selective epoxidation of soybean oil with performic acid catalyzed by acidic ionic exchange resins. *Green Processing and Synthesis* **2013**, 2 (5), 427-434.
- D. E. Salzano, A. G. Agreda, **V. Russo**, M. Di Serio, E. Santacesaria. Safety Criteria for the Epoxydation of Soybean Oil in Fed-Batch Reactor. *Chemical Engineering Transactions* **2012**, 26, 39-44.
- E. R. Tesser, M. Di Serio, R. Vitiello, **V. Russo**, E. Ranieri, E. Speranza, E. Santacesaria. Glycerol Chlorination in Gas-Liquid Semibatch Reactor: An Alternative Route for Chlorohydrins Production. *Industrial & Engineering Chemistry Research* **2012**, 51, 8768-8776.
- F. E. Santacesaria, A. Renken, **V. Russo**, R. Turco, R. Tesser, M. Di Serio. Biphasic Model Describing Soybean Oil Epoxidation with H₂O₂ in Continuous Reactors. *Industrial & Engineering Chemistry Research* **2012**, 51, 8760-8767.
- G. E. Santacesaria, R. Turco, M. Tortorelli, **V. Russo**, M. Di Serio, R. Tesser. Biodiesel Process Intensification by Using Static Mixers Tubular Reactors. *Industrial & Engineering Chemistry Research* **2012**, 51, 8777-8787.
- H. E. Santacesaria, R. Turco, M. Tortorelli, **V. Russo**, M. Di Serio, R. Tesser. Biodiesel process intensification: the role of the liquid-liquid interface area in the achievement of a complete conversion in few seconds. *Green Processing and Synthesis* **2012**, 1, 181-189.
- I. E. Santacesaria, M. Di Serio, R. Tesser, R. Turco, M. Tortorelli, **V. Russo**. Biodiesel process intensification in a very simple microchannel device. *Chemical Engineering and Processing* **2012**, 52, 47-54.
- J. D. Kralisch, I. Streckmann, D. Ott, U. Krtschil, E. Santacesaria, M. Di Serio, **V. Russo**, L. De Carlo, W. Linhart, E. Christian, B. Cortese, M. de Croon, V. Hessel. Transfer of the Epoxidation of Soybean Oil from Batch to Flow Chemistry Guided by Cost and Environmental Issues. *Chemsuschem* **2012**, 5, 300-311.
- K. E. Santacesaria, M. Di Serio, R. Tesser, M. Tortorelli, R. Turco, **V. Russo**. A simple device to test biodiesel process intensification. *Chemical Engineering and Processing* **2011**, 50, 1085-1094.
- L. E. Santacesaria, R. Tesser, M. Di Serio, R. Turco, **V. Russo**, D. Verde. A biphasic model describing soybean oil epoxidation with H₂O₂ in a fed-batch reactor. *Chemical Engineering Journal* **2011**, 173, 198-209.
- M. E. Santacesaria, R. Tesser, M. Di Serio, **V. Russo**, R. Turco. A New Simple Microchannel Device To Test Process Intensification. *Industrial & Engineering Chemistry Research* **2011**, 50, 2569-2575.

Conference contributions

- i. **V. Russo**, R. Tesser, E. Santacesaria, M. Di Serio. Kinetics of Propene Oxide Production via Hydrogen Peroxide with TS-1. Abstracts book of XVII National Congress of Catalysis GIC 2013 and XI National Congress of Zeolites Science and Technology, Riccione (IT), 15-18 September 2013.
- ii. R. Vitiello, R. Turco, R. Tesser, **V. Russo**, M. Di Serio, E. Santacesaria. Glycerol Chlorination in Gas-Liquid Semibatch Reactor: New Catalysts for Chlorhydrins Production. Abstracts book of XVII National Congress of Catalysis GIC 2013 and XI National Congress of Zeolites Science and Technology, Riccione (IT), 15-18 September 2013.
- iii. R. Turco, R. Vitiello, **V. Russo**, R. Tesser, E. Santacesaria, M. Di Serio. Selective Epoxidation of Soybean Oil using Acid Ionic Exchange Resins in Continuous Reactor. Poster session of XVII National Congress of Catalysis GIC 2013 and XI National Congress of Zeolites Science and Technology, Riccione (IT), 15-18 September 2013.
- iv. **V. Russo**, R. Tesser, M. Di Serio, E. Santacesaria. A New Kinetic Approach Applied to Biodiesel Process Intensification. Abstracts book of DGMK, Berlin (D), 8-10 October 2012.
- v. R. Turco, **V. Russo**, M. Di Serio, R. Tesser, E. Santacesaria. Epoxidation of soybean oil catalyzed by acid sulphonated resins. Abstracts book of Congresso Nazionale della Divisione di Chimica Industriale della Società Chimica Italiana, Firenze (IT), 10-14 June 2012.
- vi. R. Tesser, **V. Russo**, R. Turco, M. Di Serio, E. Santacesaria. Biocompatible lubricants starting from epoxidized soybean. Abstracts book of Congresso Nazionale della Divisione di Chimica Industriale della Società Chimica Italiana, Firenze (IT), 10-14 June 2012.
- vii. R. Turco, **V. Russo**, M. Di Serio, R. Tesser, E. Santacesaria. Epoxidation of Soybean oil: Kinetic study and modelling in fed-batch and continuous reactors. Abstracts book of XXIV SCI Congress, Lecce (IT), 11-16 September 2011.
- viii. **V. Russo**, R. Turco, M. Di Serio, R. Tesser, E. Santacesaria. A Biphasic Kinetic Approach to Biodiesel Production. Abstracts book of XXIV SCI Congress, Lecce (IT), 11-16 September 2011.
- ix. E. Santacesaria, R. Tesser, M. Di Serio, R. Vitiello, **V. Russo**. Chlorohydrins Production by Glycerol Chlorination. Abstracts book of XXIV SCI Congress, Lecce (IT), 11-16 September 2011.
- x. E. Santacesaria, M. Di Serio, R. Tesser, R. Turco, M. Tortorelli, **V. Russo**. Biodiesel process intensification in a very simple microchannel device. Abstracts book of European process intensification conference (EPIC). Manchester (UK), 20-23/06/2011.
- xi. E. Santacesaria, M. Di Serio, R. Tesser, R. Turco, **V. Russo**. Key factors in the process intensification of the soybean oil epoxidation. Abstracts book of European process intensification conference (EPIC). Manchester (UK), 22-23 June 2011.
- xii. E. Santacesaria, M. Di Serio, R. Tesser, R. Turco, **V. Russo**. Key factors in the process intensification of the soybean oil epoxidation. Intensified Poster Session of European process intensification conference (EPIC). Manchester (UK), 20-23/06/2011.
- xiii. E. Santacesaria, R. Turco, M. Tortorelli, **V. Russo**, M. Di Serio, R. Tesser. Biodiesel process intensification by using static mixers tubular reactors. Abstracts book of Catalysis in Multiphase Reactors CAMURE-8 International Symposium on Multifunctional Reactors ISMR-7. Naantali (FI), 22-25 May 2011.
- xiv. R. Tesser, E. Santacesaria, R. Turco, **V. Russo**, M. Di Serio. Epoxidation of soybean oil: kinetic study and modelling in fed-batch and continuous reactors. Abstracts book of Catalysis in Multiphase Reactors CAMURE-8 International Symposium on Multifunctional Reactors ISMR-7. Naantali (FI), 22-25 May 2011.

Contents

<i>Preface</i>	iv
<i>Abstract</i>	v
<i>List of Publications</i>	vi
<i>List of other Publications</i>	vii
<i>Conference contributions</i>	viii
<i>Contents</i>	ix
Chapter 1 – Introduction [I]	1
1.1 Propene Oxide.....	2
1.2 HPPO Process.....	5
Chapter 2 – HPPO kinetics and mechanism [II]	11
2.1 Introduction.....	12
2.2 Materials and methods.....	13
2.2.1 Chemicals and catalyst.....	13
2.2.2 Reactors and reaction procedures.....	13
2.2.3 Analytical methods.....	15
2.3 Fluid dynamic characterization.....	16
2.4 H ₂ O ₂ decomposition and methyl formate/formic acid formation.....	18
2.5 Propene oxide ring opening reaction: defective sites effect.....	22
2.6 Propene oxide synthesis kinetics and mechanism.....	25
Chapter 3 – HPPO lab-scale continuous plant	33
3.1 Introduction.....	34
3.2 Materials and methods.....	34
3.2.1 Chemicals and catalyst.....	34
3.2.2 Lab-scale HPPO pilot plant and reaction procedures.....	35
3.2.3 Analytical methods.....	42
3.3 Hydraulic tests.....	43
3.4 Fluid-dynamic tests.....	44
3.5 Kinetic tests.....	46
3.6 Kinetic modelling and simulations.....	51

Chapter 4 – Hydrogen peroxide decomposition [III-IV]	52
4.1 Introduction	53
4.2 Material and methods	53
4.2.1 Chemicals and catalysts	53
4.2.2 Catalyst characterization	55
4.2.3 Reactors and reaction procedures	56
4.2.4 Analytical methods	58
4.3 Catalyst characterization.....	59
4.4 Catalytic screening and stability tests.....	63
4.5 Kinetic investigation and model validation	67
<i>Conclusions</i>	71
<i>List of symbols</i>	73
<i>Publications</i>	75

Chapter 1 – Introduction

*"There are no secrets to success. It is the result of preparation, hard work,
learning from failure."*

Colin Luther Powell, The Leadership Secrets of Colin Powell by Oren Harari, 2003

1.1 Propene Oxide

Propene oxide (PO) is a colorless, highly volatile liquid with a sweet ether-like odour. It is flammable and extremely reactive, so care has to be paid to both storage and unloading areas. Being it so reactive, propene oxide is an excellent intermediate, in fact, it is a raw material for the production of several commercial products such as polyglycol ethers, propene glycols and propene glycol ethers. In 2010, the PO worldwide production runs at about 7.5 Mtonns/year.

The history of the PO synthesis is far to be recent and some synthetic routes have been developed till now. A list of the developed technologies is reported, while the related reaction schemes are summarized in Figure 1.

- Direct oxidation of propene: oxygen is used as direct oxidant. It would be, of course, the best synthetic route but it is still a holy grail, being the obtained PO selectivity results far from the industrial targets.
- Dehydrochlorination of chlorohydrins: the most ancient route based on the formation of chlorohydrins that give propene oxide after reacting with a basic compound. Here the coproducts are brine of chlorine salts which lead disposal problems.
- Coproduct Route (SMPO, TBA): an hydroperoxide derived from ethylbenzene or isobutene reacts with propene giving place to propene oxide and a coproduct, that is respectively styrene or *tert*-butyl alcohol. Of course, the economy of the process depends on the economy of the coproduct itself.
- Cumene hydroperoxide (CH): cumene hydroperoxide is used as oxidizing agent. This route solves the coproduct route problem, because the obtained coproduct can be reduced to the starting reagent.
- Peroxiacid route: a peroxiacid formed either in situ or ex situ reacts with propene to give propene oxide. This route did not achieve a real industrial success probably because of the intrinsic low selectivity of the process.
- HPPO process: direct use of hydrogen peroxide for epoxidizing propene. This route gives place only to water as theoretical product. Moreover, the catalyst developed for this process, TS-1, is very selective to the PO synthesis.

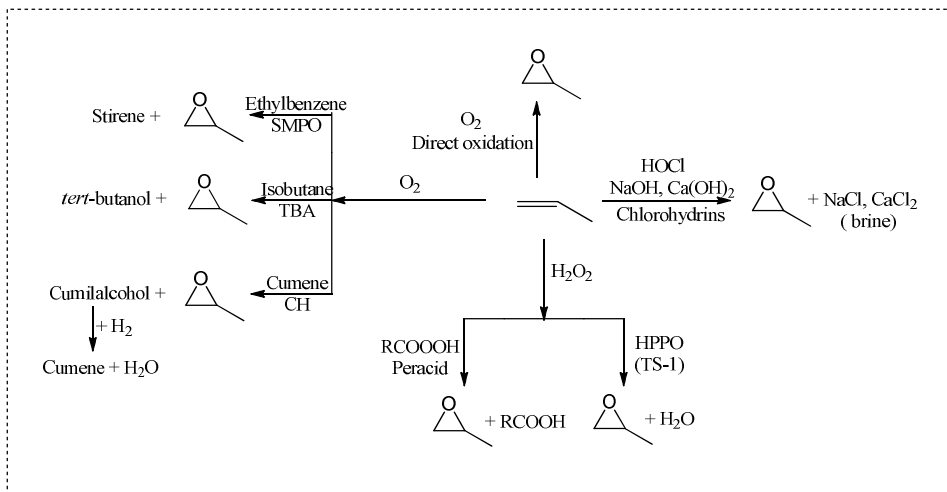


Figure 1 – Propene oxide synthetic routes.

Some of these process have already found an industrial application. At this purpose, in Figure 2 the worldwide distribution of the PO suppliers, referred to 2009, is reported.

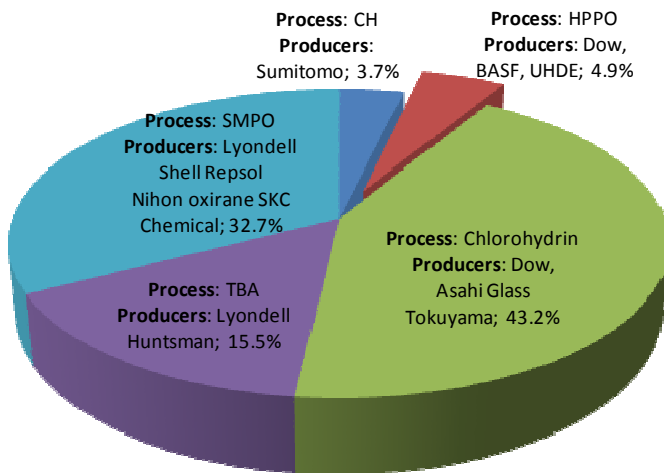


Figure 2 – PO suppliers distribution with related technologies (2009)¹.

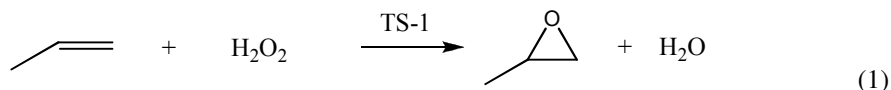
¹ Nexant Chemsystems PERP Program; Propylene Oxide, Process Technology; 2009; PERP07/08-6.

As can be seen, among the old technologies, the Chlorohydrin route is still the most diffused one, but the HPPO process can be considered the trend of the modern industry. In fact, in 2008, Evonik and SKC have launched the first commercial-scale propene oxide plant, based on the HPPO technology, with a capacity of 100 ktons/year. The next year BASF and DOW Chemical started with a new plant based on a similar technology, with a 300 ktons/year capacity. The reason of the success is the absence of the unit operations necessary for collecting and purifying the coproduct of the previous hydrogen peroxide processes, that reduces the investment cost up to 25%. Moreover HPPO process reduces the wastewater (70-80%) and the energy need (35%) with respect to the most traditional technologies². The advantage of this new technology is proven by the fact that Evonik and Uhde are going to set up another plant in China based on HPPO technology, with a capacity of 230 ktonns/year, while, DOW is setting up a 390 ktonns/year of propene oxide plant in Thailand. Being this process so economically advantageous and so eco-friendly, it has been studied in detail leading to a publication (I) that reports all the chemical and technical aspects involved. In the next paragraph, the key points of the HPPO process are reported.

² EPA, The Presidential Green Chemistry Challenge Awards Program: Summary of 2010 Award Entries and Recipients. <http://www.epa.gov/greenchemistry> (accessed Jan 2013).

1.2 HPPO Process

The use of hydrogen peroxide for epoxidizing propene is a very attractive synthetic route from both environmental and economic point of view, because, the only coproduct is water (see reaction 1).



The reaction is catalyzed by TS-1, a titanium silicalite MFI zeolite patented by ENI at the end of 1970s. The catalyst is made by $\text{Ti}(\text{OSi})_4$ tetrahedral site (called “close” sites), that contain some defective “open” $\text{Ti}(\text{OSi})_3(\text{OH})$ sites, as EXAFS studies have demonstrated on well manufactured TS-1 samples. Thanks to this structure, TS-1 shows a three-dimensional system with micropores of 5.1-5.6 Å.

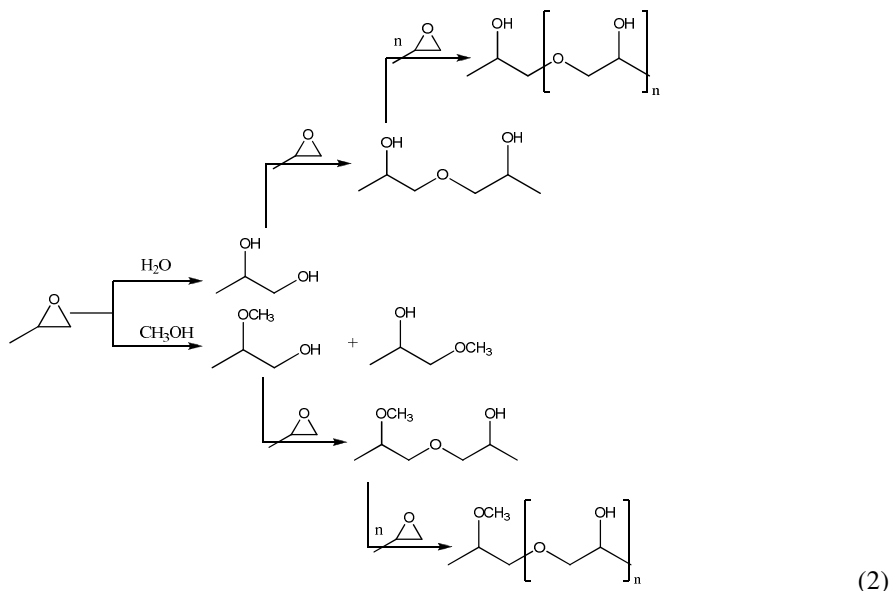
By using this catalyst, the reaction is carried out under mild conditions, in the presence of methanol as solvent, that is the best solvent in terms of both activity and selectivity for the HPPO process. The process temperature ranges between 30-50°C, while if pressure is below 16 bars, propene is in the gas phase, so three phases are present (gas-liquid-solid). Therefore, if pressure is between 20-25 bars propene is kept the liquid phase (liquid-solid system). In this last case attention has to be paid to the volumetric ratio between the two phases. In fact, in some cases two different liquid phases are present: (i) a phase rich in propene containing also propene oxide, (ii) a methanol rich phase containing water, hydrogen peroxide and some amount of propene oxide. The thermodynamic limit at 40°C and 20 bars is about 2:1 methanol:propene (vol./vol.).

Concerning the reaction mechanism, Clerici et al.³ have published that the most accredited mechanism, on the basis of spectroscopic evidences, is the Eley-Rideal one. It is important to point out that only three papers have been published till now concerning the HPPO kinetics, and these papers are all mainly focused on the main reaction

³ Clerici, M. G. *Erdöl, Erdgas, Kohle* **2006**, 122(6), OG77–OG82.

investigation. Moreover, two of the mentioned papers report kinetic runs performed by using isopropanol as solvent^{4,5}, while only one has used methanol⁶, that is, the solvent most commonly employed in the industrial plants. However, there are discrepancy about the reaction kinetic law. As a matter of fact, two of these paper confirm the Eley-Rideal mechanism, while the authors that used methanol found that the best mechanism, in terms of statistical analysis, would be a dual-site Langmuir-Hinshelwood. More experimental work is, therefore, necessary to individuate the correct kinetics in the presence of methanol as solvent and determine the related parameters.

As before mentioned, the cited paper are focused only on the main reaction, giving no kinetic information related to the side-reactions that reduce the yield of the process and increase the costs of PO purification. In fact, being propene oxide so reactive, other products can be formed by secondary reactions that lower the selectivity of the process. A detailed scheme of all the possible occurring reactions after the propene epoxidation is reported in reaction schemes 2-5.



⁴ Liang, X.; Mi, Z.; Wu, Y.; Wang, L.; Xing, E. *React. Kinet. Catal. Lett.* **2003**, 80 (2), 207-215.

⁵ Danov, S. M.; Sulimov, A. V.; Kolesnikov, V. A.; Ovcharov, A. A. *Kinetics and Catalysis* **2013**, 2, 193-198.

⁶ Shin, S. B.; Chadwick, D. *Ind. Eng. Chem. Res.* **2010**, 49, 8125-8134.



The reactions reported in the reaction scheme 2 are all related to the ring opening reactions. In particular, propene oxide can react with either water or methanol, giving place to propene glycol and methoxy propanol, respectively. These two products are the major by-products and, among them, methoxypropanol is the most abundant, being usually methanol concentration greater than the water one. Of course, propene oxide can also reacts with methoxypropanol or propene glycol giving place to dimers that can react further forming heavier adducts.

It has been shown in the literature that an increase of the reaction temperature corresponds to an increase of the hydrogen peroxide conversion, but to a corresponding decrease of the propene oxide selectivity. This fact shows that temperature needs to be kept low in order to avoid the ring opening reactions. Therefore, being the epoxidation reaction extremely exothermic, it is not very easy to keep the system at the desired temperature values, so attention must be paid to heat exchange aspect.

Hydrogen peroxide decomposition (reaction 3) must be taken into account mainly at high temperatures.

The formation of formic acid (reaction 4) and methyl formate (reaction 5) has been reported, without quantitative data, by BASF that underlined the propene oxide purification problems, because PO and methyl formate have a similar boiling point (respectively 34°C and 32°C).

In order to lower the side reactions, it is possible to add additives. Actually they affect both hydrogen peroxide conversion and propene oxide selectivity. In general, basic additives can poison the TS-1 acid sites leading to a reduction of the catalyst activity, but

also to a slower ring opening reaction rate, that means to increase propene oxide selectivity⁷.

As a first conclusion, even if the industrial interest on this technology is very high, in the scientific literature there are only studies concerning synthesis and characterization of TS-1 catalyst, while only few studies have been published on both the reaction mechanism and the kinetics of propene epoxidation reaction. These last two aspect are the main topic of this PhD thesis and are reported in “Chapter 2”.

Another very important aspect of the HPPO process is related to the reactors and all the operating units that purify the produced propene oxide. An example of plant configuration is reported in Figure 3.

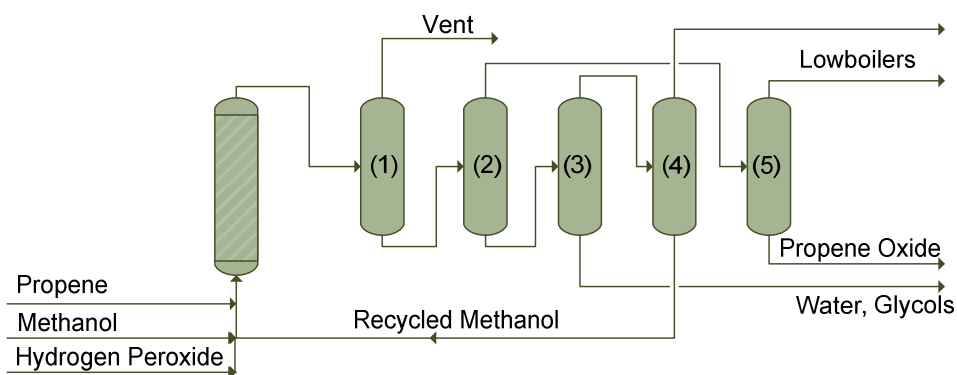


Figure 3 – DOW and BASF HPPO plant scheme⁸.

In most of the cases, the reacting unit can be either a CSTR or a tubular reactor. This last can work in different modalities, like: (i) adiabatic; (ii) adiabatic in series with intermediate cooling; (iii) isothermal; (iv) heat exchanger reactor. Also the fluid-dynamic of the system can be chosen between different options, like: (i) trickle bed reactors characterized by a gas-liquid-solid system, working at a pressure lower than 16

⁷ Crocco, G. L.; Zajacek, J. G. US 5646314, ARCO Chemical Technology, L.P.; **1997**.

⁸ Bassler, P.; Weidenbach, M.; Goebbel, H. *Chem. Eng. Trans.* **2010**, 21, 571–576.

bars; (ii) tubular reactor with a liquid-solid system; (iii) tubular reactor with a liquid-liquid-solid system.

In all the mentioned reactors, two different kind of commercial TS-1 can be used. For instance, the industrial catalyst is constituted by zeolite dispersed in a binder phase. The pellets used in packed bed are generally obtained by extruding the binder paste containing the TS-1, while, the catalyst for the slurry reactors can be obtained by spray-drying technique. The characteristics of the binder are important for the mechanical properties of the final catalyst, but also for saving the selectivity in the epoxidation reaction. Thanks to its properties, silica is used as the most common binder.

Of course, the choice of the reactor and the right catalyst is not trivial, so it would be necessary to test different kind of reactors, loaded with different kind of catalyst, and check their performances in terms of both activity and selectivity. Actually, lots of papers have been published, in the patent literature, by using tubular reactors packed with extruded TS-1, showing two main problems: (i) the thermal control, observing peaks in the temperature along the reactor axis; (ii) selectivity problems, that lead to the use of additives, probably due to either diffusion phenomena of the catalyst or to the acidity of the system. The low selectivity is hard to explain because the powdered catalyst showed, at least in batch reactor, always high selectivity. In order to solve these two problems, it could be useful to use a continuous stirred tank reactor (CSTR) that can be considered the best in terms of thermal exchange. Moreover, this reactor could be loaded directly with TS-1 in powdered form. The kinetic and validation tests performed in a lab-scale CSTR reactor, together with its fluid-dynamic characterization, is the main topic of “Chapter 3”.

Concerning the separation units, distillation columns are in general indicated like the best solution (see units 1-5 in Figure 3). The already running industrial plants are characterized by 4 to 5 distillation columns to obtain propene oxide at 98% purity.

An interesting aspect that comes out from a careful reading of the process plants is related to aqueous effluents that are normally discharged. These effluents contains unreacted hydrogen peroxide that needs to be eliminated before discharging the effluents in the environment. It is possible to eliminate hydrogen peroxide simply by creating a strong basic environment by adding NaOH to the residual hydrogen peroxide solution. In these conditions hydrogen peroxide spontaneously and promptly decomposes to water and oxygen⁹. This is a common practice in industry, because, it seems a very simple operation, but it shows many serious drawbacks. In fact, the basic environment created for decomposing hydrogen peroxide requires a successive neutralization step that is detrimental for the environment. At last, this operation is not simple for a continuous plant. A valuable alternative is the use of an heterogeneous catalyst promoting the hydrogen peroxide decomposition. Many heterogeneous catalysts have been suggested in the literature that are very active in promoting the hydrogen peroxide decomposition. Iron oxides, manganese oxides and perovskites, in particular, have shown the greatest activity in promoting this reaction. Moreover, this operation could be advantageously intensified by using packed bed tubular reactors, microreactors or sintered metal fibers.

Starting with these ideas, the detailed investigation regarding both the catalyst, the kinetics and the kind of reactor for decomposing hydrogen peroxide is the main topic of “Chapter 4”.

⁹ Santacesaria, E.; Tesser, R.; Di Serio, M.; Russo, V.; Turco, R. *Ind. Eng. Chem. Res.* **2011**, 50(5), 2569–2575.

Chapter 2 – HPPO kinetics and mechanism

“The fundamental laws necessary for the mathematical treatment [...] chemistry are thus completely known, and the difficulty lies only in the fact that application of these laws leads to equations that are too complex to be solved.”

Paul Dirac, Proceedings of the Royal Society, 1929

2.1 *Introduction*

A detailed kinetic investigation of the HPPO process, at low propene pressure, is the main topic of the present chapter. By considering that the reaction occurs in three phases (gas, liquid and solid), care has to be paid on the fluid dynamic characterization of the system, involving both the gas-liquid and liquid-solid mass transfer. Furthermore, it has to be considered that propene can be easily ignited due to the presence of oxygen developed by the hydrogen peroxide decomposition. It is evident that the most adequate experimental conditions must be chosen, so a preliminary investigation of the hydrogen peroxide decomposition in the presence of TS-1 has been performed. In order to determine the influence of the defective sites on the propene oxide ring opening reaction, some experimental runs have been performed, too.

Finally, in order to investigate the kinetics of the overall reaction network, experimental tests have been carried out at different experimental conditions of both temperature, catalyst concentration, composition and partial pressure. All the collected data have been elaborated with a single kinetic model, that takes its fundamentals on the experimental investigations of the reaction mechanism proposed by the literature.

2.2 *Materials and methods*

2.2.1 *Chemicals and catalyst*

Propene has been supplied by SIAD with a purity of 99.5 % (0.5 % propane), methanol has been supplied by Clean Consult at 99.8% purity, hydrogen peroxide (60 wt.%) has been supplied by Mythen s.r.l.. All the other reagents employed have been supplied by Aldrich at the highest level of purity available and have been used as received without further purification.

TS-1 catalyst has been supplied by Conser S.p.A. in spray-dried powdered form (average diameter of particles 35 μm ; average size of crystallites 30 nm with a titanium content of 3 wt.%). This catalyst has been used for all the experimental runs performed for publication **II**.

2.2.2 *Reactors and reaction procedures*

The HPPO kinetics has been studied in two different reactors. The experiments performed in order to study the side-reactions kinetics have been made in a hastelloy cylindrical batch reactor of 300 cm^3 , that has been supplied by Parr Instrument and allows to work at a maximum of 55 bars. The epoxidation tests have been performed in a cylindrical jacketed AISI 316 fed-batch reactor of 1000 cm^3 . This reactor has been equipped with a gaseous effect stirrer (see detail in Figure 4) in order to favor the propene mass transfer from the gas to the liquid phase. In order to avoid any catalyst loss during the withdrawn samples, a sintered AISI 316 filter of 10 μm mesh, has been used on the withdrawn line. A sketch of the used reactors, together with the related pictures, is reported in Figure 4.

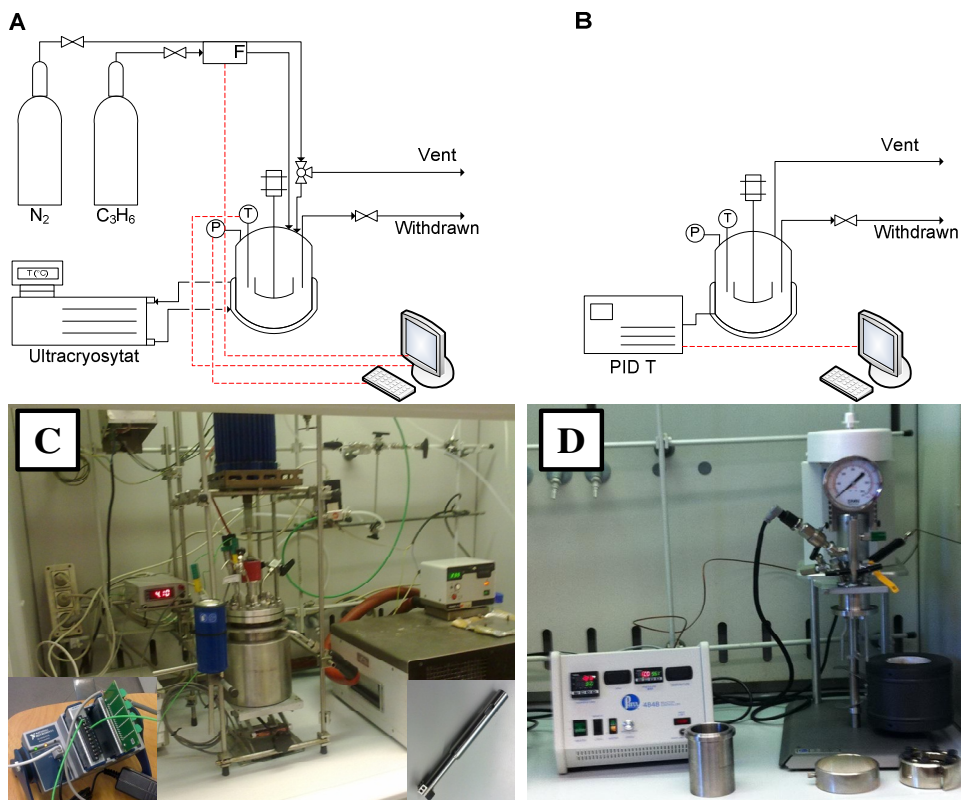


Figure 4 – Sketch, with related pictures, of the reactors used for the HPPO kinetics investigation. A,C. Main reaction investigation reactor: the details are related to the data acquisition system and the gaseous stirrer effect, B,D. Side reaction investigation reactor.

The main operative variables, such as temperature, pressure and propene flow, are recorded through a data acquisition system for both the reactors (NI cDAQ-9174) provided by National Instruments and a dedicated software written in LabVIEW 2011.

Different sets of experimental runs have been performed in order to deeply investigate the kinetics of the HPPO reaction network, studying all the reaction independently. In particular, hydrogen peroxide decomposition and the methyl formate/formic acid formation, have been studied simultaneously. The ring opening reaction kinetics have been investigated by following three different modalities: (i) considering PO degradation in the presence of methanol; (ii) studying the ring opening in the presence of both water

and methanol; (iii) considering the effect of hydrogen peroxide on the PO degradation reaction rate in the presence of both water and methanol. Finally, the propene oxide production runs have been carried out by changing the temperature, the catalyst concentration, the propene partial pressure and the methanol/water ratio. With this study it has been possible to obtain, for any reaction, the corresponding kinetic law and related kinetic parameters. In general, the experimental runs have been performed by charging a liquid solution at room temperature, pressurizing and washing the gas phase with nitrogen several time, in order to avoid the presence of oxygen, heating the system at the desired temperature and activating the propene feed to the reactor (when required). In all cases, temperature ranged between 30-70°C, with a catalyst load ranging between 1-7 wt.%. In the case of propene oxide synthesis, the propene partial pressure has been varied in the range of 0.73-3-11 bar. All the other details of the reaction procedures can be found in publication **II**.

By considering that the experimental work has been performed at low pressure, the reaction system is composed of three phases (gas-liquid-solid), so the reactor has been fluid-dynamically characterized in order to define the mass transfer parameters. The fluid-dynamic characterization of the system has been performed by propene step-wise tests on a methanol/water solution.

2.2.3 Analytical methods

The products distribution and the PO conversion have been analytically determined by gas-chromatographic analysis, using a gas chromatograph (HP 6890), equipped with a flame ionization detector (FID), a split-splitless column injector, and employing a Restek RT-Q-Bond Plot column (30 m x 0.32 mm I. D., 0.1 µm film). Before the analysis, 100 µL of ethyl acetate have been added to 5 cm³ of sample, as internal standard. The residual hydrogen peroxide concentration has been analytically determined by a iodometric titration¹⁰.

¹⁰ Kolthoff, I. M., Sandell, E. B., Meehan, E. J. Treatise on Analytical Chemistry. John Wiley & Sons: New York, **1993**.

2.3 Fluid dynamic characterization

Fluid dynamic characterizations tests have been carried out in order to determine the influence of the stirring rate on the mass transfer parameters. From the collected experimental data, the following relation for the propene Henry's constant in the reaction mixture as a function of temperature can be derived, Eq. 6.

$$H_{C_3H_6} = -0.0046 \cdot (T - 273.15) + 0.4393 \quad (6)$$

All the collected experimental data have then been subjected to mathematical regression analysis for evaluating the gas-liquid mass transfer coefficient ($k_L \cdot a_L$), by solving the mass balances related to propene present in the gas phase, where the inlet propene stream has been considered proportional to reactor pressure, and propene dissolved in the liquid phase, reported in Eqs 7-8. The ODE (Ordinary Differential Equation) system has been solved by using MatLab ode45 algorithm.

$$\frac{dn_{C_3H_6}^G}{dt} = \dot{n}_{C_3H_6}^G - J_{C_3H_6} = k_v \cdot (P^{set} - P^{actual}) - k_L \cdot a_L \cdot (P_{C_3H_6} \cdot H_{C_3H_6} - [C_3H_6]) \cdot V_L \quad (7)$$

$$\frac{dn_{C_3H_6}^L}{dt} = J_{C_3H_6} = k_L \cdot a_L \cdot (P_{C_3H_6} \cdot H_{C_3H_6} - [C_3H_6]) \cdot V_L \quad (8)$$

The trend of the evaluated gas-liquid mass transfer coefficient as a function of the stirring rate is reported in Figure 5.

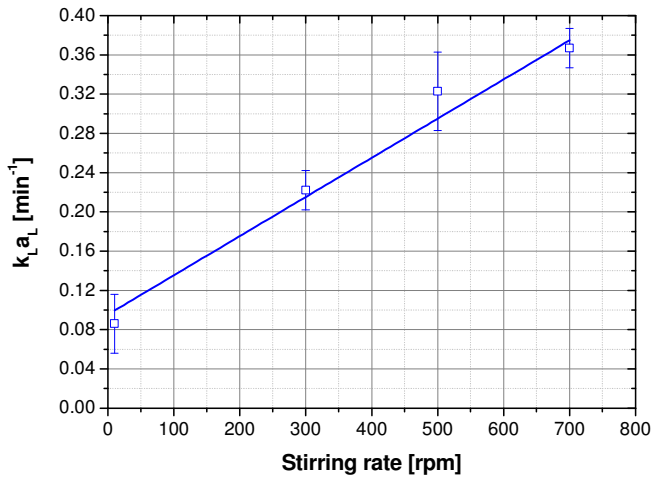


Figure 5 – Trend of the mass transfer coefficient with the stirring rate.

As can be seen the gas-liquid mass transfer parameter is quite linear in the range 10-700 rpm. With this preliminary investigation the gas-liquid mass transfer phenomena that occurs in the adopted experimental device are fully understood. Finally, by considering that gas-liquid mass transfer is always operative, in the adopted experimental conditions, it has to be taken into account when interpreting propene oxide synthesis experimental runs.

By considering that the epoxidation of propene occurs in a gas-liquid-solid system, an effort has to be made in order to estimate the liquid-solid mass transfer coefficient, too. By applying the correlations published by Sano et al.¹¹ a liquid-solid mass transfer coefficient of about $k_s=6.0$ cm/min has been estimated. By considering that the TS-1 adopted catalyst is characterized by a very high specific area ($1.7E+03$ cm²/cm³), it is possible to obtain a very high value for $k_s \cdot a_s$. For this reason, by considering that the gas-liquid resistance to the mass transfer is much greater than the liquid-solid one, that is $1/(k_L \cdot a_L) \gg 1/(k_s \cdot a_s)$, it is reasonable to consider negligible the second contribution.

Being the catalyst a solid particle, attention must be paid to the absence of internal diffusion limitation. At this purpose, by applying the Weisz-Prater correlation¹² to the propene oxide synthesis initial reaction rates values, it is possible to calculate for all cases an effectiveness factor always near to the unity.

By concluding, the gas-liquid mass transfer can be considered the only limitation for the HPPO system, so having an influence on the reaction rates. For this reason, it has to be taken into account when interpreting the propene oxide synthesis tests, in order to find a reliable intrinsic kinetics.

¹¹ Sano, Y.; Yamaguchi, N.; Adachi, T. J. *Chem. Eng. Jpn.* **1974**, 7, 255-261.

¹² Weisz, P. B.; Prater, C. D. *Advances in Catalysis* **1954**, 6, 143-196.

2.4 H_2O_2 decomposition and methyl formate/formic acid formation

The second part of the reported kinetic investigation deals with two important side reactions, that are hydrogen peroxide decomposition and methyl formate/formic acid synthesis, with the aim of choosing the adequate experimental conditions that would drastically reduce their effect. These two reactions have been studied simultaneously by reacting hydrogen peroxide and methanol in the presence of TS-1.

In the performed tests methyl formate concentration has been always very low, so that it is not possible to make a quantitative analysis on the collected data. Therefore, methyl formate concentration could be measured at temperature greater than 50°C and at high TS-1 concentration. By considering that this compound has a similar boiling point than propene oxide (respectively 32°C and 34°C), its formation could lead problems in propene oxide purification, that is normally performed in distillation columns. For this reason, it is necessary to avoid its formation working at low temperature and catalyst concentration. This fact has to be taken into account overall in designing HPPO recirculation plants, where methyl formate can be accumulated.

Then, concerning the hydrogen peroxide decomposition, several experimental runs have been performed, all described by the following kinetic rate law, Eq. 9.

$$r_d = k_d \cdot [TS - 1] \cdot [H_2O_2] \quad (9)$$

The reported law takes into account the experimental evidences, showing that the hydrogen peroxide decomposition linearly depends on the TS-1 concentration, as it can be seen in Figure 6 for two different sets of experiments, performed at 40 and 60 °C. Moreover, this reaction shows a strong dependence on the temperature, with an estimated activation energy of 19.5 Kcal/mol. At this purpose, the Arrhenius plot is reported in Figure 7.

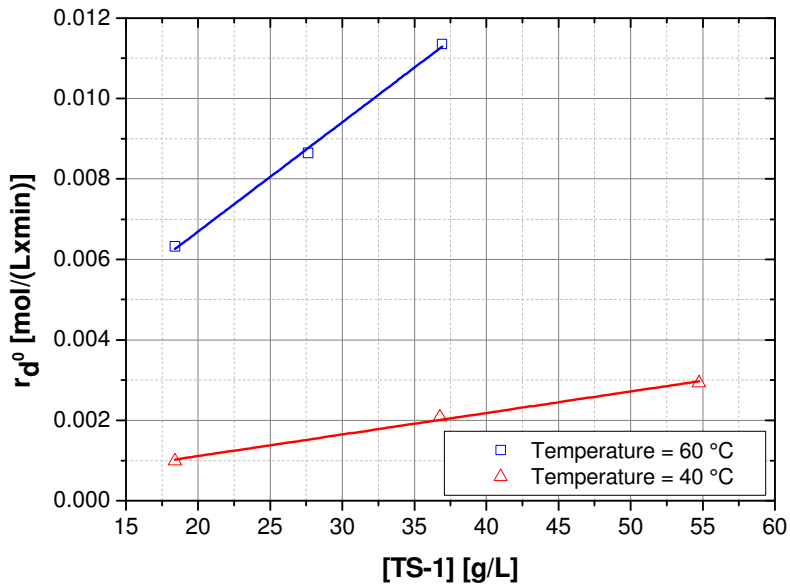


Figure 6 – Initial hydrogen peroxide decomposition rate as function of the TS-1 concentration with related simulation. Symbols are experimental data, lines calculated values.

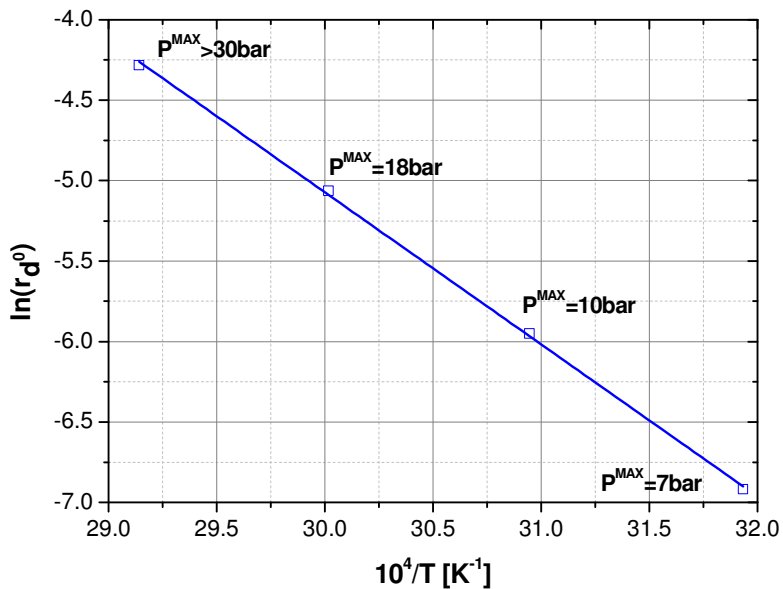


Figure 7 – Arrhenius plot on hydrogen peroxide decomposition and related simulation. Symbols are experimental data, lines calculated values.

So, by increasing the temperature, a strong increase in the hydrogen peroxide conversion can be observed. Moreover, starting from a nitrogen pressure of 5 bars, the global pressure of the system increases as a consequence of the oxygen development due to the hydrogen peroxide decomposition.

In order to interpret the collected experimental data, Eq. 10 has been used to solve the mass balance for each component.

$$\frac{dn_i}{dt} = \pm v_{i,d} \cdot r_d \cdot V_L \quad (10)$$

Moreover, the kinetic constant dependence on the temperature has been taken into account by applying the modified Arrhenius equation reported in Eq. 11, written in general form because will be used from now on.

$$k_m = k_m^{ref} \cdot \exp \left[-\frac{E_{a,m}}{R} \cdot \left(\frac{1}{T} - \frac{1}{T_{ref}} \right) \right] \quad (11)$$

All the kinetic parameters that have been estimated on the experimental data are reported in Table 1, together with the statistical information. The calculations have been performed by using MatLab, with ode45 as ODE solver algorithm.

Table 1 – Hydrogen peroxide decomposition kinetic parameters, at a reference temperature of 313 K, together with the related statistical information. C.I.: confidence interval. σ : standard deviation.

		Value	90% C.I.	95% C.I.	99% C.I.	σ
k_d^{ref}	[L/(g _{TS-1} ·min)]	2.45E-05	6.82E-08	8.15E-08	1.09E-07	2.43E-06
$E_{a,d}$	[Kcal/mol]	1.95E+01	2.84E-02	3.40E-02	4.54E-02	1.69E-02

The agreements can be appreciated in Figures 6, 7 and in the parity plot reported in Figure 8. The average difference between the experimental data and the corresponding calculated values is about 3%.

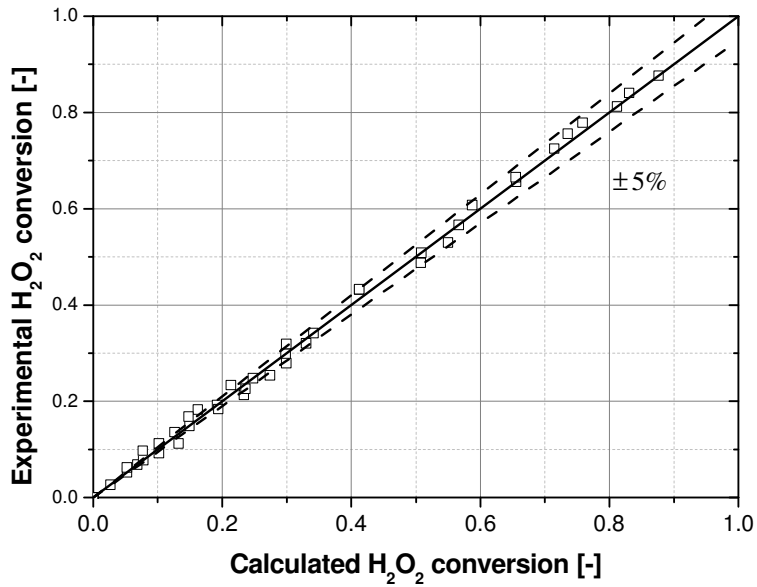
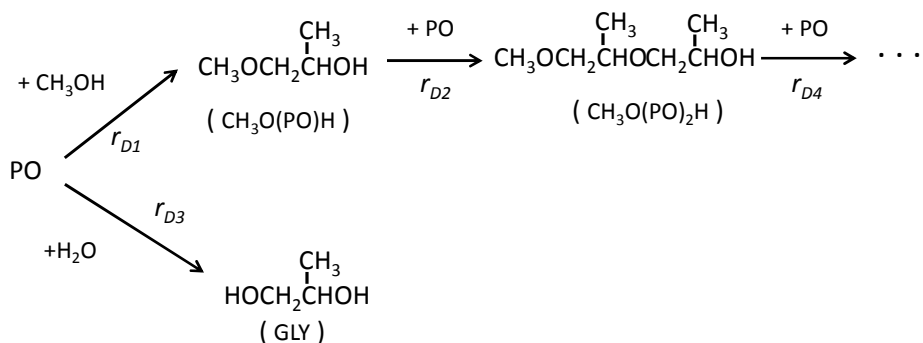


Figure 8 – Parity plot for the hydrogen peroxide decomposition tests.

It is possible to conclude that in the industrial plants the choice of the reaction conditions is fundamental, because both the hydrogen peroxide decomposition and the formation of both methyl formate and formic acid are favored by the high catalyst concentration and by the possible presence of hot spot along the reactor: care must be made on controlling these two variables.

2.5 Propene oxide ring opening reaction: defective sites effect

An important aspect that must be taken into account, when studying the HPPO kinetics, is that TS-1 defective sites can have a catalytic behavior on the ring opening reactions¹³. In this case, no mechanism suggestions are given by literature and actually it is very hard to understand which sites are responsible of these reactions. In order to interpret the collected experimental data we have considered the reaction scheme reported in scheme 1.



Scheme 1 - Reaction scheme of epoxide ring opening.

The corresponding reaction rates are reported in Eqs 12-15.

$$r_{D1} = k_{D1} \cdot [TS - 1] \cdot [PO] \cdot [CH_3OH] \quad (12)$$

$$r_{D2} = k_{D2} \cdot [TS - 1] \cdot [PO] \cdot [CH_3O(PO)H] \quad (13)$$

$$r_{D3} = k_{D3} \cdot [TS - 1] \cdot [PO] \cdot [H_2O] \quad (14)$$

$$r_{D4} = k_{D4} \cdot [TS - 1] \cdot [PO] \cdot [Oligom] \quad [Oligom] = \sum_{i=2, \dots} [CH_3O(PO)_i H] \quad (15)$$

¹³ Thiele, G.F., Roland, E. *Journal of Molecular Catalysis A: Chemical* **1997**, 117, 351-356.

The kinetic constant of the kinetic law (13) and (15) can be assumed the same for both the reaction of PO with methoxy propanol and its oligomers, independently on their molecular weight, because, all these side reactions (reaction to methoxy propanol and to oligomers) occur according to the same mechanism, where PO reacts with an alcoholic group¹⁴.

The reaction rate laws have been successfully applied to describe a great number of experimental runs performed with two different modalities: (i) TS-1, propene oxide and methanol; (ii) TS-1, propene oxide, methanol and water. The data have been elaborated by applying the mass balance reported in Eq. 16, considering the Arrhenius law reported in Eq. 11. The estimated parameters are reported in Table 2.

$$\frac{dn_i}{dt} = \pm \sum v_{i,m} \cdot r_{Dm} \cdot V_L \quad (16)$$

The mass balance reported in Eq. 16 has been solved by using MatLab ode45 ODE solver. In every case an average difference between experimental data and calculated value of 5% has been determined, as it can be appreciated from Figure 9, where an overall parity plot is reported.

¹⁴ Di Serio, M.; Tesser, R.; Dimiccoli, A.; Santacesaria, E. *Ind. Eng. Chem. Res.* **2002**, 41, 6772.

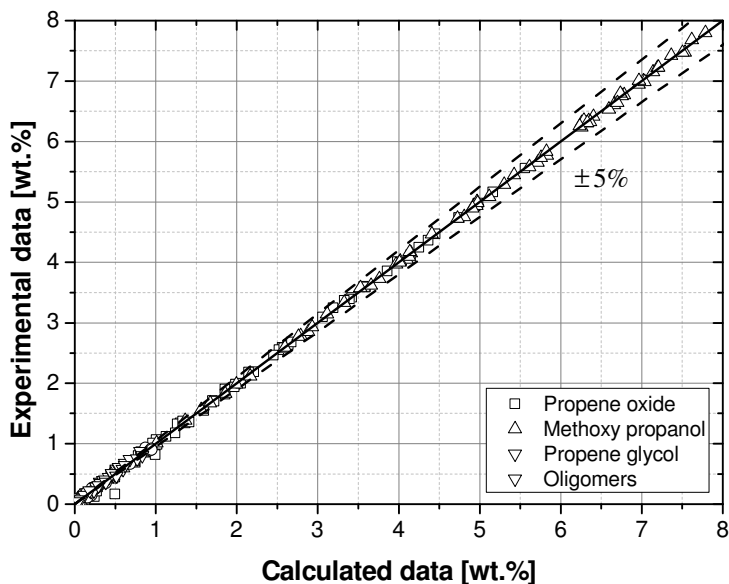


Figure 9 – Parity plot for the ring opening reaction in absence of hydrogen peroxide.

Table 2 – HPPO ring opening reactions kinetic parameters, calculated at a reference temperature of 313 K, together with the related statistical information. C.I.: confidence interval. σ : standard deviation.

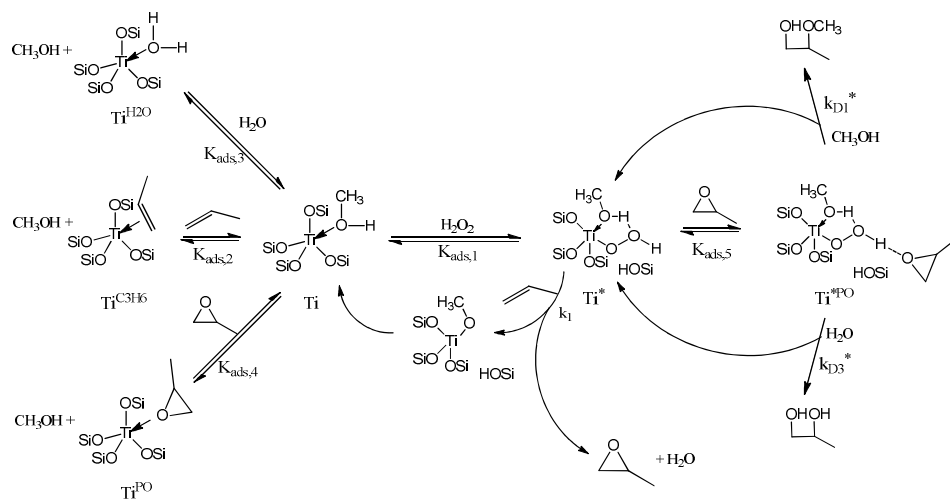
		Value	90% C.I.	95% C.I.	99% C.I.	σ
k_{D1}^{ref}	$[L^2/(g_{TS} \cdot mol \cdot min)]$	9.48E-06	2.94E-07	3.51E-07	4.63E-07	1.78E-07
k_{D2}^{ref}	$[L^2/(g_{TS} \cdot mol \cdot min)]$	6.07E-06	7.28E-06	8.69E-06	1.15E-05	4.41E-06
k_{D3}^{ref}	$[L^2/(g_{TS} \cdot mol \cdot min)]$	1.14E-05	2.20E-06	2.62E-06	3.46E-06	1.33E-06
$E_{a,D1}$	[Kcal/mol]	1.07E+01	1.17E+00	1.39E+00	1.84E+00	7.07E-01
$E_{a,D2}$	[Kcal/mol]	3.40E+01	1.28E+01	1.53E+01	2.02E+01	7.78E+00
$E_{a,D3}$	[Kcal/mol]	1.60E+01	5.78E+00	6.90E+00	9.09E+00	3.50E+00

2.6 Propene oxide synthesis kinetics and mechanism

The HPPO kinetics has been investigated by considering a reliable mechanism based on the observations already reported in the literature. A first evidence that comes out from the study reported in reference [III] is that all the reactions occurring the HPPO process are linearly dependent on the catalyst concentration and are dependent by temperature.

Clerici et al.¹⁵ have reported that the key factor of the propene epoxidation mechanism is the reversible splitting of a Ti-O-Si (Ti) bond by H₂O₂ leading to a Ti-OOH (Ti*) specie and the coadsorption of one alcohol or water molecule stabilizing the hydroperoxide through a five-membered ring, as it is reported in scheme 2 (Ti*). Then, the epoxidation step occurs, where the peroxy oxygen vicinal to Ti is transferred to the double bond, with the contemporary formation of a Ti-alkoxide specie, a molecule of water, and a molecule of propene oxide. Finally, Ti-OR quickly reforms the initial Ti-O-Si bond completing the catalytic cycle.

Starting from this mechanism, and on the basis of the experimental evidences reported in [III], a complete reaction scheme can be written as in scheme 2.



Scheme 2 - Propene oxide formation mechanism.

¹⁵ Bellussi, G.; Carati, A.; Clerici, M. G.; Maddinelli, G.; Millini, R. *Journal of Catalysis* **1992**, 133, 220-230.

The propene oxide synthesis is catalyzed by Ti-OOH specie. The formation of Ti-OOH specie is favored by the coordination on Ti-O-Si site of methanol, however other species can coordinate the Ti-O-Si sites. These equilibria reduce the concentration of active sites and, as a consequence, the reaction rate, as it has been observed by performing experimental runs at different propene/hydrogen peroxide ratios. For instance in Figure 10, the initial propene oxidation reaction rate as a function of the propene partial pressure is reported.

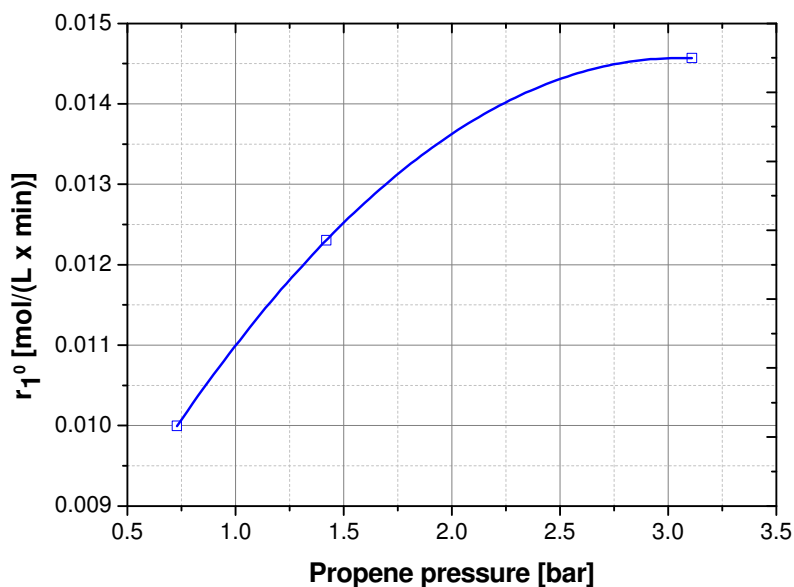


Figure 10 – Initial propene oxidation reaction rate as a function of the propene partial pressure. Symbols are experimental data, lines calculated data.

All these effects have been taken into account introducing the corresponding adsorption equilibrium constants. Moreover, by considering that the literature findings propose an Eley-Rideal mechanism for propene, it is possible to derive the following propene oxide synthesis reaction rate, Eq. 17.

$$r_1 = k_1 \cdot [TS - 1] \cdot \frac{K_{ads1} \cdot [H_2O_2] \cdot [C_3H_6]}{1 + K_{ads1} \cdot [H_2O_2] + K_{ads2} \cdot [C_3H_6] + K_{ads3} \cdot [H_2O] + K_{ads4} \cdot [PO]} \quad (17)$$

As it can be seen, the reaction rate has been considered linearly dependent on the catalyst concentration, as experimentally observed (see Figure 11), and depends on the main components concentration.

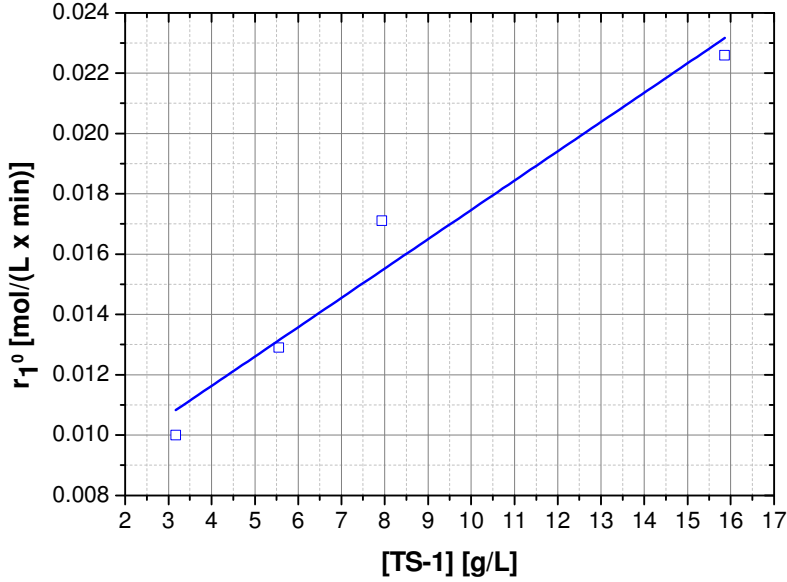


Figure 11 – Initial propene oxidation reaction rate as a function of the TS-1 concentration. Symbols are experimental data, lines calculated data.

As demonstrated by the collected experimental evidences, Ti^* specie can catalyze also the side reactions, interacting with the epoxide, forming the activate specie Ti^{*PO} , which concentration has been considered always very low, so the ring opening kinetic rate laws becomes directly dependent on Ti^* concentration. Starting from the made assumption, it is possible to write the following reaction rate expressions, Eqs 18-21.

$$r_{D1}^* = k_{D1}^* \cdot [TS-1] \cdot \frac{K_{ads1} \cdot [H_2O_2] \cdot [PO] \cdot [CH_3OH]}{1 + K_{ads1} \cdot [H_2O_2] + K_{ads2} \cdot [C_3H_6] + K_{ads3} \cdot [H_2O] + K_{ads4} \cdot [PO]} \quad (18)$$

$$r_{D2}^* = k_{D2}^* \cdot [TS-1] \cdot \frac{K_{ads1} \cdot [H_2O_2] \cdot [PO] \cdot [CH_3O(PO)H]}{1 + K_{ads1} \cdot [H_2O_2] + K_{ads2} \cdot [C_3H_6] + K_{ads3} \cdot [H_2O] + K_{ads4} \cdot [PO]} \quad (19)$$

$$r_{D3}^* = k_{D3}^* \cdot [TS-1] \cdot \frac{K_{ads1} \cdot [H_2O_2] \cdot [PO] \cdot [H_2O]}{1 + K_{ads1} \cdot [H_2O_2] + K_{ads2} \cdot [C_3H_6] + K_{ads3} \cdot [H_2O] + K_{ads4} \cdot [PO]} \quad (20)$$

$$r_{D4}^* = k_{D4}^* \cdot [TS-1] \cdot \frac{K_{ads1} \cdot [H_2O_2] \cdot [PO] \cdot [Oligom]}{1 + K_{ads1} \cdot [H_2O_2] + K_{ads2} \cdot [C_3H_6] + K_{ads3} \cdot [H_2O] + K_{ads4} \cdot [PO]} \quad (21)$$

The kinetic constant of the kinetic law (19) and (21) can be assumed the same for both the reaction of PO with methoxy propanol and its oligomers, independently on their molecular weight, because, all these side reactions (reaction to methoxy propanol and to oligomers) occur according to the same mechanism, where PO reacts with an alcoholic group.

As can be seen, the ring opening reaction rate laws depend linearly on the catalyst concentration and propene partial pressure is not influent. These aspects can be observed by plotting the initial reaction rate for r_{D1}^* , r_{D2}^* , r_{D3}^* and r_{D4}^* as a function of either the catalyst concentration or the propene partial pressure, Figures 12 and 13.

Moreover, the ring opening reaction rates depend also on the hydrogen peroxide concentration, as observed in the literature^{16,17}. This aspect has been also observed from ring opening experimental runs performed in the presence of TS-1, propene oxide, water, methanol and hydrogen peroxide. The results with related fitting are reported in Figure 14.

¹⁶ Bellussi, G.; Carati, A.; Clerici, M. G.; Maddinelli, G.; Millini, R. *J. Catal.* **1992**, 133, 220-230.

¹⁷ Bonino, F.; Damin, A.; Ricchiardi, G.; Ricci, M.; Spanò, G.; D'Aloisio, R.; Zecchina, A.; Lamberti, C.; Prestipino, C.; Bordiga, S. *J. Phys. Chem. B* **2004**, 108, 3573-3583.

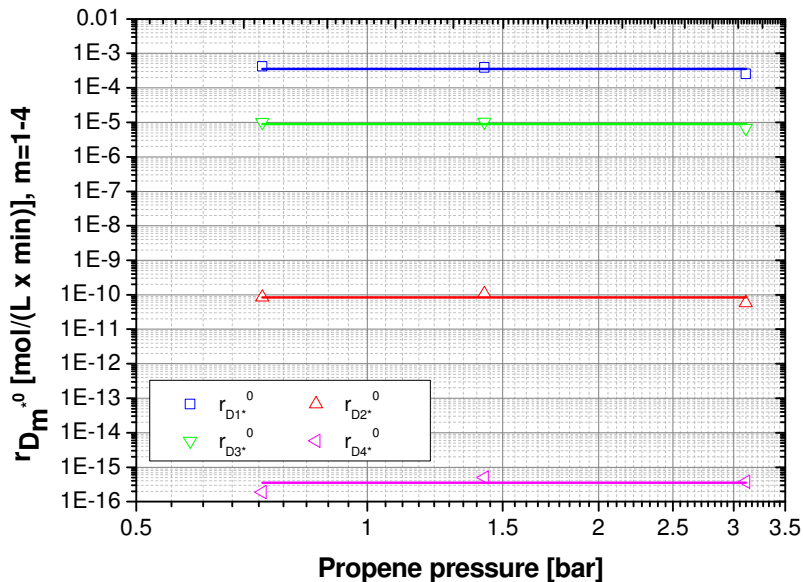


Figure 12 – Initial ring opening reaction rates as a function of the propene partial pressure. Symbols are experimental data, lines calculated data.

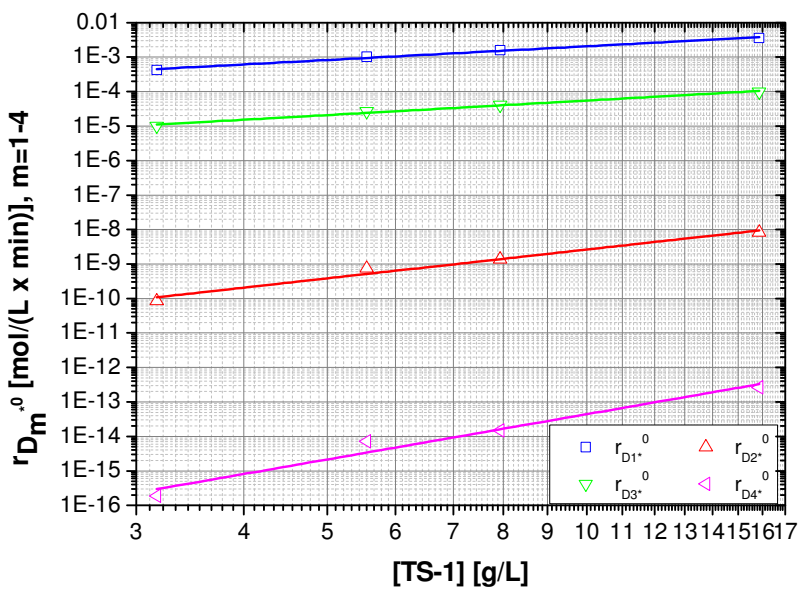


Figure 13 – Initial ring opening reaction rates as a function of the TS-1 concentration. Symbols are experimental data, lines calculated data.

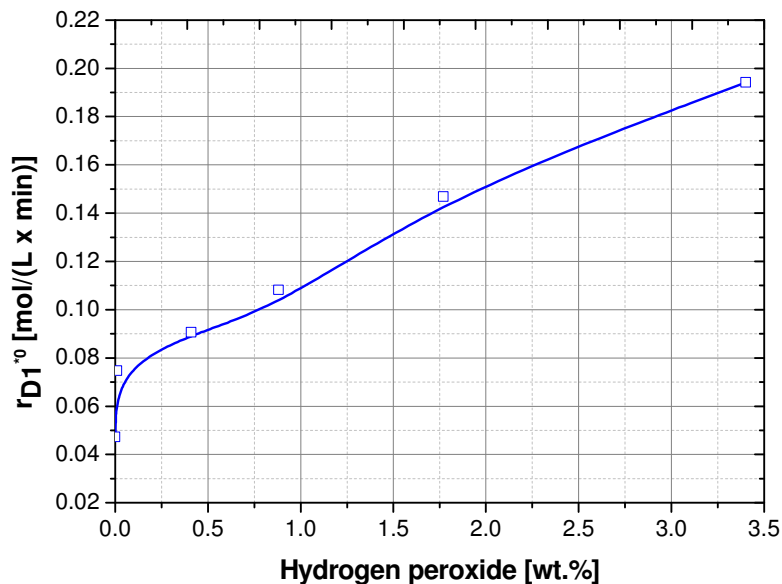


Figure 14 – Initial reaction rate trend for the ring opening reactions as a function of the hydrogen peroxide conversion. Symbols are experimental data, lines calculated data.

The initial reaction rate shows an interesting trend. It is evident that at very low hydrogen peroxide concentrations there is a sharp increase of the reaction rate, then, the slope slows down. Probably, two different mechanisms are operative both involving acid sites that are present on the catalyst surface, that are, silanols, on the correspondence of crystal defects, and the Ti-OOH specie formed as a consequence of the interaction between the catalyst and hydrogen peroxide. However, the first type of catalytic sites are not active in producing PO but can decompose it, while, the second type of sites can promote both the PO synthesis and the successive decomposition.

Moreover, by comparing the ring opening reaction rates catalyzed by Ti* and the ones catalyzed by the defective sites, it is possible to conclude that the first ones are about three time faster than the second one. Even so, it is not appropriate to neglect the influence of the defective sites on the overall reaction network.

Starting from this study, it has been possible to correctly interpret all the collected experimental data, that have been simulated by applying the general mass balance reported in Eq. 22.

$$\frac{dn_i}{dt} = J_i + \sum v_{i,m} \cdot r_m \cdot V_L \quad (22)$$

The kinetic constant dependence on the temperature has been taken into account by applying the modified Arrhenius equation reported in Eq. 11, while the gas-liquid mass transfer (J_i), with related parameters, obtained in the fluid-dynamic characterization have been applied with no changes.

All the kinetic parameters that have been estimated on the experimental data are reported in Table 3, together with the statistical information. The parameter estimation has been performed by using MatLab with ode23s as ODE solver algorithm.

Table 3 – HPPO kinetic parameters together with the related statistical information. The reference temperature is 313K. C.I.: confidence interval. σ : standard deviation.

		Value	90% C.I.	95% C.I.	99% C.I.	σ
k_1^{ref}	[L/(g _{TS-1} ·min)]	2.98E+01	1.32E+00	1.57E+00	2.08E+00	7.96E-01
$k_{D1}^{*,ref}$	[L ² /(g _{TS-1} ·mol·min)]	1.18E-01	2.87E-02	3.56E-02	4.54E-02	1.45E-06
$k_{D2}^{*,ref}$	[L ² /(g _{TS-1} ·mol·min)]	3.11E-04	7.32E-05	8.73E-05	1.23E-05	4.38E-05
$k_{D3}^{*,ref}$	[L ² /(g _{TS-1} ·mol·min)]	4.40E-02	2.23E-03	2.58E-03	3.34E-03	1.57E-05
K_{ads1}	[L/mol]	3.47E-03	2.73E-06	3.25E-06	4.30E-06	1.65E-06
K_{ads2}	[L/mol]	8.28E+00	4.93E-02	5.89E-02	7.77E-02	2.98E-02
K_{ads3}	[L/mol]	4.54E-01	2.21E-03	2.63E-03	3.48E-03	1.33E-03
K_{ads4}	[L/mol]	7.58E+00	1.01E-01	1.21E-01	1.59E-01	6.10E-02
$E_{a,1}$	[Kcal/mol]	1.09E+01	4.66E-02	5.56E-02	7.34E-02	2.82E-02
$E_{a,D1}^*$	[Kcal/mol]	2.54E+01	1.28E+00	1.37E+00	1.97E+00	7.05E-01
$E_{a,D2}^*$	[Kcal/mol]	3.02E+01	1.32E+01	1.15E+01	1.98E+01	7.75E+00
$E_{a,D3}^*$	[Kcal/mol]	3.51E+01	5.62E+00	6.84E+00	9.12E+00	3.45E+00

All the collected experimental have been satisfactory described, with an error always less than 5%, as it can be appreciated from Figures 10-14 and the parity plot reported in Figure 15. The side reaction kinetic rate laws have been tested on both the propene oxide synthesis runs and ring opening reactions performed in the presence of propene oxide,

water, methanol and hydrogen peroxide, obtaining good fittings in every case (error less than 5%).

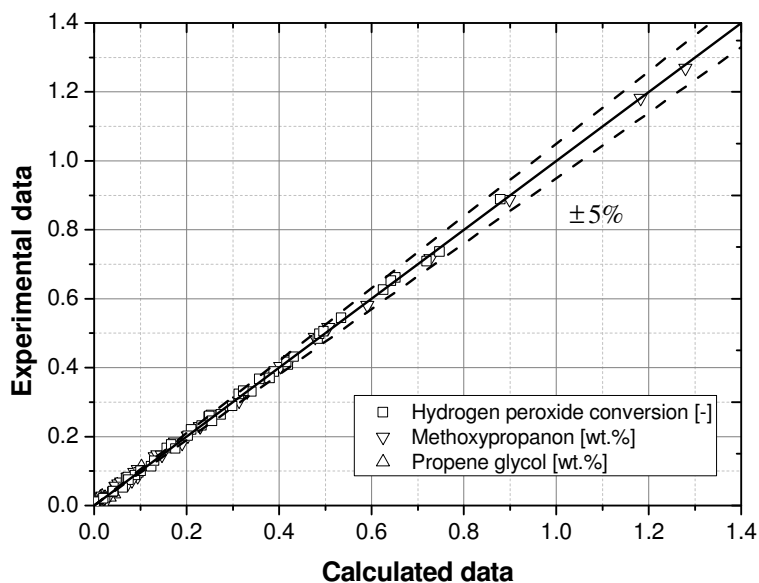


Figure 15 – Parity plot for the propene oxide synthesis tests.

Finally, as can be seen in Table 3, among the equilibrium constants, the biggest ones are K_{ads2} (8.28 L/mol) and K_{ads4} (7.58 L/mol) respectively related to propene and propene oxide. This means that these two species are competitive in the adsorption on the catalytic sites. As a consequence an increase of the propene concentration does not give a linear increase of the reaction rate (see Figure 10). Moreover, high propene oxide concentration in the system slow down the reaction. Both these aspects must be taken into account in designing a continuous plant. An idea, for example, could be to separate propene oxide at the end of a continuous reactor and feed the resulting part of the mixture to another reactor.

Chapter 3 – HPPO lab-scale continuous plant

*“The three great essentials to achieve anything worthwhile are, first, hard work;
second, stick-to-itiveness; third, common sense.”*

Thomas A. Edison, Men who made America great by Bertie Charles Forbes, 1917

3.1 *Introduction*

An HPPO lab scale continuous plant has been designed, installed and tested in order to validate the kinetic investigation performed in the first part of this work.

The lab scale plant is composed by a continuous stirred tank reactor (CSTR) that operates under a pressure of 20 bars, so allowing to work with liquid propene. The plant has been first characterized, then tested in propene oxide synthesis.

The collected data have been discussed and properly simulated with the developed kinetic model.

3.2 *Materials and methods*

3.2.1 *Chemicals and catalyst*

Propene has been supplied by SIAD with a purity of 99.5 % (0.5 % propane), methanol has been supplied by Clean Consult at 99.8% purity, hydrogen peroxide (60 wt.%) has been supplied by Mythen s.r.l.. All the other reagents employed have been supplied by Aldrich at the highest level of purity available and have been used as received without further purification.

TS-1 catalyst has been supplied by Conser S.p.A. in spray-dried powdered form (average diameter of particles 35 μm ; average size of crystallites 30 nm with a titanium content of 3 wt.%).

3.2.2 *Lab-scale HPPO pilot plant and reaction procedures*

The propene oxide synthesis experimental runs have been performed in a lab-scale pilot plant, where the reactor is a continuous stirred tank (CSTR). A sketch of the realized plant is reported in Figure 16.

As it can be seen, a piston pump is used to feed the oxidizing solution composed by 93.2 wt.% methanol, 3.5 wt.% hydrogen peroxide and 3.3 wt.% water. Propene is fed to the reactor through a liquid mass-flow-meter controller based on the Coriolis principle. Propene is stored in a tank under the pressure of 35 bar, so pressure is the driving force of the feeding while the flow-meter is the regulator. Both the pumping systems are fixed at the desired flow-rate that is kept constant during the test.

A static mixer has been installed and tested in order to verify if the oxidizing solution and propene are properly mixed before feeding them in the CSTR. The mentioned mixer is an AISI 316 stainless steel tube of 10 cm length and 3/4" OD (1.54 cm ID) filled with glassy spheres of 2.4 mm diameter. The mixer presents a void degree of 0.4.

The reactor is a continuous stirred tank reactor (CSTR). The design of this unit is not trivial. In fact, there is the necessity to build up a complex reaction system, deriving from different properties of the reaction itself.

First of all, being the reaction extremely exothermic ($\Delta H = 57$ Kcal/mol), it is needed a proper heat exchange system, capable to subtract the heat released by all the reactions and keep the reaction temperature at the desired level. For this reason, a stainless steel AISI 316 cooling coil of 2 m length and 1/8" outer diameter, where water flows at a flow-rate of 6 L/min. A thermocouple is installed in the reactor in order to check the reaction temperature. A sketch of the reactor is reported in Figure 17, while a photo of the overall HPPO plant is reported in Figure 18 A. The reactor has been built by Advanced Couplings Limited.

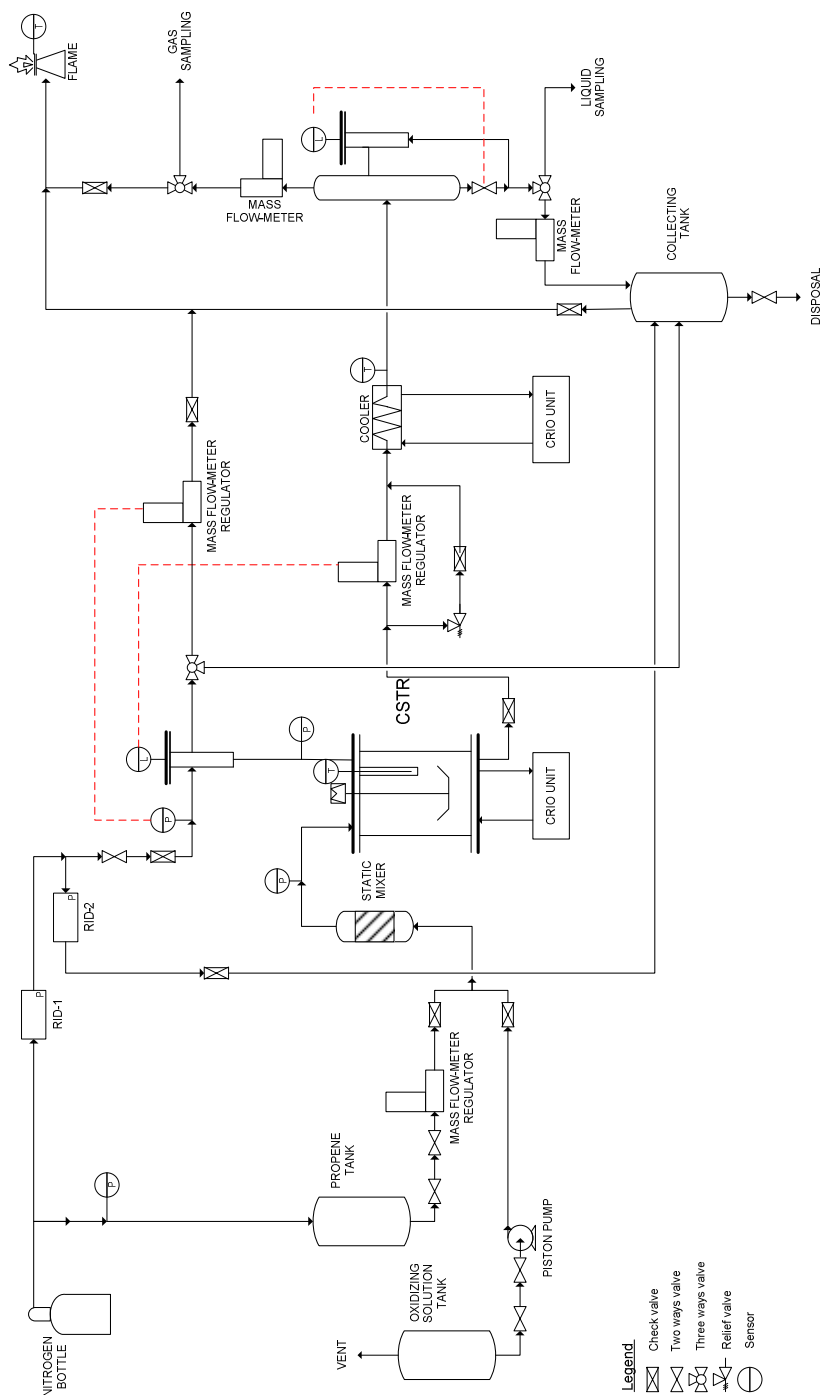


Figure 16 – HPPO lab-scale continuous plant.

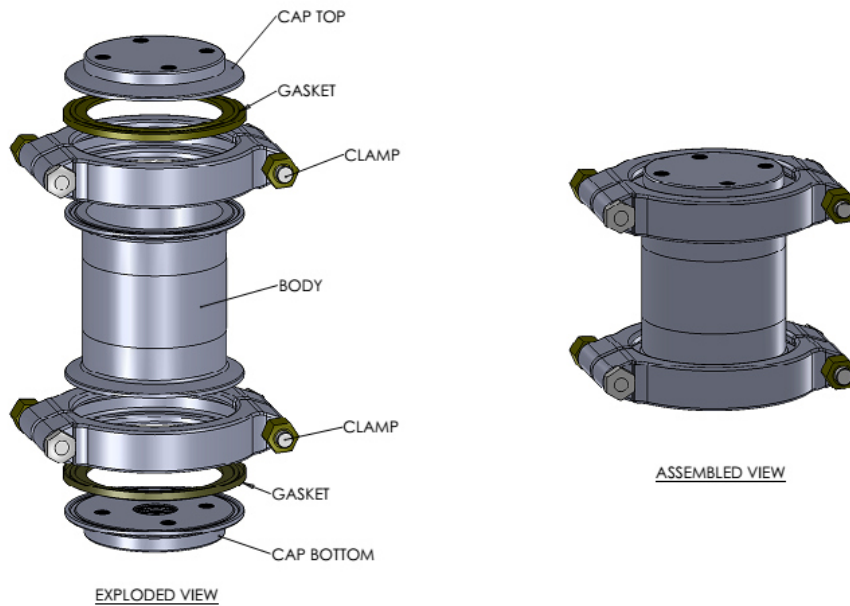


Figure 17 – Sketches of the designed CSTR.

Secondly, the system has to be pressurized at pressure greater than 16 bars, in order to keep propene in the liquid phase. For this reason, an auxiliary tank connected to the top of the reactor is connected to a nitrogen bottle through a pressure regulator. All the tests have been performed at 20 bars. A filter has been introduced on line, in order to avoid any catalyst drainage from the CSTR to the mentioned tank.

Therefore, there is the necessity to keep all the reactor filled with liquid, in order to avoid high catalyst concentration in the CSTR and to warrantee a good heat transfer. For this reason, in the auxiliary tank, a liquid level sensor has been installed.

Oxygen can be released due to the eventual hydrogen peroxide decomposition, it would be dangerous an eventual accumulation in the auxiliary tank. For this reason, the top of the mentioned tank is continuously flushed by regulating the gas outer flow with a mass flow-meter controller. This equipment is driven by the pressure of the gas phase, with a PID controller. For a better safety, a mechanical relief valve is installed on the outlet

stream, calibrated at 50 bars, so if suddenly the pressure gets higher than the mentioned value, the valve opens and everything is sent to the final collecting tank.

By considering that the pumps are always in action during the test, it is necessary to warrant a continuous and regular outlet liquid flux from the reactor in order to avoid either a liquid accumulation or a reactor emptying. In order to solve this problem, a liquid mass flow-meter controlled based on the Coriolis principle has been installed on the outlet line. The mentioned flow-meter is automatically driven by the liquid level sensor previously described, so if the level increases, there is an accumulation and the flow-meter proportionally opens. This operation is made by a PID controller.

Finally, an adequate filtering system has to be installed on the outlet line being the catalyst in an extremely fine powdered form. In order to avoid the filter obstruction by the catalyst, the feed/outlet streams are automatically alternate.

The outlet liquid phase is composed of course by the reaction products and the unreacted reagents. This solution has to be de-pressurized at atmospheric pressure. In this way, propene, methanol and propene oxide would directly flash in two streams, a liquid one containing the heavy products and a gas phase containing mainly propene and the a certain amount of the light components, such as propene oxide and methanol, with consequent mistakes in measuring the selectivity of the system. In order to keep propene oxide and methanol in the liquid phase and to properly flash the product stream, two operation units have been put in series: (i) a cooler system, that lead the product stream at 5°C, composed by a stainless steel AISI 316 cooling coil of 2 m length 1/8" outer diameter immersed in a cylindrical vessel (Figure 18 B); (ii) a flash unit composed by a stainless steel AISI 316 pipe of 30 cm length and 1" outer diameter, fed at the center. The flash unit is connected to a second auxiliary tank where a liquid level sensor is installed in order to keep the flash unit filled with liquid for 1/3 of its length (Figure 18 C).

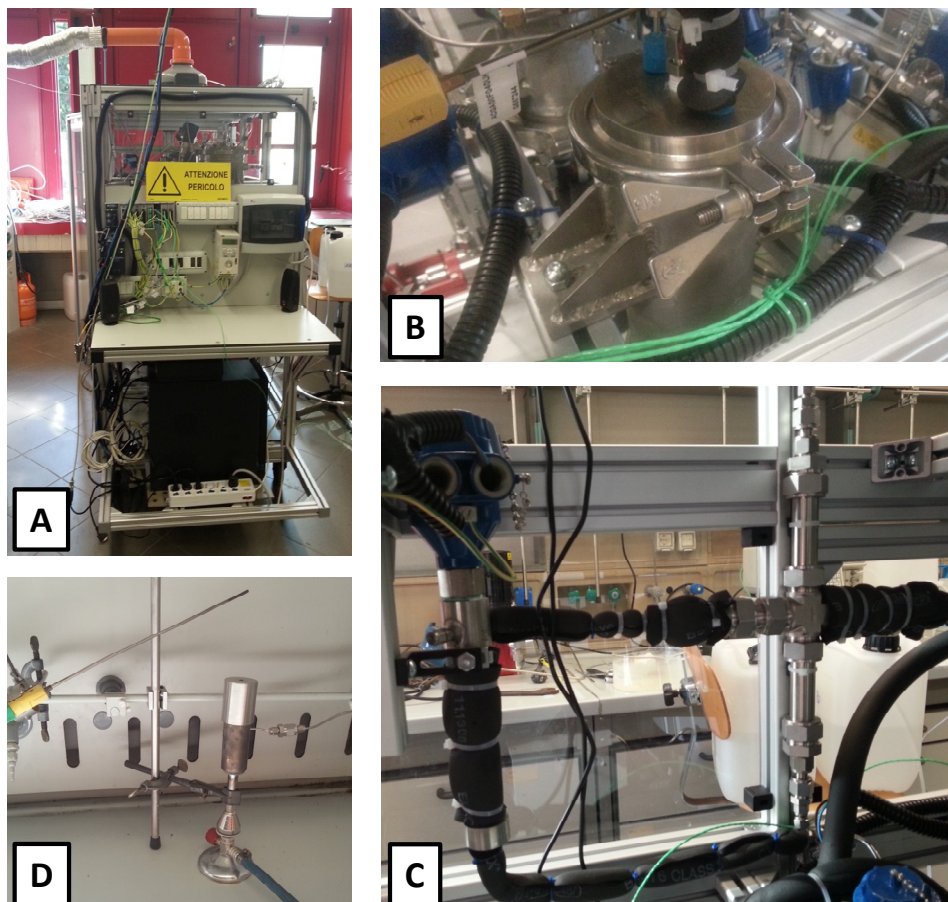


Figure 18 – A. HPPO plant: overall view. B. Heat exchanger. C. Flash unit. D. Torch.

The liquid stream coming out from the flash unit is measured through a liquid mass flow-meter controller based on Coriolis principle and further collected and analyzed to determine the hydrogen peroxide conversion and the propene oxide selectivity. The liquid solution is stored in a 5 L tank continuously flushed with nitrogen in order to avoid eventual ignitions.

The gas stream is measured through a mass flow-meter controller and analyzed to verify if propene oxide is present in the gas phase. By considering that this last stream contains also the unreacted propene, it is sent to a burner working at 900°C in order to be converted in CO₂ and water (Figure 18 D). A thermocouple is installed on the flame in

order to verify if it is working, while a pilot flame has been provided by feeding external butane to the burner in order to avoid its turning off. Of course, all the gas purges of the system are connected to the same flame.

All the described operations and all the valves connecting the described units are automated through to a data acquisition system (NI cDAQ-9178) provided by National Instruments and a dedicated software written in LabVIEW 2011. The mentioned software contains also several kind of alarms on the main operating variables, in order to keep everything is safe conditions. A picture of the developed software is reported in Figure 19 A-B.

Each test, both the hydraulic, the fluid-dynamic and the kinetic ones, have been performed with the same experimental procedure. The lab scale continuous plant has been firstly loaded with the liquid setting an overall volumetric flow-rate of $30 \text{ cm}^3/\text{min}$, under atmospheric and inert pressure. In the meantime, both the reactor and the cooler are brought at the set temperature value, while the stirring rate set at 300 rpm. As the system is full and at the right temperature, a pressure of 20 bars has been applied. Dependently on the test, three different procedures have been applied.

- (i) Hydraulic test: the system is kept under fluid pumping at 20 bars. Some temperature changes are made in order to verify the proper working of all the installed units.
- (ii) Fluid-dynamic tests: the flow-rate is adjusted and the solution tracer (toluene 9wt.% in methanol) is pumped to the reactor. The tracer concentration is monitored by UV-Vis method.
- (iii) Kinetic tests: both the oxidizing solution and propene are pumped to the reactor at a fixed flow-rate.

At the end of each test, the reactor is first washed with methanol, then the liquid phase discharged.

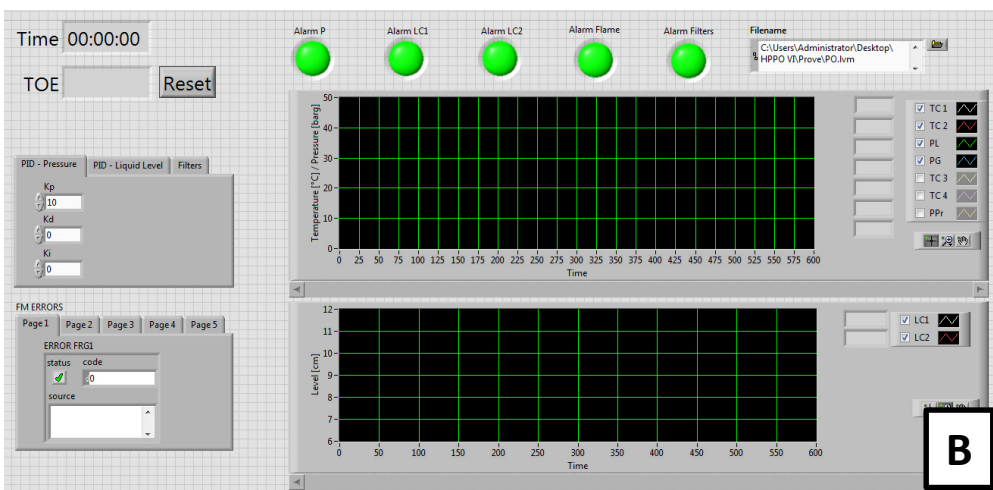
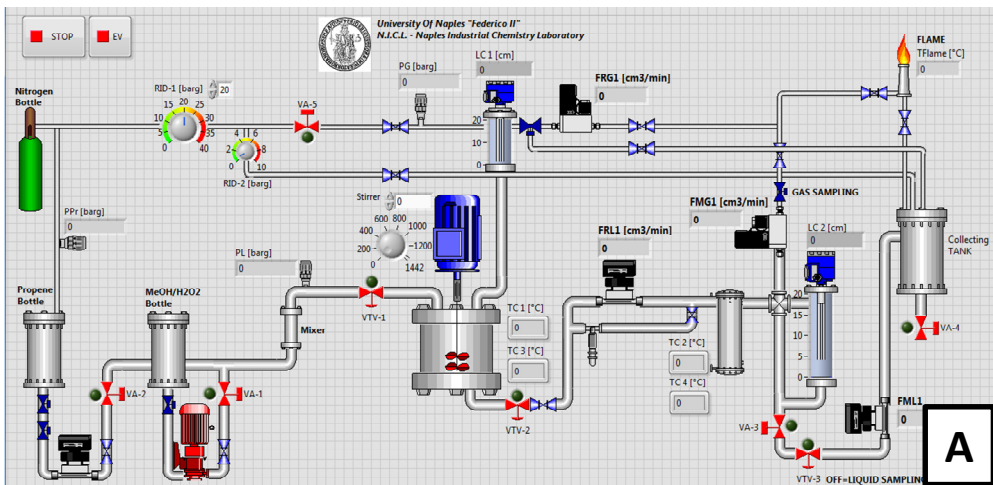


Figure 19 – LabVIEW software: A Control panel; B. Monitor and alarms.

3.2.3 Analytical methods

The products distribution and the PO conversion have been analytically determined by gas-chromatographic analysis, using a gas chromatograph (HP 6890), equipped with a flame ionization detector (FID), a split-splitless column injector, and employing a Restek RT-Q-Bond Plot column (30 m x 0.32 mm I. D., 0.1 μm film). Before the analysis, 100 μL of ethyl acetate have been added to 5 cm^3 of sample, as internal standard. The residual hydrogen peroxide concentration has been analytically determined by a iodometric titration.

The UV-Vis measurements for the CSTR fluid-dynamic tests have been performed by using a Jasco UV-975 spectrophotometer in continuous, setting $\lambda=286$ nm and using toluene as tracer molecule.

3.3 Hydraulic tests

The HPPO lab scale continuous plant has been submitted firstly to several hydraulic test in order to verify the leak and the hydraulic of the system. In these tests, water has been pumped to the reactor previously made empty, setting an overall volumetric flow-rate of $30 \text{ cm}^3/\text{min}$, under atmospheric and inert pressure. In Figure 20, it is possible to appreciate an example of the obtained results.

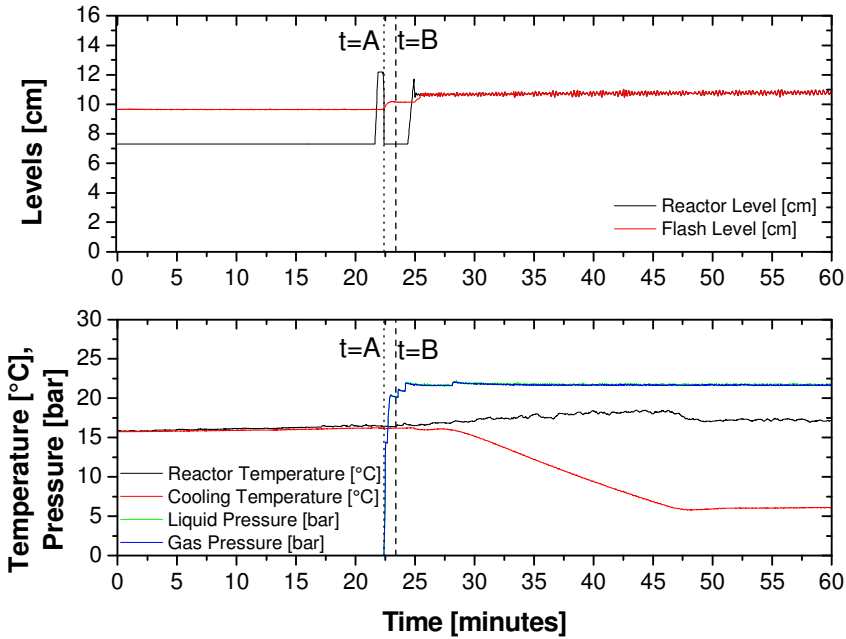


Figure 20 – Hydraulic test performed by fixing a volumetric flow-rate of $30 \text{ cm}^3/\text{min}$.

At time <A, water has been pumped at atmospheric pressure till the liquid sensor installed above the reactor has measured a level of 10 cm. At this point, the two pumps have been stopped, and the system has been pressurized at about 22 bar (time=A). Here the liquid level has decreased as pressure increased. As soon as the system has reached the set pressure, the two pumps have been activated again. At time=B, the ultra cryostat connected to the cooler has been set to 5°C . From this point, the temperature outside the cooler started to decrease till 6°C , temperature that has kept stable till the end of the test.

Of course, during this operation, both the levels and the system pressure have not shown any kind of variation, fact that show the goodness of the PID that regulates the levels of both the reactor and the flash units and the pressure of the reactor itself.

This kind of test demonstrated that the HPPO lab scale plant has been properly installed and no problems, related to both the hydraulic and the leak of the system have been observed.

3.4 *Fluid-dynamic tests*

The CSTR have been tested in order to study the fluid dynamics of the reactor. The summary of the performed fluid-dynamic tests is reported in Table 4, together with the results of the measured average residence time. Of course, the dead volumes have been subtracted from the residence time calculation.

Table 4 –Summary of the experimental conditions and main results.

Test	Average residence time [minutes]
CSTR-1	6.90
CSTR-2	4.53
CSTR-3	13.93

In Figure 21, an example of the experimental profiles obtained for the CSTR fluid-dynamic tests is reported. The figure refers to the CSTR-1 test. Here F is the dimensionless tracer concentration, obtained dividing toluene concentration by its inlet value.

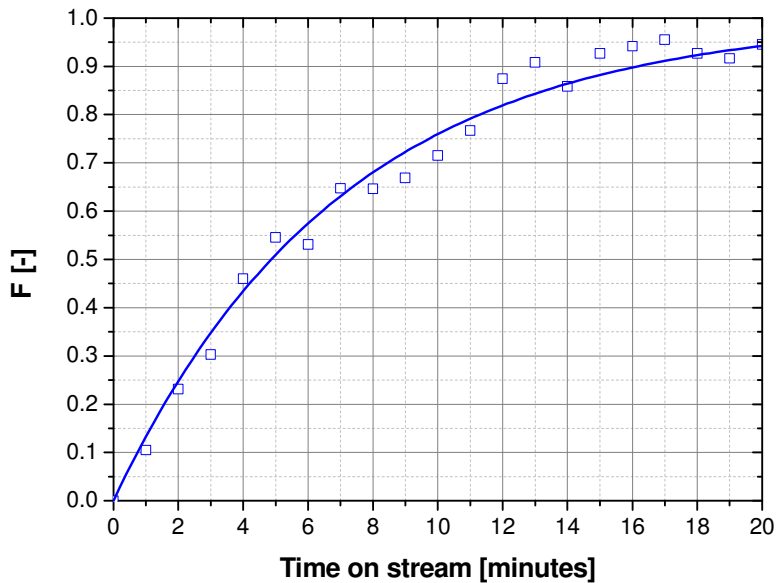


Figure 21 – Fluid-dynamic test: F function versus time on stream.

The average residence time, \bar{t} , can be obtained by fitting on the collected experimental data, applying Eq. 23, valid for a CSTR ideal behavior¹⁸.

$$F = 1 - e^{-t/\bar{t}} \quad (23)$$

The fit can be appreciated in Figure 21, while the fitted value are reported in Table 4. The measured residence time values will be used in interpreting the kinetic tests reported in the next paragraph.

¹⁸ Levenspiel, O. Chemical Reaction Engineering, John Wiley & Sons: New York, 1999.

3.5 Kinetic tests

Some different experimental runs in the designed continuous stirred tank reactor (CSTR) have been performed. These runs are useful to validate the model developed in the fed-batch reactor. In fact, in both the fed-batch and the CSTR reactor the same TS-1 powdered catalyst has been used, so the same activity and selectivity should be observed.

A list of the performed experimental runs with related experimental conditions is reported in Table 5. All the runs have been performed in isothermal condition.

Table 5 – Summary of the performed tests with related experimental conditions. RPM: stirring rate. *Run performed by mixing methanol and propene before entering the reactor.

Run	P [bar]	RPM	T _R [°C]	CH ₃ OH ^{IN} [wt. %]	H ₂ O ₂ ^{IN} [wt. %]	C ₃ H ₆ /H ₂ O ₂ [mol/mol]
1	21	300	30	93.2	3.58	0.14
2	21	300	40	93.2	3.58	0.14
3	21	300	40	93.2	3.55	0.28
4	21	300	40	93.2	3.55	0.56
5*	21	300	40	93.2	3.60	0.27

The first run has been performed for 5 hours in order to verify that the system reached the stationary state. In order to demonstrate it, the profiles of hydrogen peroxide conversion/propene oxide selectivity and reactor's temperature are reported (see Figure 22).

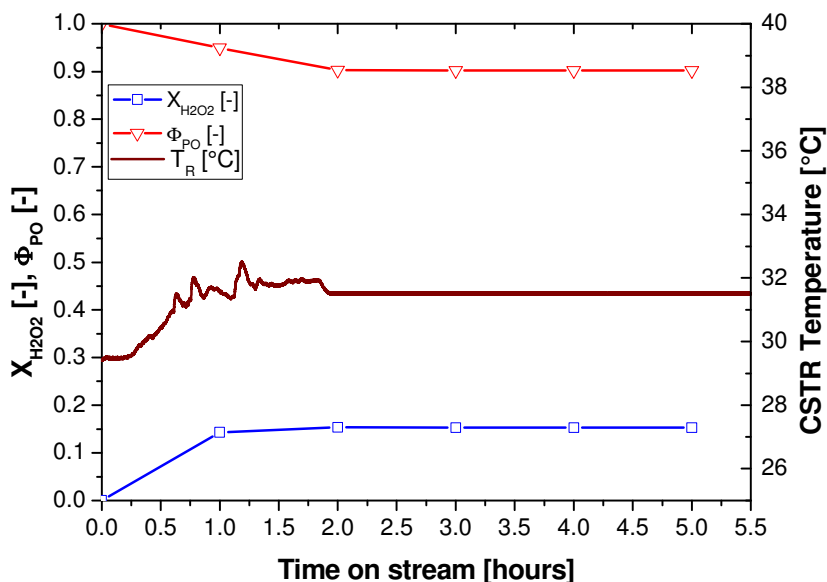


Figure 22 – Hydrogen peroxide conversion, propene oxide selectivity and CSTR temperature, against time of stream, of Run 1 of Table 5.

As it can be seen, the system can be considered stationary already after 2 hours. On the basis of the kinetic study performed in a fed-batch reactor, and in order to keep the system safe, it has been decided to work at low propene/hydrogen peroxide molar ratio, keeping hydrogen peroxide in excess, and low TS-1 loading. In this way, it has been possible to work under isothermal conditions, avoiding any hydrogen peroxide decomposition. At this purpose, four experimental runs have been performed and the comparison of the data in terms of hydrogen peroxide conversion ($X_{H_2O_2}$) and propene oxide selectivity (Φ_{PO}) are reported in Figures 23-26. The collected results show that by increasing the oxidizing solution flow-rate, so decreasing the residence time, a decrease in the hydrogen peroxide conversion is observed but the selectivity to propene oxide significantly increases (see Figure 23). This fact is reasonable because by lowering the residence time the conversion of the main reaction decreases as expected but as the side reactions are consecutive to the main one the occurrence of by products is more lowered.

The two runs performed at different temperatures demonstrate that by increasing the temperature the hydrogen peroxide conversion increases while the propene oxide

selectivity decreases (see Figure 24). Two runs have been performed at different propene/hydrogen peroxide molar ratio by keeping constant the temperature more or less the residence time. The results of the two runs show that by doubling the propene concentration in the reactor, the conversion increases only by a factor of 1.7 (see Figure 25). This fact is in agreement with the not linear dependence of the propene concentration on the propene oxide formation reaction rate. The last run of Table 5 has been performed by putting in series a static mixer to the CSTR, in order to verify that the oxidizing solution and propene are efficiently mixed before entering the reactor. In this way, a new run has been performed (Run 5 of Table 5), where the oxidizing solution and propene are mixed before entering the reactor. By using the mentioned mixer, only a slight increase of the hydrogen peroxide conversion has been obtained, so demonstrating that also in the previous runs the two reactant feeds are well mixed (see Figure 26).

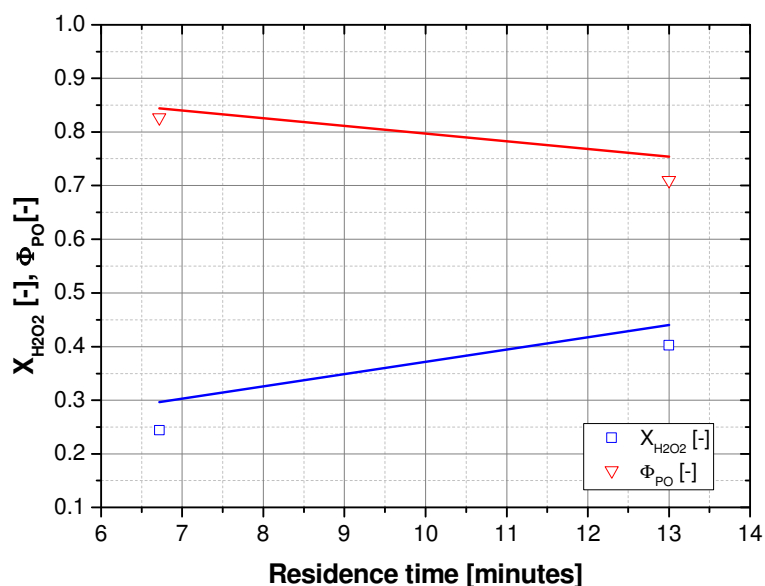


Figure 23 – Residence time dependence on hydrogen peroxide conversion and propene oxide selectivity.

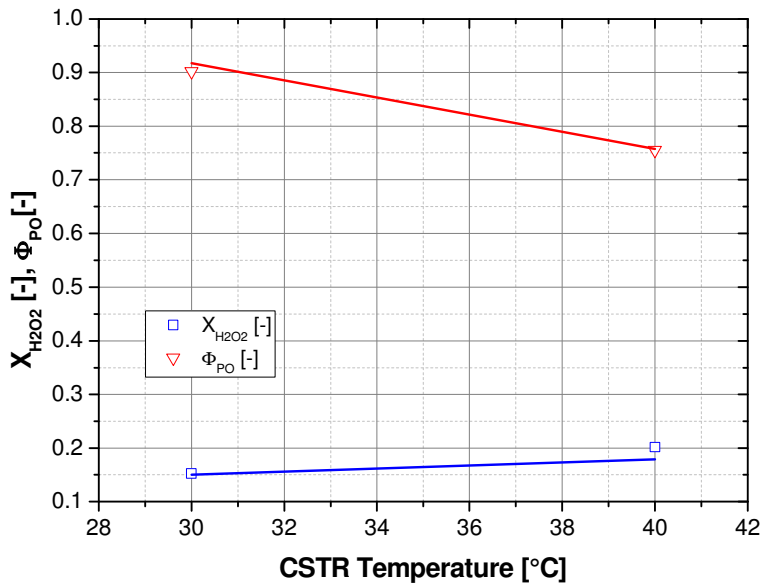


Figure 24 – Temperature dependence on hydrogen peroxide conversion and propene oxide selectivity.

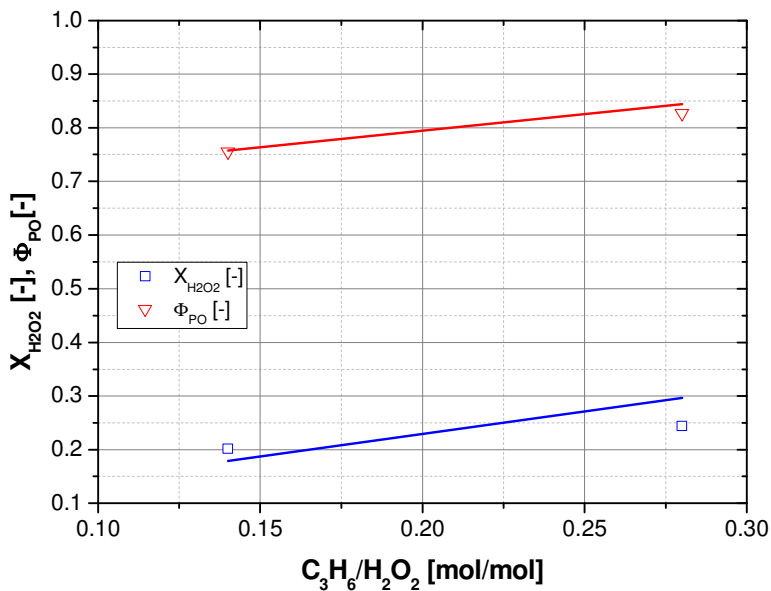


Figure 25 – Propene/hydrogen peroxide molar ratio dependence on hydrogen peroxide conversion and propene oxide selectivity.

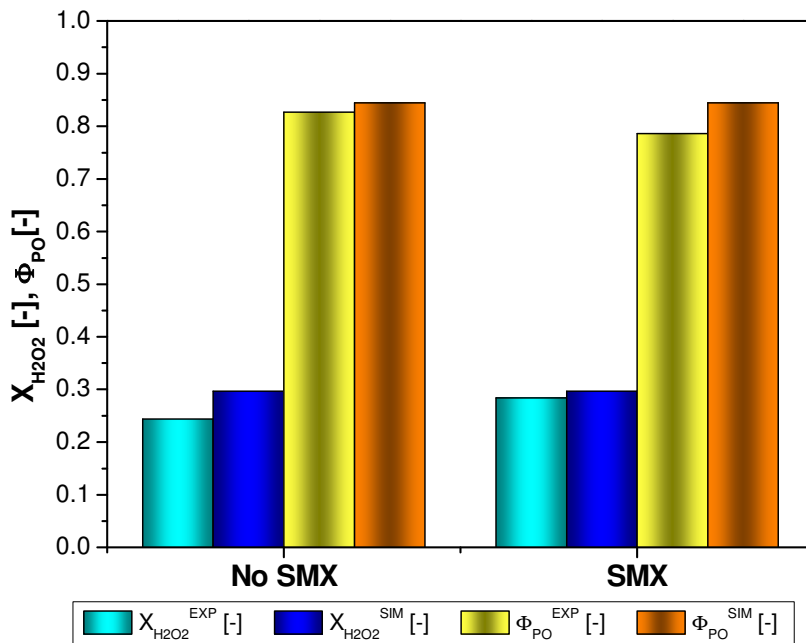


Figure 26 – Mixing effect on hydrogen peroxide conversion and propene oxide selectivity.

3.6 Kinetic modelling and simulations

The experimental data collected in the HPPO lab scale plant have been simulated by considering a dynamic CSTR isothermal model. The mass balances that have been used to interpret the collected data are reported in Eq. 24, solved numerically by using ode45s ODE solver algorithm implemented in MatLab.

$$\frac{d[I]}{dt} = \frac{[I]^{IN} - [I]^{OUT}}{\tau} \pm \sum v_{i,m} \cdot r_m \quad (24)$$

In order to appreciate the goodness of the fitting, in Figure 27 the parity plot, between calculated and experimental data, is reported, concerning both the hydrogen peroxide conversion and propene oxide selectivity. As it can be seen, all the data are in a window of 20%, so the model can be considered validated.

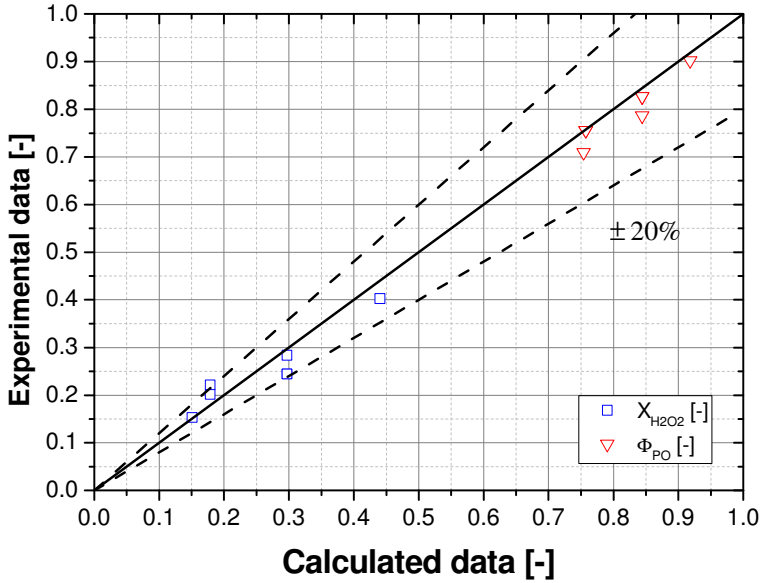


Figure 27 – CSTR parity plot for both hydrogen peroxide conversion and propene oxide selectivity.

Chapter 4 – Hydrogen peroxide decomposition

“Science is no more than an investigation of a miracle we can never explain,

and art is an interpretation of that miracle.”

Ray Bradbury, The Martian Chronicles, 1950

4.1 Introduction

The waste water treatment of the HPPO plant has been studied in the present section of this work, investigating the possibility to decompose the unreacted hydrogen peroxide with an heterogeneous catalyst.

An depth catalyst screening has been performed, finding that manganese base catalysts can be good candidates for the scope. Moreover, depending on the catalyst preparation, it is possible to prepare stable catalyst in slightly acid conditions.

At this purpose, the kinetics of the most stable and active catalyst has been studied, validating the derived kinetic model in a structured micro reactor.

4.2 Material and methods

4.2.1 Chemicals and catalysts

Hydrogen peroxide (60 wt.%) has been supplied by Mythen s.r.l.. Boehmite (Pural SB-1) has been obtained from Sasol, γ -Al₂O₃ from Fluka and Alfa Aesar, urea from Merck.

MnO_x catalysts for hydrogen peroxide decomposition have been prepared with dry impregnation technique on both powdered and pelletized γ -Al₂O₃. Different kind of catalysts have been prepared by varying the Mn amount or the receipt. The nomenclature of the catalysts is Mn(X)-Y-Z, with X the Mn weight percentage (0.2-5wt.%), Y the support preparation procedure and Z impregnation procedure.

The impregnation have followed three different procedures: A. impregnation of alumina coatings with Mn precursor solution [Mn(CH₃COO)₂·4H₂O in water]; B. deposition of Mn containing alumina sol, 22 mg Mn(CH₃COO)₂·4H₂O and 4.7 mg Al₂O₃; C. deposition of Mn containing alumina sol, 4.7 mg Mn(CH₃COO)₂·4H₂O and 4.7 mg Al₂O₃. The details related to the support preparation can be found in publication **III**.

The catalyst supported on SMFSS (i.e. perovskite 5 wt.% La_{0.4}Ca_{0.6}MnO₃/SMFSS, 5 wt.% (NiO+Al₂O₃+ MgO)/SMFSS, 5 wt.% (Al₂O₃+MgO)/SMFSS) have been prepared by incipient wetness impregnation method. The structured support used for the active

phase deposition is a stainless steel AISI 316L sintered metal fiber, SMFSS, (Southwest Screens & Filters SA, Belgium), with a fiber diameter of 20 μm , a filter thickness of 0.3 mm and a porosity of 0.83. The prepared catalysts with the detailed compositions are reported in Table 6.

Table 6 – Hydrogen peroxide decomposition catalysts supported on SMFSS.

Catalyst	Composition
20NiO	5wt.%(20wt.%NiO+Al ₂ O ₃ +MgO)/SMFSS
50NiO	5wt.%(50wt.%NiO+Al ₂ O ₃ +MgO)/SMFSS
MnO _x	5wt.%MnO _x /5wt.%(Al ₂ O ₃ +MgO)/SMFSS
Perovskite	5wt.%La _{0.4} Ca _{0.6} MnO ₃ /SMFSS

All the details concerning the procedures in catalyst preparations are reported in publication **IV**.

All the other reagents and supports employed have been supplied by Aldrich at the highest level of purity available and have been used as received without further purification.

4.2.2 Catalyst characterization

The Brunauer–Emmett–Teller (BET) surface areas, pore sizes, and pore volumes of the powders have been determined either with a Micromeritics ASAP 2400 instrument using nitrogen adsorption at 77 K (publication **III**) or with a Sorptomatic 1990 (publication **IV**), both according to the method of Dollimore and Heal.

The scanning electron microscopy (SEM) has been performed with either a Quanta 3D FEG microscope at 30 kV with a resolution of 1.2 nm (publication **III**) or a Philips FEI XL30-FEG equipped with an Everhart–Thornley secondary-electron (SE) detector, operated at an accelerating voltage of 15 kV (publication **IV**). Before analysis, the sample underwent a hydrocarbon decontamination treatment using a plasma-cleaner (EVACTRON).

XRD spectra have been recorded on a Rigaku Geigerflex device with Cu K α radiation (40 kV, 40 mA) by continuous scan (1.5°/min).

In coating resistance tests (publication **III**), adherence has been determined in terms of the weight loss of the coated plates after a drop test in which the plates have been placed in a holder and dropped from a distance of 65 cm; the procedure has been repeated five times. Weight loss for has been calculated as in Eq. 25.

$$x = \frac{(w_{cp1} - w_p) - (w_{cp2} - w_p)}{(w_{cp1} - w_p)} \cdot 100 \quad (25)$$

Where w_{cp1} is the weight of the coated plate before the drop test, w_{cp2} is the weight of the coated plate after the drop test, and w_p is the weight of the uncoated plate.

4.2.3 Reactors and reaction procedures

Three different types of reactors have been used. A glass-jacketed batch reactor with a volume of 100 cm³ has been used for both the catalytic screenings and the kinetic study of the powdered catalysts. The catalyst screening tests have been performed at a fixed temperature (50-60°C), with a fixed hydrogen peroxide initial concentration (2-10wt.% H₂O₂/H₂O) but at different catalyst concentration. Therefore, the kinetic tests have been performed by using a solution of 10wt.% H₂O₂/H₂O varying both temperature and catalyst concentration. Details can be found in publication **III**.

The continuous runs have been performed in two different reactors. A packed-bed tubular reactor (length, 20 cm; inner diameter, 1 cm) has been used to study the stability on stream of the manganese oxide catalyst. The reactor has been packed with 3 g of catalyst in spherical pellets of 2.5-mm diameter containing 5 wt.% manganese. The catalyst has been diluted along the bed with 17 g of glass spheres of 2.5-mm diameter. The tests have been performed pumping a 10wt.% H₂O₂/H₂O solution, at room temperature, to the reactor trough a HPLC pump, working at a fixed flow-rate (4 cm³/min). A sketch, with related picture of the used plant is reported in Figure 28.

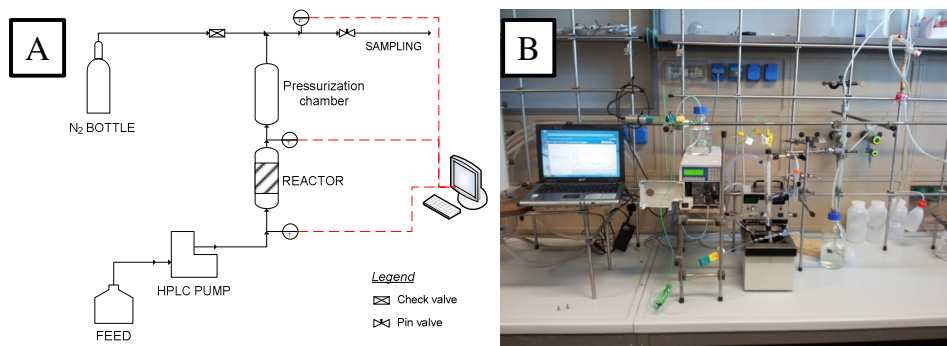


Figure 28 – Laboratory scale continuous plant for hydrogen peroxide decomposition. A: sketch; B: picture.

Temperature and pressure have been monitored by data acquisition system (NI cDAQ-9174) provided by National Instruments and a dedicated software written in LabVIEW 2011.

Another continuous reactor (a disk-shaped single-plate microreactor with a void volume of 1.78 cm³) has been used with an internal geometry that favors local micromixing, with channels of 0.4 mm. The metallic walls of the reactor have been coated with 50 mg of a catalyst whose composition has been optimized by means of the runs performed in the previously described reactor. The metallic plate has been covered with a polytetrafluoroethylene (PTFE) sheet held in place with another metallic plate. The continuous setup has been arranged to operate between 1 and 5 bar, to allow for the investigation of the effect of pressure on the decomposition of hydrogen peroxide. A picture of the mentioned reactor is reported in Figure 29.

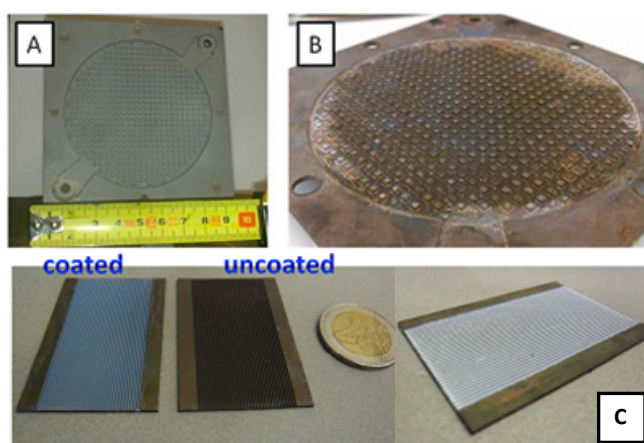


Figure 29 – Disk-shaped single-plate stainless steel AISI 316 microreactor. A. Original plate; B. Coated plate; C. Stainless steel plates for catalytic tests, coated and uncoated.

In this case, the experiments have been performed pumping a 9.6wt.% H₂O₂/H₂O solution, at room temperature, to the reactor through a HPLC pump (flow-rate range 0.25-1 cm³/min), working under a pressure ranging from 1 to 5 bars. The liquid has been pressurized with nitrogen through the pressurization chamber, an empty pipe that avoided the reactor emptying, while the outlet flow-rate has been adjusted with a manual pin valve. A scheme of the laboratory scale continuous plant adopted is reported in Figure 29 A.

Finally, the catalyst stability tests have been performed using stainless steel plates (50×35×1mm) with a channel depth of 400µm and a channel diameter of 600µm. The plates have been pretreated before the deposition of the coating. The coatings have been deposited by the wash-coating technique whereby the suspension has been deposited on the substrate and the excess has been then wiped off. The described plates are shown in Figure 29 C. All the details can be found in publication **III**.

The hydrogen peroxide decomposition tests dealing with the catalyst supported on SMFSS, have all been performed in a glass reactor equipped with a mechanical stirrer (stirring rate 1900 rpm) and immersed in a thermostatic water bath. The catalyst has been fixed to the terminal part of the stirrer. Temperature has been set either at 25 or 60°C, catalyst content has been with 0.3 or 1.5 g, while the initial hydrogen peroxide content ranged between 5-10wt.% H₂O₂/H₂O. The absolute values have been chosen dependently on the catalyst activity. All the other details can be found in publication **IV**.

4.2.4 Analytical methods

The residual hydrogen peroxide concentration has been analytically determined by a iodometric titration for publications (**III**, **IV**). The evolution with time of the hydrogen peroxide decomposition rate, in publications **III** and **IV**, has been monitored by gas-volumetric analysis in terms of the volume of oxygen produced. The used equipment consists in two graduated cylinders filled with water, turned upside down and deep in a beaker. The oxygen released during the reaction is collected at the top of the cylinder and water is correspondingly displaced allowing the measurement of the volume of oxygen delivered as function of time.

4.3 Catalyst characterization

Different kind of manganese supported on γ -alumina powdered catalysts have been prepared in order to optimize the wash-coating procedure. The XRD patterns of different manganese alumina catalysts, calcined at 500°C are shown in Figure 30.

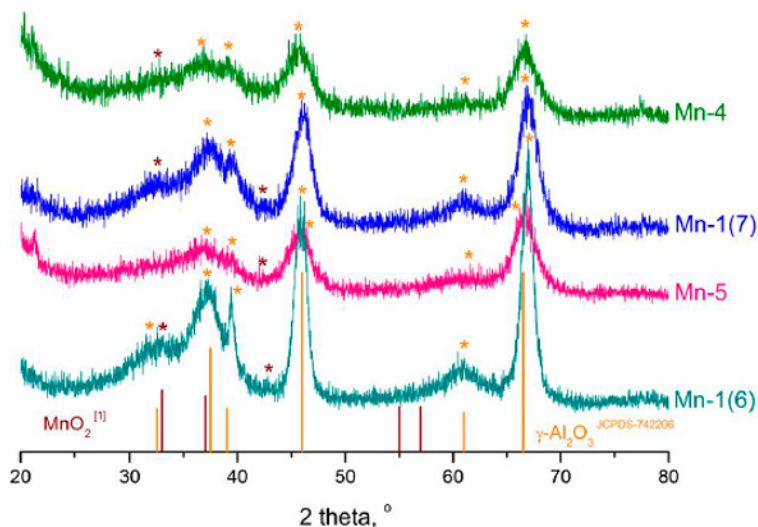


Figure 30 – XRD patterns of manganese on alumina catalysts.

The background XRD pattern is the γ -Al₂O₃ one^{19,20}. The dark stars are related to some small peaks corresponding to the MnO₂ phase, although the peaks are not clearly pronounced and some of them probably overlap alumina peaks.

For each catalysts, the BET surface area has been measured. Actually, it has been determined by the initial surface area of the alumina precursor (see Table 7), decreasing after Mn impregnation.

¹⁹ Zapf, R.; Kolb, G.; Penneman, H.; Hessel, V. *Chem. Eng. Technol.* **2006**, 29(12), 1509–1512.

²⁰ Zapf, R.; Becker-Willinger, C.; Berresheim, K.; Bolz, H.; Gnaser, H.; Hessel, V.; Kolb, G.; Löb, P.; Pannwitt, A. K.; Ziogas, A. *Trans. Inst. Chem. Eng. A* **2003**, 81, 721–729

Table 7 – Mn doped alumina coatings with related properties. a_{sp}^{BET} : surface area, n.d.: not determined. x: weight loss.

Catalyst	Mn [wt.%]	Al_2O_3 a_{sp}^{BET} [m^2/g]	a_{sp}^{BET} [m^2/g]	x [wt.%]	Coating thickness [μm]	Mn content per unit surface area
Mn(0.5)-2-A	0.5	78	65	2	31±3.4	0.008
Mn(0.5)-3-A	0.5	214	200	11	7±1.4	0.003
Mn(2)-2-A	2	78	97	10	60±10.2	0.021
Mn(2)-3-A	2	214	209	1	5±1.0	0.010
Mn(0.5)-1-B	0.5	320	276	5	8±1.6	0.002
Mn(2)-1-C	2	320	250	n.d.	13±3.3	0.008
Mn(5)-2-A	2	78	95	8	40±3.2	0.053

Stability tests have shown that all of the coatings are stable and uniform, so reasonably adhesive, being the weight loss always lower than 15%. The coatings are uniform, as the deviation in thickness has been within 20–25%. SEM images have been recorded in different locations on the micro structured plates. At this purpose, the enlarged SEM images of the Mn(2)-3-A catalytic coating are shown as an example, Figure 31.

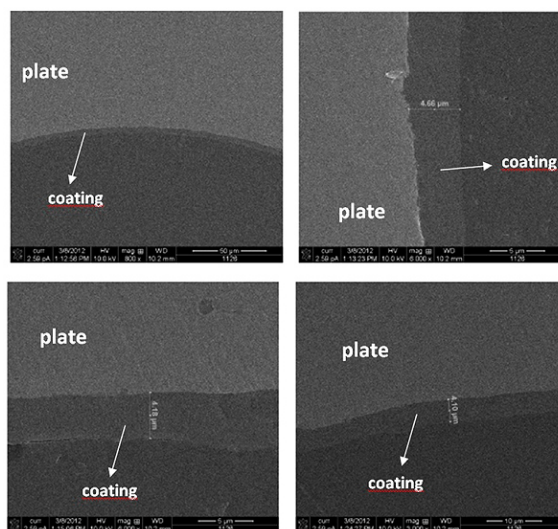


Figure 31 – SEM image of catalyst Mn(2)-3-A.

As can be seen, a thick alumina layer has been obtained near the channel walls, much more than in the center of the channel, because of its strong surface tension of the aqueous suspension.

Concerning the SMFSS supported catalysts, the BET measurements have been carried out with $(\text{Al}_2\text{O}_3+\text{MgO})$ in powder form, because the introduction of sufficient amount of SMFSS based catalyst into the apparatus is not feasible. A total surface area of $83 \text{ m}^2/\text{g}$ of $(\text{Al}_2\text{O}_3+\text{MgO})$ has been determined. Assuming a similar structure of the oxide mixture $(\text{Al}_2\text{O}_3+\text{MgO})$ on the SMFSS surface, a specific area of about $4 \text{ m}^2/(\text{g of SMFSS})$ can be estimated. In Figure 32, some SEM micrographs, before and after deposition of the oxide mixture $(\text{Al}_2\text{O}_3+\text{MgO})$ layer by incipient wetness impregnation method, are reported.

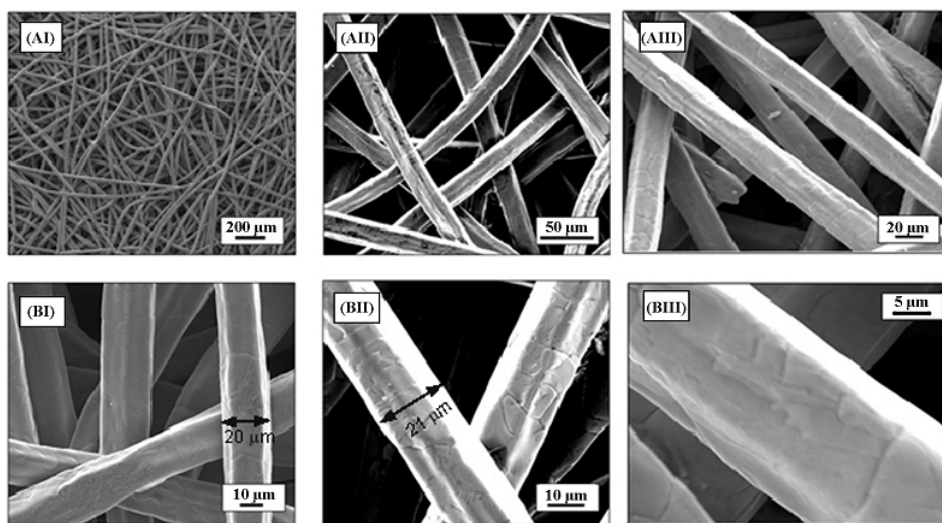


Figure 32 – SFMSS SEM images. A. medium; B. high resolution images, pre- (I) and post- (II) covered with homogeneous 5 wt.% $(\text{Al}_2\text{O}_3+\text{MgO})$ layer and (III) final 5 wt.% $\text{MnO}_x/5 \text{ wt.}\% (\text{Al}_2\text{O}_3+\text{MgO})/\text{SMFSS}$.

The metallic network shows a random distribution of fibers with relatively high porosity (see Figure 32 A(I)), while the fibers show a tetragonal-like structure with diameters of ca. $20 \mu\text{m}$ (see Figure 32 A(II)). Series II shows the formation of a thin homogeneous

oxide layer, of about 0.5 μm thickness, where the macroporosity of the network is kept, being the deposition homogeneous with a low oxide loading. Even by impregnating MnO_x catalyst, the structure is kept (see Figure 32 A(III)–B(III)). The coating preserves the SMFSS network. Moreover, the catalyst stability is ensured by the thin and uniform layer which strongly interacts with the SMFSS support and prevents any leaching.

Finally, the pore size distribution of SMFSS is reported in Figure 33. As can be seen, the catalyst showed a bi-modal micro- and meso-porous material with almost half of the pore volume consisting of pores in the range of 10–100 nm.

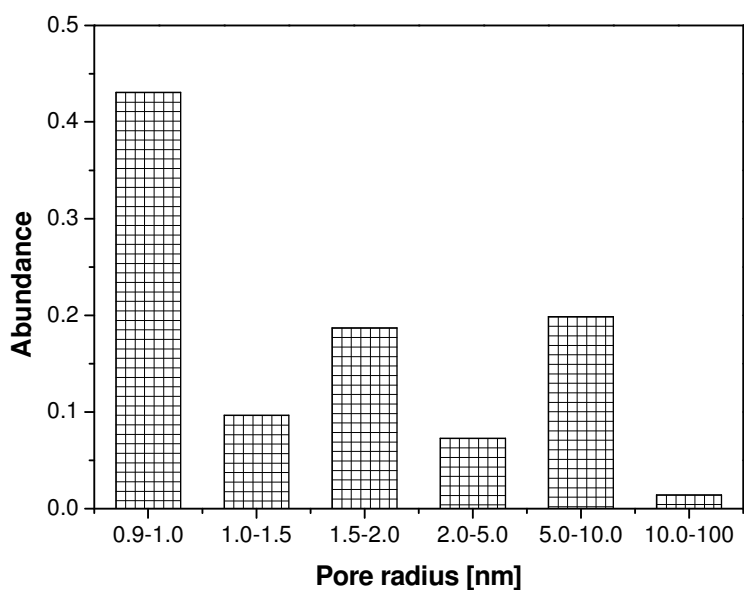


Figure 33 – Pore size distribution in $\text{Al}_2\text{O}_3+\text{MgO}/\text{SMFSS}$.

This morphology together with the thin coating layer, that is $<1 \mu\text{m}$, provides a good internal mass-transfer, avoiding eventual diffusion limitations and ensures an optimal availability of catalytic phase.

4.4 Catalytic screening and stability tests

An intensive catalytic screening investigation has been performed to find the most active heterogeneous catalysts for the hydrogen peroxide decomposition. These catalysts have been tested by in batch reactors by setting the temperature, catalyst concentration and initial hydrogen peroxide concentration values on the basis of preliminary tests where the activity of each catalyst has been investigated. In order to compare the activity of each catalyst, the experimental runs have been all interpreted by applying a first order kinetics referred to hydrogen peroxide concentration, Eq. 26.

$$r_c = k_c \cdot [H_2O_2] \quad (26)$$

The evolution with time of the hydrogen peroxide concentration have been solved using the mass balance reported in Eq. 27, using MatLab ode45 ODE solver algorithm.

$$\frac{dn_{H_2O_2}}{dt} = -r_c \cdot V_L \quad (27)$$

Of course, each runs has been performed at different catalyst amount. For this reason, the apparent kinetic constant has been divided by the mass of the catalyst and the active phase fraction, for an homogeneous comparison. Temperature could not be homogeneous because of the extremely different activity of the tested catalysts. In Figure 34, the results of the performed catalytic screening are shown, comparing both powdered and SMFSS supported catalysts.

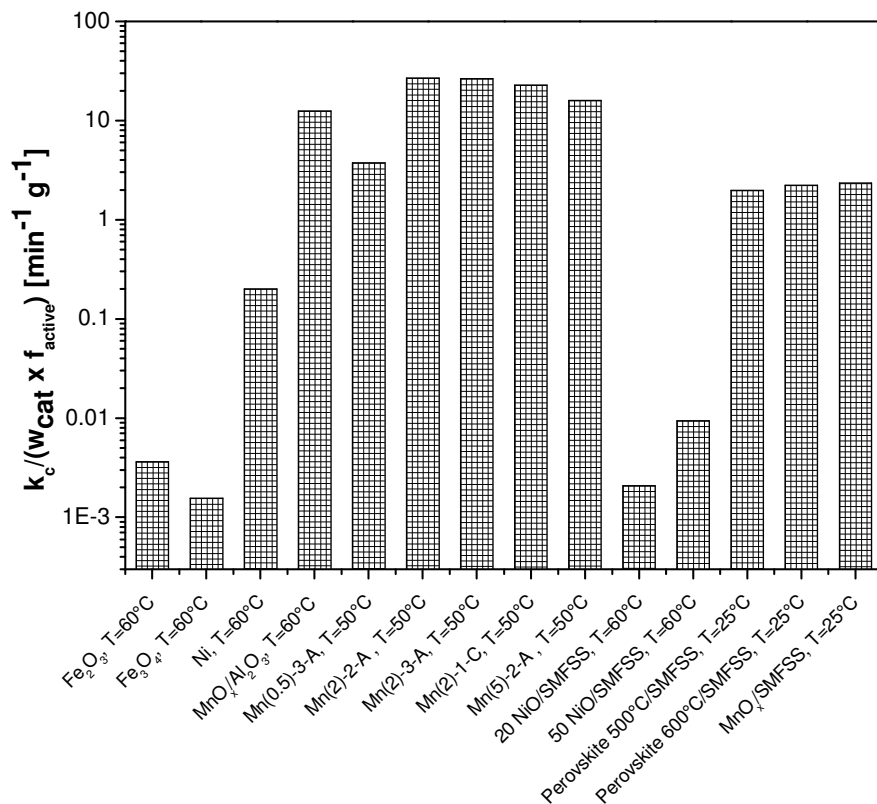


Figure 34 – Catalytic screening for hydrogen peroxide decomposition results. The apparent kinetic constant divided by the catalyst mass (w_{cat}) and the active phase fraction (f_{active}) for different heterogeneous catalysts. Ni: Engelhard Ni 3298 GE 3/64 in.×3F, 60.0 wt % Ni. $\text{MnO}_x/\text{Al}_2\text{O}_3$: MnO_x catalyst supported on $\gamma\text{-Al}_2\text{O}_3$, 5 wt.% Mn, prepared by dry impregnation of a solution of $\text{Mn}(\text{CH}_3\text{COO})_2 \cdot 4\text{H}_2\text{O}$ in water.

Preliminary investigations have been performed testing some commercial traditional catalysts, such as Fe_xO_y and Ni catalysts and comparing them with MnO_x and NiO supported catalysts. As a first conclusion, manganese oxide-based catalysts have shown the highest activity compared to iron, nickel and niobium based catalysts, so the investigation have been deepened in manganese oxides base catalysts. Moreover, all the Mn based catalysts have shown comparable activities, with the exception of the $\text{Mn}(0.5)\text{-}3\text{-A}$ catalyst, which exhibited a very poor activity.

By comparing the activities of the SMFSS supported catalysts, it has been observed that with a 2.5-fold increase of NiO loading on the SMFSS, the rate constant increased by a factor of 4.5. This behavior can be explained only by assuming that the lower amount of NiO corresponds to a coating of NiO strongly interacting with Al₂O₃ and less active in promoting the reaction with respect to the not interacting NiO which is more abundant in the 50 NiO sample. However, as the other catalysts showed better results, no further investigation has been done on the NiO-based SMFSS. Concerning the perovskite catalysts supported on SMFSS, no significant difference in activity has been noted by calcining them at different temperatures (500-600°C). Manganese oxide based structured catalyst showed activity comparable with perovskite.

By concluding, the powdered MnO_x/Al₂O₃ based catalyst have shown the highest activity. For this reason, the MnO_x/Al₂O₃ catalyst stability has been tested in long-time continuous runs performed in a tubular reactor, packing it with a Mn catalyst supported on γ-Al₂O₃ spheres by dry impregnation and calcined at 500°C. Two runs have been performed by changing the Mn content (2-5 wt.%). The obtained results are reported in Figure 35.

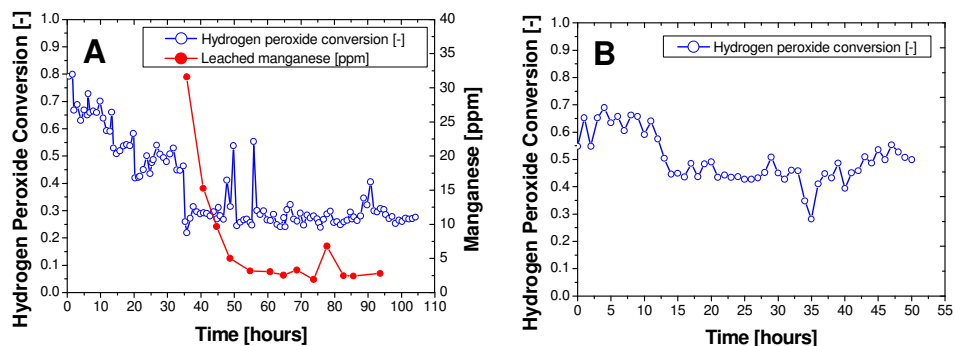


Figure 35 – Hydrogen peroxide decomposition trend as a function of reaction time for: A. 5 wt % Mn catalyst supported on γ-Al₂O₃ and calcined at 500°C; B. 2 wt % Mn catalyst supported on γ-Al₂O₃ and calcined at 500°C.

By loading the highest content of manganese, a decrease of the hydrogen peroxide conversion from about 80% to 30% occurred with increasing time on stream, becoming then constant. This phenomenon has been explained by analyzing the manganese content

in the collected samples, observing that active phase leaching occurs (see Figure 35 A). Therefore, it is possible to conclude that, after impregnation, manganese deposited on the alumina in two forms, one of which is strongly bonded to the surface and stable to leaching and another that is poorly interacting and prone to dissolve in the slightly acidic hydrogen peroxide solution. For the preparation of a more stable catalyst, it is important to load less manganese, eventually increasing the calcination temperature to favor the interaction of MnO_x with the surface support. At this purpose, two catalysts have prepared by first reducing the manganese content to 2 wt.% and then calcining them at two different temperatures, namely, 500 and 800 °C. In both cases, the catalysts gained better stability, with negligible leaching of manganese. The trend of the conversion as a function of time for the catalyst calcined at 500°C is presented in Figure 35 B. The scattering of the conversion data is not due to the leaching of manganese, which is negligible, but rather to both temperature scattering and changes in catalyst wetting in this complex gas–liquid flow system in which a copious gas volume is produced on the surface and inside the pores, preventing the liquid access to the active sites. The calcination at 800 °C resulted in a lower conversion (ca. 30%), probably because of the decrease of the specific surface area from 170 to 123 m^2/g , for the calcinations at 500 and 800 °C, respectively.

By considering that manganese supported catalyst can be considered stable at low manganese content, and by considering that they show a good activity, they are good candidates for hydrogen peroxide decomposition flow treatment. For this reason, the kinetics of the hydrogen peroxide decomposition using most active catalyst found in the screening tests, that is Mn(2)-3-A, has been studied.

4.5 Kinetic investigation and model validation

The kinetic investigation has been performed by varying both the catalyst concentration and the temperature to determine the reaction order with respect to the catalyst concentration and the kinetic parameters. The collected data have been interpreted with a first order kinetics respect to both hydrogen peroxide and catalyst concentrations, Eq. 28, while the temperature dependence has been explicated by using the modified Arrhenius equation reported, Eq. 29.

$$r_{Mn} = k_{Mn} \cdot [Mn(2) - 3 - A] \cdot [H_2O_2] \quad (28)$$

$$k_{Mn} = k_{Mn}^{ref} \cdot \exp\left[-\frac{E_a}{R} \cdot \left(\frac{1}{T} - \frac{1}{T_{ref}}\right)\right] \quad (29)$$

The evolution with time of the hydrogen peroxide concentration have been solved using the mass balance reported in Eq. 30, by using MatLab ode45 ODE solver.

$$\frac{dn_{H_2O_2}}{dt} = -r_{Mn} \cdot V_L \quad (30)$$

The effect of both temperature and catalyst concentration on the initial reaction rate can be observed in Figure 36. As can be seen, the reaction rate shows a relatively high dependence with temperature (see Figure 36 A) and it linearly depends on the catalyst concentration (see Figure 36 B).

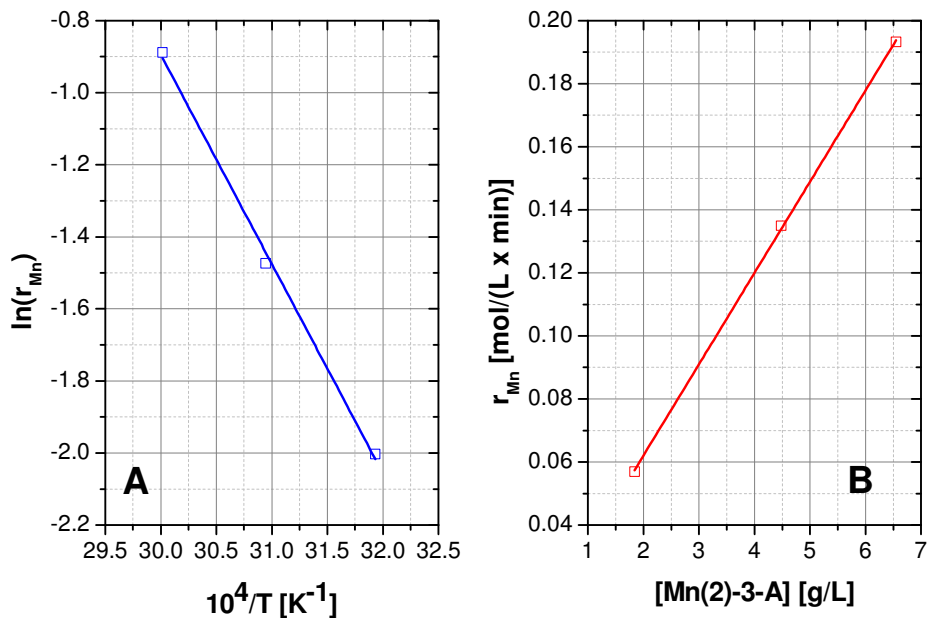


Figure 36 – Kinetic investigation of Mn(2)-3-A catalyst. A. Arrhenius plot. B. Initial reaction rate trend with the catalyst concentration. Symbols are experimental data, lines calculated values.

The kinetic parameters that best fitted the experimental data are listed in Table 8. The relatively low activation energy confirms the strong dependence of the reaction rate on the temperature.

Table 8 – Hydrogen peroxide decomposition catalyzed by Mn(2)-3-A kinetic parameters, evaluated at 313 K, together with the related statistical information. C.I.: confidence interval. σ : standard deviation.

		Value	90% C.I.	95% C.I.	99% C.I.	σ
k_{Mn}^{ref}	[L/(g _{cat} ·min)]	1.26E+01	1.79E-04	2.15E-04	2.85E-04	5.86E+04
$E_{a,Mn}$	[Kcal/mol]	1.04E-02	1.03E-07	1.23E-07	1.64E-07	8.46E+04

In order to validate the investigated kinetics, Mn(2)-3-A catalyst has been coated on the surface of a stainless steel single-plate microreactor. Different continuous runs have been performed under various conditions of pressure, volumetric flow rate, and temperature. By working at atmospheric pressure and 25°C and varying the flow rate, the hydrogen peroxide conversion decreased, as can be seen in Figure 37.

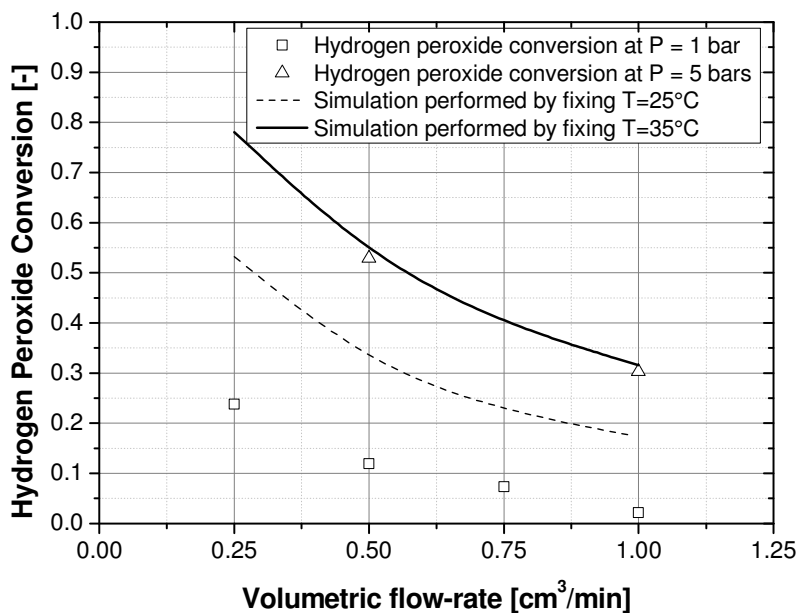


Figure 37 – Hydrogen peroxide decomposition runs performed in a continuous coated-disk-shaped single-plate microreactor at different pressures and flow rates. Symbols are experimental data; lines are simulated results.

The performed experiments have been simulated by fixing the kinetic rate law, Eq. 31, and the related parameters, applying the mass balance equation reported below, valid for a plug flow model. The reported mass balance has been solved by using MatLab ode45 ODE solver algorithm

$$\frac{d\dot{n}_{H_2O}}{dV} = -r_{Mn} \quad (31)$$

The plug flow approach is rough but useful for comparison purposes. In fact, by simulating the experimental runs performed at atmospheric pressure, the simulation predicts higher conversion values than the experimental ones. This fact can be considered reasonable because the oxygen developed as a consequence of the reaction gives rise to a consistent gas hold-up in the reactor, thereby strongly reducing the liquid residence time and consequently the H_2O_2 conversion. To solve this problem, some runs have been performed at moderately higher pressure (5 bar), thereby compressing the gas and increasing the liquid residence time and the related conversion.

As a consequence, a higher hydrogen peroxide decomposition has been observed, with an increase in the temperature in the reactor from 25 to about 38 °C, because of the high exothermicity of the reaction. The temperature has been measured by a thermocouple positioned at the reactor outlet. The experimental data collected at a pressure of 5 bar have been fitted by assuming an average temperature of 35°C inside the reactor, which is a reasonable value (see Figure 37). Clearly, in this way, the thermal profile has been neglected. On the other hand, the thermal profile is not easily measurable because of both the geometry of the reactor and the evaluation of the heat released from the device. However, the developed kinetic model with appropriately adjusted kinetic parameters can be used for the design of a continuous reactor for hydrogen peroxide decomposition.

Conclusions

The literature findings demonstrated that one of the most convenient synthetic strategies, in both environmental and economical point of view for producing propene oxide is the partial oxidation of propene with hydrogen peroxide, in the presence of titanium silicalite catalyst (TS-1). This process is known as HPPO (Hydrogen Peroxide Propene Oxide) and even if some industrial plants, based on this technology, are already running, no detailed information are published dealing with the kinetics of the overall reaction network, with some dark spots dealing with the by-products formation.

For the mentioned reasons, in this PhD work, a detailed study on the kinetics of the overall reaction network, deepening the investigation on both the main and side reactions, has been performed. In order to investigate the operative conditions to be adopted in the propene oxide synthesis tests, both the methyl formate synthesis and hydrogen peroxide decomposition catalyzed by TS-1 have been studied, finding that methyl formate is formed only in harsh conditions, but hydrogen peroxide decomposition is strongly influenced by both temperature and catalyst concentration. In order to both avoid hydrogen peroxide decomposition (explosive gaseous mixture with propene) and methyl formate production (difficulties in propene oxide purification), the propene oxide synthesis tests have so been performed at low temperature and catalyst concentration. The results have shown that the reaction occurs with an Eley-Rideal mechanism, where propene from the liquid bulk reacts with adsorbed hydrogen peroxide. Two kind of oxirane cleavage have been individuated: (i) Ti-OOH sites, acid enough to promote the propene oxide ring opening; (ii) defective sites. These two phenomena have been studied independently, finding that the first one is three times faster than the second.

For kinetic validation purpose, a lab-scale continue plant has been installed, where the reactor is a continuous stirred tank reactor (CSTR). The developed kinetic model is able to satisfactory describe all the collected experimental data. In this way, the developed

kinetic model could be useful to predict the operation of an HPPO industrial plant working with powdered TS-1.

The final part of the presented PhD thesis, deals with the hydrogen peroxide decomposition, that is needed to decompose the unreacted hydrogen peroxide streams before disposal. An intensive catalytic screening has been performed in order to find a good heterogeneous catalyst, supporting them either on powder or on sintered metal fibers. The kinetics of the best catalyst have been investigated, validating it in a disk-shaped microreactor obtaining a good agreement between experimental and calculated data.

List of symbols

a_L	Gas-liquid interfacial area [cm^2/cm^3]
a_S	Catalyst specific area [cm^2/cm^3]
a_{sp}^{BET}	Catalyst specific area evaluated with BET method, [m^2/g]
<i>C.I.</i>	Confidence interval
$E_{a,m}$	Activation energy of the reaction m , [Kcal/mol]
F	Dimensionless tracer concentration, [-]
f_{active}	Catalyst active phase, [-]
H_i	Henry constant of component i , [$\text{mol}/(\text{L}\cdot\text{bar})$]
$[I]$	Concentration of the i component, [mol/L]
$[I]^{IN}$	Inlet concentration, [mol/L]
$[I]^{OUT}$	Outlet concentration, [mol/L]
J_i	Mass transfer flux of component i , [mol/min]
K_{adsn}	Equilibrium constant ($n=1,5$), [L/mol]
k_L	Gas-liquid mass transfer coefficient [cm/min]
k_m	Kinetic constant of the reaction m . Units depend on the reaction.
k_m^{ref}	Kinetic constant of the reaction m at a reference temperature. Units depend on the reaction.
k_S	Liquid-solid mass transfer coefficient [cm/min]
k_v	Valve opening constant [$\text{mol}/(\text{min}\cdot\text{bar})$]
$[Mn(2)-3-A]$	Mn(2)-3-A concentration, [g/L]
$Mn(X)-Y-Z$	Manganese based catalyst with X wt.% Mn, Y support preparation, Z impregnation procedure
n_i^j	Moles of the component i in the phase j , [mol]
\dot{n}_i^j	Molar flow-rate of the component i in the phase j , [mol/min]
<i>Oligom</i>	Polymerization oligomer
P	Pressure, [bar]
P^{actual}	Reactor's pressure varying with time, [bar]
P_i	Partial pressure of component i , [bar]
P^{set}	Set pressure, [bar]

PO	Propene oxide
R	Ideal gas constant, [Kcal/(K·mol)]
r_m	Reaction rate of the reaction m , [mol/(L·min)]
r_m^0	Initial reaction rate of the reaction m , [mol/(L·min)]
RPM	Stirring rate, [rpm]
T	Temperature, [K]
t	Time, [min]
\bar{t}	Average residence time, [min]
T_R	Reactor's temperature, [°C]
T_{ref}	Reference temperature, [K]
Ti^α	α site on titanium
$[TS-1]$	TS-1 concentration, [g/L]
V	Volume, [L]
V_L	Liquid volume, [L]
w_{cat}	Catalyst mass, [g]
w	Weight, [g]
x	Weight loss, [wt.%]
$X_{H_2O_2}$	Hydrogen peroxide conversion, [-]

Greek letters

σ	Standard deviation
τ	Residence time, [min]
$\nu_{i,m}$	Stoichiometric coefficient for component i in reaction m , [-]
Φ_{PO}	Propene oxide selectivity, [-]

Publications

Chemical and Technical Aspects of Propene Oxide Production via Hydrogen Peroxide (HPPO Process)

V. Russo, R. Tesser, E. Santacesaria, and M. Di Serio*

Department of Chemical Sciences, University of Naples "Federico II", via Cintia 80126 Napoli, Italy

ABSTRACT: Propene oxide is a very important chemical whose production technology has changed a lot during the last 30 years. Nowadays, the most promising technology is the HPPO process in which the propene oxide is produced by oxidizing propene with hydrogen peroxide, via titanium silicalite-1 (TS-1) catalysis. Even if this technology has been patented in the early 1980s and some chemical plants are already in production, only few papers have been published until now dealing with the catalytic and kinetic aspects of the process. In this paper, the state of the art of the scientific knowledge and technical aspects related to propene oxide synthesis in the presence of TS-1 catalyst have been reviewed.

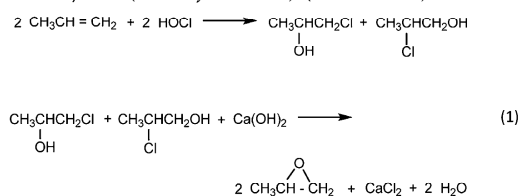
1. INTRODUCTION

Propene oxide (formula C_3H_6O) is a colorless, low boiling, highly volatile liquid with a sweet ether-like odor. It is flammable and reactive, so storage and unloading areas must be specifically designed and monitored. Propene oxide is a highly reactive chemical used as an intermediate for the production of several commercial materials. It reacts readily with compounds containing active hydrogen atoms, such as alcohols, amines, and acids. Therefore, propene oxide is used worldwide to produce versatile products as polyether polyols (polyglycol ethers), propene glycols, and propene glycol ethers.¹ In 2010, the PO worldwide production runs at about 7.5 Mtonns/y.²

Even though until now a lot of synthetic routes have been developed to produce PO,^{1,3} in this paper, only the most important processes that have found an application in the modern chemical industry will be reviewed.

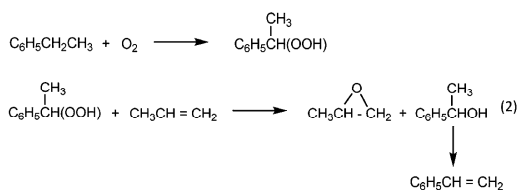
The direct oxidation of propene, in gas phase, with oxygen is still a holy grail. Several catalysts and several reaction conditions have been tested until now, but the results are very far from the industrial targets.^{4–7} Duma and Hönicke in 2000 have proposed the use of N_2O as oxidant for propene epoxidation to PO in gaseous phase, using silica supported iron oxide promoted with Na.⁸ However, this route suffers of low selectivity due to the formation of both carbonaceous deposits and other high molecular weight products.⁹

The most ancient industrial process developed to produce PO from propene is based on the dehydrochlorination of chlorohydrins (*Chlorohydrin Route*) (see scheme 1).

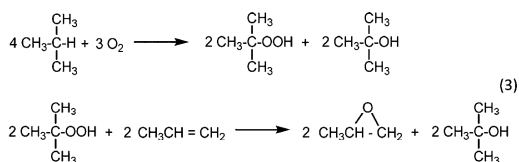


However, the coproducts of this process are brine of chlorine salts which lead to great problems in their disposal because it can also contain harmful byproducts.

Successively, some processes based on the use of oxygen as oxidant via the preformation of hydroperoxide have been developed. The hydroperoxide formed in a first stage is used to epoxidize propene via homogeneous organometallic catalysis (Mo based catalyst¹⁰) or heterogeneous catalysis (Ti support on silica^{11,12}); in this reaction an alcohol is formed as coproduct (*Coproduct Route*). Eventually in a third stage the obtained alcohols are dehydrated to olefinic products. The more diffuse processes are based on the use of hydroperoxide derived from ethylbenzene or isobutane. The process based on ethylbenzene is called styrene monomer propene oxide (SMPO) process, because, styrene is the related coproduct (see scheme 2).



The process based on isobutane is called the Ter-butyl Alcohol (TBA) process because its coproduct is the ter-butyl alcohol which can eventually be dehydrated to iso-butene (see scheme 3).



The coproduct route was more environmentally safe than the chlorohydrin one, but its economy depends strongly on the marketability of the obtained coproducts. To solve this

Received: September 4, 2012

Revised: December 11, 2012

Accepted: December 24, 2012

Published: December 24, 2012

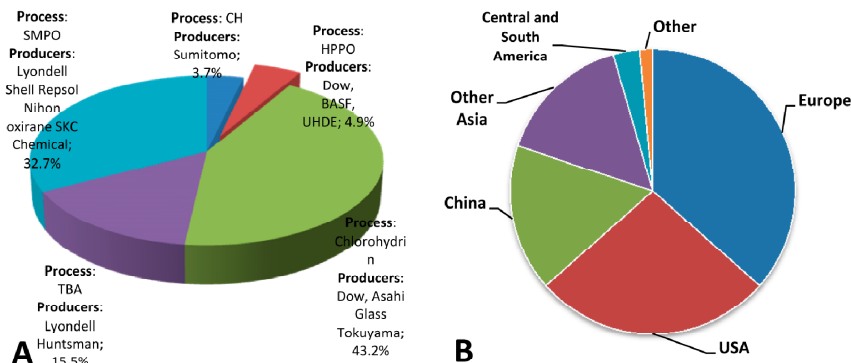
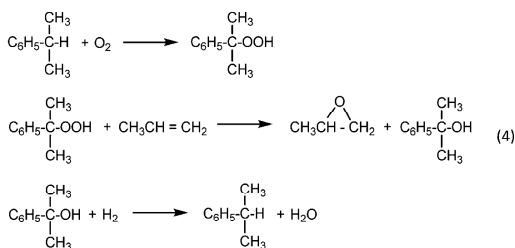
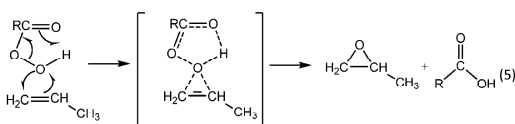


Figure 1. (A) PO suppliers distribution with related technologies (2009).³³ (B) Worldwide PO consumption (2012).³⁴

problem, in 2006 the Sumitomo Co. started a new process based on cumene hydroperoxide (CH process) in which the final alcohol is reduced to the starting cumene (see scheme 4). In this case, the catalyst was a silicon oxide catalyst with a mesoporous structure containing Ti in the framework.¹³

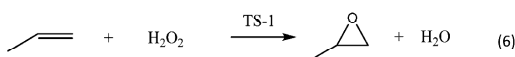


The use of peroxiacids was developed by Bayer and Degussa. Hydrogen peroxide was used to produce peracids via acid catalysis (peracetic or perpropionic).^{14–16} The peracid was used as an epoxidizing agent (Prilezhaev reaction) for producing PO, and the related acid that can be recycled (see scheme 5).



However this route did not achieve a real industrial success probably because of the intrinsic low selectivity of the process.

The direct use of hydrogen peroxide for epoxidizing propene is a much more interesting from both environmental and economic points of view, because the only coproduct is water (see scheme 6).



Several attempts have been made to find the right catalyst to epoxidize propene directly with hydrogen peroxide.^{17–22} The right catalyst was found by ENI at the end of the 1970s, that patented the use of titanium silicalite-1 (TS-1) for the *direct epoxidation of propene* with hydrogen peroxide (HPPO—hydrogen peroxide propene oxide).²¹ The TS-1 catalyst opened the possibility to the use of hydrogen peroxide as an oxidizing

reagent, allowing its use as an aqueous solution without catalyst deactivation.^{23–27} By using this catalyst, the reaction is carried out under mild conditions (around 40 °C), and theoretically, only water is generated as byproduct. In 2008, after about 25 years from the first ENI patent, Evonik (former Degussa), and SKC have launched the first commercial-scale propene oxide plant, based on the HPPO technology,²⁸ with a capacity of 100 kton/y. The next year BASF and DOW Chemical started with a new plant based on a similar technology, with a 300 kton/y capacity.^{2,29}

The absence of the unit operations, necessary for collecting and purifying the coproduct of the previous hydrogen peroxide processes, reduces the investment cost up to 25%. Moreover the HPPO process reduces the wastewater (70–80%) and the energy need (35%) with respect to the most traditional technologies.³⁰

The advantage of this new technology is proven by the fact that Evonik (formerly Degussa) and Uhde are going to set up another plant in China based on HPPO technology, with a capacity of 230 kton/y,³¹ while DOW is setting up a 390 kton/y of propene oxide plant in Thailand.³²

However, the previously described processes are still the more diffused ones; in Figure 1A, the worldwide distribution of the PO suppliers, referred to 2009, is reported,³³ while in Figure 1B, the worldwide consumption of propene oxide referred to 2012 is shown.³⁴

As can be seen, among the old technologies, the chlorohydrin route is still the most diffused one, but the HPPO process is the trend of the modern industry, considering the advantages expressed before.

Even if in the scientific literature there are a lot of studies on the synthesis and characterization of TS-1 catalyst,^{26,35,36} only few studies have been published on both the reaction mechanism^{1,26} and the kinetics of the propene epoxidation reaction.^{35,36} On the contrary, a large number of patents have been published on propene epoxidation claiming different process conditions, reactors, and additives, to improve the conversion and selectivity to propene oxide.

All the previous cited aspects (both chemical and technical) will be reviewed in this paper for presenting a complete state of the art of propene oxide production, via epoxidation with hydrogen peroxide, in the presence of titanium silicalite catalyst.

2. TS-1 CATALYST

Titanium silicalite is a crystalline zeolite material in which tetrahedral $[\text{TiO}_4]$ and $[\text{SiO}_4]$ units are arranged in a MFI structure.³⁷ The chemical nature of Ti species in TS-1 catalyst is made by $\text{Ti}(\text{OSi})_4$ tetrahedral sites (called “close” sites), that contain some defective “open” $\text{Ti}(\text{OSi})_3(\text{OH})$ sites, as EXAFS studies have demonstrated on well manufactured TS-1 samples.^{23–25,38} Owing to this structure, TS-1 shows a three-dimensional system of channels having molecular dimension of 5.1–5.6 Å and which constitutes the zeolitic micropores of the material.

The TEM micrograph exhibits well-ordered lattice fringes of the MFI structure of TS-1, which is indicative of high crystallinity. This confirms that the TS-1 catalyst has uniformly sized micropores of about 0.5 nm.^{39–42}

BET analysis has been applied to TS-1 catalyst to obtain the specific surface area, although the BET theory do not take into account micropore filling. In this case, a linear “BET” range is found at $0.005 < P/P^0 < 0.1$ that is lower than the usual used one $0.05 < P/P^0 < 0.3$. Starting from this approximation, the results of the BET analysis reported in the literature gave a surface area of 420–450 $\text{m}^2 \text{g}^{-1}$ and a pore volume of 0.18–0.26 $\text{cm}^3 \text{g}^{-1}$.^{23,35}

The synthesis of TS-1 catalyst, normally, starts with the hydrothermal crystallization of zeolite structure by using different silicon (for example: TEOS, fumed silica, colloidal silica, amorphous silica) and titanium sources (for example: TEOT, TBOT, TOPT, TiCl_3 , TiCl_4 , rutile), templating (for example: TPA^+ , $\text{TBP}^+/\text{TEP}^+$, $\text{TPA}^+/\text{TEA}^+$), and mineralizing agents (for example: OH^- , NH_3) (see the work of Perego and reference therein⁴³). Then, the obtained solid is dried (100 °C) and calcined at high temperatures (500–550 °C). The different synthesis routes produce crystal agglomerates in a mean size of 0.1–80 μm ⁴³ and also the structural properties can change (the Ti dispersion and its coordination number).⁴⁴

The use of a right synthesis route is fundamental to obtain an active and stable catalyst. As a matter of fact the TS-1 activity is correlated with the presence of isolated framework Ti(IV) sites²⁷ and to the crystal morphology of the zeolite,²⁷ while an increase in local disorder and/or coordination number of Ti (from IV to VI) is responsible for the lower stability under H_2O_2 treatment of the catalyst.⁴⁴

IR, XRD, and UV–vis are the characterization methods usually applied to confirm the presence of Ti(IV) in the framework.⁴³

The XRD pattern of TS-1 catalyst presents single peaks at 24.4° and 29.3° demonstrating a conversion from a monoclinic symmetry (silicalite) to an orthorhombic symmetry (titanium silicalite).^{23,45} The Ti sites, in the TS-1 catalyst, lead to a regular change in unit cell volume (UCV), with a correlation between UCV and Ti in the order of 3% (as TiO_2) of Ti loading, after which the correlation starts to be no longer valid, clearly indicating an upper limit for Ti (IV) insertion in the zeolite framework.⁴⁵

From the FT-IR spectrum of TS-1 catalyst it is possible to observe an absorption band at about 970 cm^{-1} that is not present in the spectrum of either pure silicalites or titanium oxides. In general, the intensity of this band increases with the amount of titanium that substitutes the silicon in the framework of silicalites.^{23,46} The UV–vis spectrum shows an absorption band near 215 nm indicating the presence of tetrahedral Ti

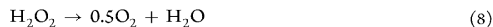
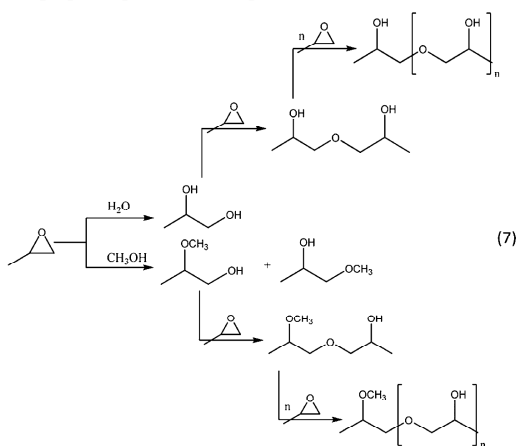
species in TS-1.^{23,47} The absence of other peaks demonstrates that there is no octahedral Ti or anatase TiO_2 .^{47–49}

TS-1 catalyst is normally used in both packed bed and continuous slurry reactors (see section 6). The industrial catalyst is constituted by zeolite dispersed in a binder phase. The pellets used in packed bed are generally obtained by extruding the binder paste containing the TS-1, while, the catalyst for the slurry reactors can be obtained by spray-drying technique.⁵⁰ The characteristics of the binder are important for the mechanical proprieties of the final catalyst, but also for saving the selectivity in the epoxidation reaction.⁵¹ As a matter of fact, for example, Li et al.⁵¹ have demonstrated that the use of alumina as binder, instead of silica, leads to a strong increase in byproducts formation, giving place to a PO selectivity of respectively 32.39 and 73.90% with the same hydrogen peroxide conversion, of about 95%.

3. REACTIONS OCCURRING IN THE HPPO PROCESS AND THE CATALYST DEACTIVATION

In general, propene epoxidation with hydrogen peroxide is performed at 40–60 °C, keeping propene at 20–25 bar and using methanol as solvent (see scheme 6). However in addition to propene oxide other products can be formed by secondary reactions that lower the yield.^{52–55}

A detailed scheme of all the possible occurring reactions after the propene epoxidation is reported in schemes 7–10.



The reactions of scheme 7 are all related to the ring-opening reactions. Two possible main reactions can occur between propene oxide and either water or methanol, giving propene glycol and methoxy propanol, respectively. These two products are the major byproducts reported in every paper or patent published in the literature; moreover, with the methanol concentration usually being greater than that of water, the probability to form methoxypropanol instead of glycol is very high²⁶ (for example, Papparatto et al.⁵⁶ for the output stream of a first reactor operating at 50 °C reported the following composition: 4.83 wt % propene oxide, 0.12 wt % methoxypropanol, 0.03 wt % 1,2-propene glycol). Of course,

propene oxide can also react with methoxypropanol or glycol giving dimers that can react further forming heavier adducts. The formation of these byproducts reducing the selectivity is also one of the causes of catalyst deactivation.^{26,35}

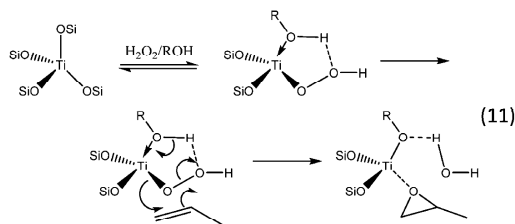
Hydrogen peroxide decomposition (reaction 8) must be taken into account mainly at high temperatures.⁵⁷

The formation of formic acid (reaction 9) and methylformate (reaction 10) has been reported (without quantitative data) by BASF⁵⁸ that underlined the propene oxide purification problems.

Several papers and patents have been published until now devoted to the catalyst deactivation and catalyst regeneration.^{36,59–69} Zuo et al.⁶⁹ have shown that in a tubular reactor the catalyst deactivation increases along the bed, being maximum at the reactor outlet where also the concentration of byproducts is maximum. The most commonly used techniques to regenerate the TS-1 catalyst are thermal treatment, at temperatures from 300 to 700 °C in the presence of different media, such as air, steam, and inert gas,^{60–65} oxidation by diluted hydrogen peroxide, at temperatures below than 100 °C,^{62,67,68} and extraction by different solvents, such as methanol, at different temperatures in the range of 140–240 °C.^{70–72} In particular, Wang et al.³⁶ have very recently performed a detailed study on the TS-1 deactivation and its regeneration. The authors have verified that the best performances, in terms of activity, in the TS-1 regeneration, are obtainable by calcinations and by treatment with hydrogen peroxide. From BET analysis, it has been verified that these two methods warrant an almost complete recovery of the surface area, while, the treatment with the solvent does not lead to a satisfactory recovering of the surface area. This fact has been justified by the presence of the propene oxide condensation products that are produced as byproducts in the PO synthesis, such as dimers of propene oxide and methoxypropanol. As a matter of fact, the molecules of these compounds, formed in the micropores of the zeolites, cannot diffuse outside from the channels, and part of them resides there. The regeneration with hydrogen peroxide has also been patented by Degussa, that performed batch runs in order to verify the possibility of regenerating the catalyst with a treatment of different solvents/reactants (methanol, water, a solution of H₂O₂ at 5 wt %) at reflux condition.⁷³ Degussa claimed the reflux treatment with hydrogen peroxide for 4 h as the best method, because, with this treatment, the catalyst recovers almost completely the activity of a fresh catalyst.⁷³

4. REACTION MECHANISM AND KINETICS

In both the scientific literature and the patent library only the mechanism of the main reaction of the HPPO process has been studied. Clerici et al.²¹ have shown that the key factor for this mechanism is the reversible splitting of one Ti–OSi bond by H₂O₂ with the resulting formation of a Ti–OOH species and the coadsorption of one alcohol or water molecule stabilizing the hydroperoxide through a five-membered ring (see scheme 11).^{27,74} Then, the epoxidation step occurs, where the peroxy oxygen vicinal to Ti is transferred to the double bond, with the contemporary formation of a Ti-alkoxide and a molecule of water. Finally, the desorption of the epoxide and the reaction of Ti–OR with H₂O₂, to form again the active species, complete the catalytic cycle (see scheme 11).²¹



Alternative mechanistic proposals are generally based on density functional theory (DFT) studies with sometimes the support of spectroscopic evidence. However, these data are normally obtained under conditions that are very different from the real ones present in industrial reactors.⁷⁵

It is important to point out that only two papers have been published until now concerning the HPPO kinetics,^{35,76} and these papers are both focused only on the main reaction.

Liang et al.⁷⁶ have tested several possible kinetic equations deriving from different hypothesized reaction mechanism to simulate their kinetic data. Even if the experimental runs have been performed in conditions far from the one used in the industrial reactors ($T = 30–50$ °C, $P = 0.1–0.6$ MPa, $H_2O_2 = 2$ wt %, solvent = isopropanol⁷⁶), the results seem to confirm the reaction mechanism proposed by Clerici et al. on the basis of spectroscopic studies.²¹ As a matter of fact, the kinetic analysis performed by Liang et al.⁷⁶ pointed out that the best kinetic equation for fitting the experimental data obeys an Eley–Rideal model (see eq 12).

$$r = \frac{kK_1[H_2O_2][C_3H_6]}{1 + K_1[I_2O_2] + K_2[C_3H_6] + K_3[PO]} \quad (12)$$

According to the mentioned authors, the reaction takes place between the adsorbed hydrogen peroxide on the titanium active sites and propene in the free state.

Recently, Shin et al.³⁵ have published a kinetic study using methanol as solvent ($T = 40$ °C, $P = 0.7–7$ bar, $H_2O_2 = 0.34$ wt %, solvent = methanol at 40–90 wt %³⁵). Also in this case, the conditions were far from the industrial reactors. The authors have tested different kinetic rate laws, on the collected experimental data, finding that the best mechanism, in terms of statistical analysis, is a dual-site Langmuir–Hinshelwood (see eq 13).

$$r = \frac{kK_1K_2[H_2O_2][C_3H_6]}{(1 + K_1[H_2O_2] + K_3[CH_3OH])(1 + K_2[C_3H_6] + K_4[CH_3OH])} \quad (13)$$

However, these kinetic expressions contains four adsorption parameters ($K_1–K_4$) and one kinetic constant (k), with a total of five adjustable parameters that have been regressed on a few number of experimental data, and the conclusions of the authors cannot be considered definitive. More experimental work is, therefore, necessary to individuate the correct kinetics in the presence of methanol as solvent and determine the related parameters.

5. REACTION CONDITIONS

5.1. Role of Temperature and Pressure. Shin et al.³⁵ have reported that an increase of the reaction temperature corresponds to an increase of the hydrogen peroxide conversion. In particular, passing from 30 to 50 °C, the

hydrogen peroxide conversion increases 1.3 times, working at 0.7 bar of propene, 0.35 wt % H_2O_2 , 50 wt % CH_3OH , and 0.28 g TS-1 in powder for 1 h of reaction time. In the meantime, the selectivity to propene oxide decreased from 99 to 96%. The same evidence has been described by Clerici et al.²⁶ This fact shows that temperature needs to be kept low in order to avoid the ring-opening reactions. At this purpose, being the epoxidation reaction extremely exothermic, Degussa reported in a patent⁷⁷ that by working with a jacketed packed bed tubular reactor, it was not possible to work under isothermal conditions, and they attributed the lowering of selectivity to this aspect.

The pressure is also a very important operative variable. In fact, as propene is gaseous at standard conditions, the operative pressure needs to be chosen carefully in order to decide to work either in a gas–liquid–solid state or in a liquid–liquid–solid state. Actually, at pressure lower than 16 bar and at 40 °C, propene is in a gas state. By working in gas–liquid–solid state and by increasing the propene pressure, the propene concentration in the liquid phase increases, consequently increasing the reaction rate.^{35,76} Recently, some patents published by Degussa^{78–80} have verified and claimed that the HPPO system, at pressures greater than 16 bar, is composed by two different liquid phases: (i) a phase rich in propene containing also propene oxide and (ii) a methanol rich phase containing water, hydrogen peroxide, and some amount of propene oxide. They have experimentally observed that by working at 40–60 °C, at a pressure of 25 bar, with a 300 cm^3 tubular reactor (4 m length and 1 cm diameter) and using methanol as solvent, it is possible to obtain a 96% H_2O_2 conversion with a 96–97% of propene oxide selectivity. By observing the samples in a sight glass window, two immiscible liquid phases have been observed.

5.2. Role of the Solvent. The propene epoxidation reaction rate strictly depends on the reaction medium in which the reaction is carried out. As a matter of fact, several papers have pointed out that methanol is the best solvent.^{76,81–84} In general, the epoxidation rate decreases in alcohol solvents in the order, methanol > ethanol > *i*-propanol > *t*-butanol, with the two extremes differing by more than 1 order of magnitude.^{26,27,84,85} Moreover, by using methanol also the selectivity to propene oxide is strongly increased. A comparison of several tested solvents for the propene oxidation to PO, in terms of both hydrogen peroxide conversion and PO selectivity is reported in Figure 2.⁸³ It is evident from the figure that methanol is the best solvent for the HPPO process.

Figure 2 shows also that the activity to propene oxide is not increased by using an aprotic solvent like acetone (MeCOMe).⁸³ In this case, selectivity stays high because acetone is not a nucleophilic molecule which can react with a PO ring.

It has been further verified that water dissolved in methanol solvent has a moderately negative effect on the reaction, because of both competing in the adsorption on the TS-1 sites and lowering the concentration of propene in solution; propene being much more soluble in methanol (2.6×10^{-1} mol/(L·atm), at 40 °C) than in water (8.3×10^{-3} mol/(L·atm), at 40 °C).^{85,86} This fact can also be appreciated from Figure 2, comparing the results obtained by two experimental runs performed in the same operating conditions but by using pure methanol or water as solvent (92% and 40% H_2O_2 conversion, respectively).

5.3. Role of Additives. ARCO and Degussa companies have investigated in several patents the role of the additives on

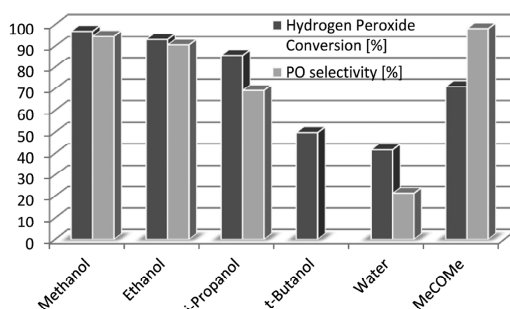


Figure 2. Influence of the reaction media on the epoxidation of propene, at 60 °C, 0.4 MPa, 0.4 wt % TS-1, 32 cm^3 solvent, 2 cm^3 30 wt % H_2O_2 , time 1.5 h.⁸³

both hydrogen peroxide conversion and propene oxide selectivity. In particular, the ARCO company has performed a deep investigation on the role of both basic (B) and nonbasic (NB) salts by performing experimental runs with different salts in the same experimental conditions.⁸⁷ In particular, it has been found that the nonbasic salts lead to a higher hydrogen peroxide conversion and propene oxide selectivity. Then, in a much more recent patent,⁸⁸ the role of ammine on the TS-1 activity and selectivity has been investigated finding that in general the addition of an amine leads to a higher propene oxide selectivity but to a higher decrease in the hydrogen peroxide conversion degree.

In general, the behavior of both the salts and the additives containing nitrogen on TS-1 activity has been also observed by Degussa.^{73,89–91} In particular, they have demonstrated that by treating TS-1 catalyst with salts, such as Na_2SO_4 , $(\text{NH}_4)_2\text{SO}_4$, NH_4NO_3 , and NaH_2PO_4 , the catalyst shows a lowering in activity but an increase in propene oxide selectivity.⁷³ Then, Degussa has demonstrated that by working at pH > 7, by using NaOH, it is possible to increase the propene oxide selectivity against a lowering in hydrogen peroxide conversion.⁸⁹ In further patents,^{90,91} Degussa has claimed that by using ammonia salts, it is possible to obtain the same results.

The same kind of behavior has also been observed both by Polimeri Europa^{56,92} and then by Dow.⁹³ In particular Dow found that by adding zinc carbonate to the solution, it is possible to keep the same hydrogen peroxide conversion but the selectivity to PO is increased from 93 to 98%.

In conclusion, it has been demonstrated that basic additives poison the acid sites of TS-1 catalyst leading to a reduction of the catalyst activity, but also to a slower ring-opening reaction rate, that means to increase propene oxide selectivity.

6. REACTORS

A detailed analysis on the existing patent literature showed that there is a large variety of reactor setups that have been used until now for the HPPO process. In particular, in Table 1, a list of all the patented type of reactors and related reaction conditions is reported.

Stirred batch reactors^{39,73,88,92,94–98} have normally been employed to test both the activity and the selectivity of TS-1 catalyst in powder, evaluating the effect of the presence of several salts and basic substances.

For what concerns the continuously stirred tank reactor (CSTR) use, Degussa⁶⁷ found that the best operating

Table 1. Reaction Conditions and Reactor Types Patented until 2012

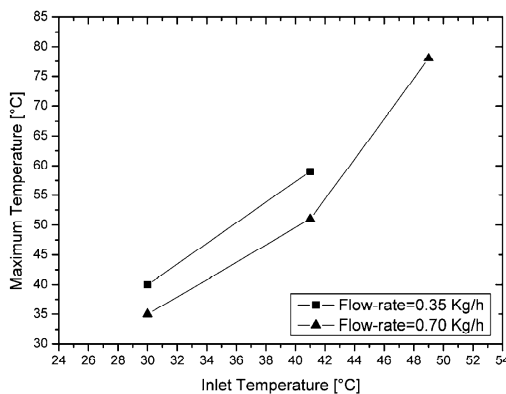
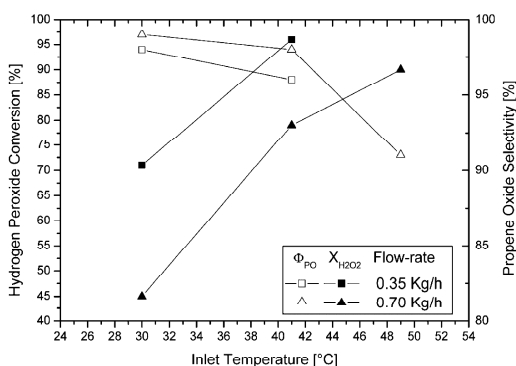
reactor	T (°C)	P (bar)	ref
batch reactor	0–40	1–20	39, 73, 88, 92, 94–98
continuously stirred tank reactor (CSTR)	50–65	13	56, 67, 99
packed bed reactor (PBR)	40–50	15–20	67, 77, 100–103
trickle bed reactor (down-flow)	40	25	89, 104
bubble siphon reactor	35–56	1	98, 105, 106
recycle reactor	55	>15	107
heat exchangers reactor	30–60	25	79, 103, 108, 109

conditions have been reached by working at a medium pH of 8.12, reaching an hydrogen peroxide conversion of 50% and a propene oxide selectivity of 92.1% ($T = 65\text{ }^{\circ}\text{C}$, $P = 6\text{ bar}$, $\text{TS-1} = 0.12\text{ g/cm}^3$, $\text{H}_2\text{O}_2/\text{methanol} = 0.17\text{ w/w}$, $\text{LHSV (liquid hourly space velocity)} \approx 1.5\text{ h}^{-1}$). Polimeri Europa^{36,99} reported that by using a CSTR reactor working at $50\text{ }^{\circ}\text{C}$, 1.2 bar, with a hydrogen peroxide solution pH of 6.5 and a TS-1 concentration of 6 wt %, it is possible to obtain a hydrogen peroxide conversion of 96% and a propene oxide selectivity of 97% (no information are given about the residence time).

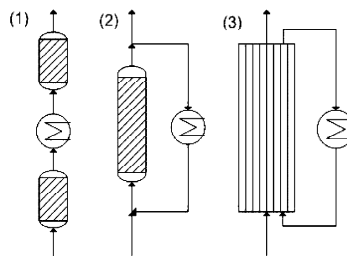
Some reactors operated as PBR, using TS-1 is in the form of pellets, by working at $40\text{--}60\text{ }^{\circ}\text{C}$, feeding propene as liquid (pressures of 20–25 bar), with an inlet hydrogen peroxide concentration in a range of 3–8 wt %. Obviously, for this type of reactor, the liquid–solid transport phenomena both inside and outside of the catalytic particle must be considered, because, they strongly affect the catalyst efficiency.⁹² For what concerns the spatial velocities, some patents have worked with LHSV values ranging from 3 to $5\text{ cm}^3\text{ g}_{\text{cat}}^{-1}\text{ h}^{-1}$.^{100–102} By considering, instead, the LHSV values, BASF has worked with two different reactors. In the first patent, 20 g of catalyst in pellets were loaded in a 50 cm^3 reactor ($\text{LHSV} \approx 0.8\text{ h}^{-1}$),¹⁰⁰ while, in the second patent 20 g of catalyst were loaded in two reactors each of 190 cm^3 ($\text{LHSV} \approx 3.7\text{ h}^{-1}$).¹⁰¹ Being the TS-1 extruded density of about 0.48 g/cm^3 , in the second case the catalytic bed has been diluted with an inert material (no information are given about this aspect). This fact is crucial, because, by diluting the catalytic bed with an inert material, it is possible to reach a better thermal control of the reactor, during the epoxidation reaction, and to work with higher spatial velocities, that means much more turbulent regimes with a lowering in the liquid–solid mass transfer limitations. At this purpose, Degussa⁷⁷ has claimed the use of a jacketed packed bed tubular reactor of 1 cm of diameter and 4 m length for the propene oxide synthesis. By packing completely the tubular reactor with extruded TS-1 catalyst, hot-spots have been observed due to the exothermicity of the epoxidation reaction. In Figure 3, the maximum temperature reached inside the catalytic bed is plotted against the inlet temperature, at different flow-rates, while in Figure 4, both the hydrogen peroxide conversion ($X_{\text{H}_2\text{O}_2}$) and propene oxide selectivity (Φ_{PO}) are plotted against the inlet temperature, varying the flowrates.

As it can be seen, by increasing the inlet temperature, the maximum temperature reached in the catalytic bed increases too, both at 0.35 and 0.7 kg/h. Moreover, even if at higher temperatures the hydrogen peroxide conversion is higher, Degussa has observed a decrease in the propene oxide selectivity, due to the higher ring opening reaction rate.

The problem of temperature control is common also to other epoxidation processes.¹⁰⁸ In order to keep the reaction

**Figure 3.** Maximum temperature reached inside the catalytic bed is plotted against the inlet temperature.⁷⁷**Figure 4.** Hydrogen peroxide conversion ($X_{\text{H}_2\text{O}_2}$) and propene oxide selectivity (Φ_{PO}) against the inlet temperature, at different flowrates.⁷⁷

temperature at a desired safety level, solving the heat transfer problem, BASF and DOW described the use of reactors with high thermal exchange efficiency for olefin epoxidation (see Figure 5).¹⁰³ DOW and BASF proposed different solutions, ranging from PBR in series with an external heat exchanger (Figure 5-1), recycle PBR reactors with external heat exchanger (Figure 5-2), and heat exchanger plate reactors filled with TS-1 (Figure 5-3). In all cases, hydrogen peroxide conversion of 95–

**Figure 5.** Efficient heat exchange reactors: (1) PBR in series with external heat exchange, (2) recycle PBR reactors with external heat exchange, (3) heat exchanger plate reactors.

97% can be reached, with a propene oxide selectivity in the range of 90–95%.

Degussa and Uhde have, then, patented the use of heat exchanger reactors,⁷⁹ working in a trickle bed state, to produce propene oxide, by either packing or coating the catalyst on the heat exchanger walls. Even if the pressure drops for this type of reactor are higher, it is possible to obtain a very good thermal control. Degussa has claimed that the use of a trickle bed reactor with down-flow feeding produces the formation of two liquid phases: one rich in propene, the other in methanol, water, and hydrogen peroxide. In this case, propene oxide is partitioned between the two liquid phases, and the amount that is dissolved in the apolar phase cannot degrade. This fact leads to an increase of the overall propene oxide selectivity.¹⁰⁴

BASF and DOW have recently demonstrated that by working with two reactors in series, separating the produced propene oxide in between, it is possible to increase the selectivity from 80.3% to 96%, with hydrogen peroxide conversion greater than 95%. As a matter of fact, by separating propene oxide, the ring-opening reactions rate are prevented and the selectivity increases.² Then, Solvay has patented the use of a bubble siphon reactor.^{98,105,106} In this case, the reactor works with a propene gaseous feeding at 1 bar. Working with this reactor, propene oxide is stripped away with the unreacted propene, while the alcoholic solution is partially recycled. The catalyst regeneration, is performed in flux with air at 300 °C for about 7 h. This system has recently been improved¹⁰⁷ using a reactor, that works under pressure, with recycle, taking a contact time with the catalyst of 5.5 min and an overall residence time of 4 h. Also in this case, good results have been obtained in terms of both hydrogen peroxide conversion and propene oxide selectivity.

7. PRODUCTION OF HYDROGEN PEROXIDE

One of the main problems related to the technologies using hydrogen peroxide is the reduction of the cost of this reagent and, in general, the economy of the HPPO process is justified only if the HPPO reactor is coupled with a hydrogen peroxide synthesis plant. Nowadays, the developed commercial HPPO plants produce hydrogen peroxide by the oxidation and reduction of anthraquinones.^{110–112}

The BASF–DOW plant in Antwerp is fed with hydrogen peroxide produced with Solvay's high-productivity hydrogen peroxide technology.¹¹³ Solvay's technology is based on ethylanthraquinones reduction/oxidation cycle.

Polimeri Europa has patented an integrated plant where hydrogen peroxide is produced in situ via anthraquinones reduction/oxidation cycle in methanol.⁹⁵ This process has the advantage to eliminate the necessity of hydrogen peroxide extraction with water from the anthraquinones working solution and the successive concentration by distillation. However the reported yield of propene oxide was lower than that reported for ex-situ HPPO processes.¹¹⁴

A very interesting approach from the conceptual point of view is the use of a bifunctional catalyst to produce hydrogen peroxide from direct reaction of oxygen and hydrogen and in the meantime catalyze the epoxidation reaction of propene (see for example^{115–117}). The catalyst are in general TS-1 supporting metals (Pt, Pd, Os, Ru, Ir;¹¹⁵ Au,¹¹⁶ Pd, Re¹¹⁷). However, this approach suffers from low selectivity, because of the hydrogenation of propene to propane.¹¹⁷

Polimeri Europa proposed an integrated plant in which hydrogen peroxide is produced from hydrogen and oxygen in

the presence of a their developed catalyst. The claimed plant is composed by three sections:^{56,92,118} a first section for the hydrogen peroxide formation, from the reaction between hydrogen and oxygen catalyzed by a Pd/Pt catalyst,^{56,92,118} operating directly in methanol, reaching a composition of about 6 wt % hydrogen peroxide, 89.7 wt % methanol, and the resulting parts in water; a second section where hydrogen peroxide reacts with propene in a CSTR in the presence of TS-1; and a third purification section where it is possible to reach 99.99 wt % in propene oxide.

8. HPPO INDUSTRIAL PLANTS

BASF and DOW patented a process^{102,119} in which propene oxide is formed in a high efficient heat exchanger reactor, with a hydrogen peroxide conversion of 99.8% and a propene oxide selectivity of 93.2%. This type of plant has been in production since 2008 in Antwerp with a plant capacity of 300 kton/y of propene oxide.² A scheme of the plant is reported in Figure 6.

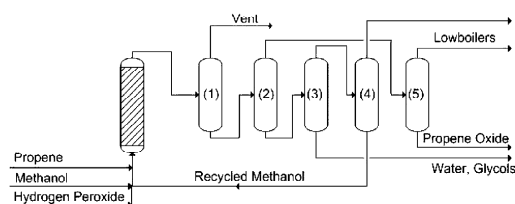


Figure 6. DOW and BASF HPPO plant scheme (after the work of Bassler et al.²).

The reactor is a tubular reactor working at about complete conversion. The purification section is composed by five distillation columns in series, useful to remove first the off-gas (1), then to purify propene oxide (2 and then 5), separate water and glycols (3), and recycle methanol (4). In order to obtain a better separation of propene oxide, BASF and DOW have patented an extractive distillation column that uses either water or glycol as solvent.¹²⁰

Evonik (formerly Degussa) and Uhde have built in 2008 in Ulsan, Korea, an HPPO plant based on TS-1 catalyst of 100 kton/y of propene oxide¹²¹ (see the scheme in Figure 7). The reaction is carried out in one of the patented very efficient heat removal reactors.⁷⁹ As the reaction mixture leaves the reactor, it is sent to a flash unit (1) that separates propene from the liquid phase. Propene is purified and recycled to the reactor (2), while the liquid phase is treated in a battery of three distillation columns (3–5). The first (3) is a pre-separation column that separates propene oxide from water/methanol; the second (4) is a stripping column where propene is recycled to the flash unit (2). Finally, propene oxide is purified in the last column and is obtained at 99.9% purity. Water and methanol are collected in a final distillation column (6), and methanol is recycled to the oxidation reactor.

9. CONCLUSION

Propene oxide is an important product for the chemical industries because of its wide range of applications. A new production technology (HPPO) has been developed in several years of research activity but only recently have new plants been built on the basis of this very competitive technology, with respect to the older ones. In the HPPO technology, propene

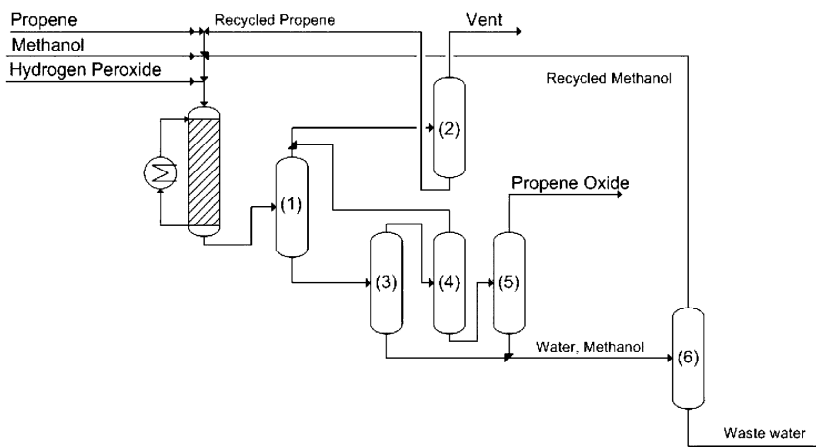


Figure 7. Evonik and Uhde HPPO plant scheme.¹²²

oxide is produced starting from propene and hydrogen peroxide in the presence of TS-1 as catalyst. The process is environmental friendly, because, only water is formed as a byproduct of the main reaction. In the patented processes, hydrogen peroxide conversion, that is the limiting reagent, is reported between 95 and 98% with a selectivity to PO of 90–98%. The problems related to this technology are the following: the high exothermicity of the reaction, the catalyst mass transfer limitation, the factors affecting the selectivity, the catalyst deactivation and regeneration, and the need of a dedicated hydrogen peroxide production plant. All these aspects have been considered and widely discussed on the basis of the published literature, and we have seen that they bring to different choices of operative conditions and plant design.

At last, the kinetic interpretation of the whole reaction network of the HPPO process has not been sufficiently investigated yet and more investigation, therefore, are necessary for getting a fruitful optimization of the HPPO process.

AUTHOR INFORMATION

Corresponding Author

*E-mail: diserio@unina.it

Notes

The authors declare no competing financial interest.

ACKNOWLEDGMENTS

This study was funded by CONSER S.p.A.

REFERENCES

- (1) Nijhuis, T. A.; Makkee, M.; Moulijn, J. A.; Weckhuysen, B. M. The Production of Propene Oxide: Catalytic Processes and Recent Developments. *Ind. Eng. Chem. Res.* **2006**, *45* (10), 3447–3459.
- (2) Bassler, P.; Weidenbach, M.; Goebbel, H. The new HPPO Process for Propylene Oxide: From Joint Development to worldscale Production. *Chem. Eng. Trans.* **2010**, *21*, 571–576.
- (3) Ishino, M. Development of New Propylene Oxide Process. *16th Saudi Arabia-Japan Joint Symposium*; Dhahran, Saudi Arabia, November 5–6, 2006.
- (4) Lee, W. S.; Akatay, M. C.; Stach, E. A.; Ribeiro, F. H.; Delgass, W. N. Reproducible preparation of Au/TS-1 with high reaction rate for gas phase epoxidation of propylene. *J. Catal.* **2012**, *287*, 178–189.
- (5) Ren, Y.; Xu, L.; Zhang, L.; Wang, J.; Liu, Y.; He, M.; Wu, P. Selective epoxidation of propylene to propylene oxide with H₂ and O₂ over Au/Ti-MWW catalysts. *Pure Appl. Chem.* **2012**, *84* (3), 561–578.
- (6) Zheng, X.; Zhang, Q.; Guo, Y.; Zhan, W.; Guo, Y.; Wang, Y.; Lu, G. Epoxidation of propylene by molecular oxygen over supported Ag–Cu bimetallic catalysts with low Ag loading. *J. Mol. Catal. A: Chem.* **2012**, *357*, 106–111.
- (7) Pulido, A.; Concepción, P.; Boronat, M.; Corma, A. Aerobic epoxidation of propene over silver (111) and (100) facet catalysts. *J. Catal.* **2012**, *292*, 138–147.
- (8) Duma, V.; Hönicke, D. Gas Phase Epoxidation of Propene by Nitrous Oxide over Silica-Supported Iron Oxide Catalysts. *J. Catal.* **2000**, *191*, 93–104.
- (9) Thömmes, T.; Gräf, I.; Reitzmann, A.; Kraushaar-Czarnetzki, B. Catalytic Vapor Phase Epoxidation of Propene with Nitrous Oxide as an Oxidant: Investigations on Catalyst Composition and Reaction Conditions. *Ind. Eng. Chem. Res.* **2010**, *49*, 2624–2637.
- (10) Lines, E. L.; Fairbrother, R. J.; Herbst, J. A. *Catalytic epoxidation of alkylene compounds*. US 4157346, Olin Corporation; 1979.
- (11) Rameswaran, M.; Cochran, R. N. *Epoxidation process*. US 5081267, Arco Chemical Technology, L.P.; 1992.
- (12) Zajacek, J. G.; Pa, D.; Crocco, G. L. Integrated process for epoxide production. US 5214168, Arco Chemical Technology, L.P.; 1993.
- (13) http://www.sumitomo-chem.co.jp/english/rd/report/theses/docs/20060100_ely.pdf (accessed Jan 2013).
- (14) Prescher, G.; Schreyer, G.; Weiberg, O.; Wirthwein, R.; Waldmann, H.; Seifert, H.; Schwerdtel, W.; Swodenk, W. *Process for the preparation of propylene oxide*. US 4137242, Bayer Aktiengesellschaft, Deutsche Gold- und Silber-Scheideanstalt Vormals Roessler; 1979.
- (15) Prescher, G.; Schreyer, G.; Weiberg, O.; Wirthwein, R.; Waldmann, H.; Seifert, H.; Schwerdtel, W.; Swodenk, W. *Process for the preparation of propylene oxide*. US 4113747, Bayer Aktiengesellschaft, Deutsche Gold- und Silber-Scheideanstalt Vormals Roessler; 1978.
- (16) Weissermel, K.; Arpe, H.-J. *Industrielle Organische Chemie*; Wiley: New York, 1994; p 295.
- (17) Saxton, R. J.; Zajacek, J. G.; Crocco, G. L. Epoxidation process and catalyst therefore. US 5374747, Arco Chemical Technology, L.P.; 1994.
- (18) Saxton, R. J.; Zajacek, J. G.; Crocco, G. L. Epoxidation process. US 5412122, Arco Chemical Technology, L.P.; 1995.
- (19) Saxton, R. J.; Zajacek, J. G.; Crocco, G. L. Epoxidation process. US 5684170, Arco Chemical Technology, L.P.; 1997.

- (20) Buchler, J.; Schmidt, M.; Prescher, G. Method for the catalytic epoxidation of olefins with hydrogen peroxide. US 4973718, Degussa Aktiengesellschaft; 1990.
- (21) Clerici, M. G. TS-1 and Propylene Oxide, 20 Years Later. *Erdöl, Erdgas, Kohle* **2006**, *122* (6), OG77–OG82.
- (22) Weissmermel, K.; Arpe, H. J. *Industrial Organic Chemistry*, third completely revised ed.; Wiley: New York, 1997; p 273.
- (23) Taramasso, M.; Perego, G.; Notari, B. Preparation of porous crystalline synthetic material comprised of silicon and titanium oxides. US 4410501, Snamprogetti S.p.A.; 1983.
- (24) Neri, C.; Anfossi, B.; Esposito, A.; Buonomo, F. Process for the epoxidation of olefinic compounds. IT 22608, ANIC S.p.A.; 1982.
- (25) Neri, C.; Anfossi, B.; Esposito, A.; Buonomo, F. Process for the epoxidation of olefinic compounds. EP 100119, ANIC S.p.A.; 1986.
- (26) Clerici, M. G.; Bellussi, G.; Romano, U. Synthesis of Propylene Oxide from Propylene and Hydrogen Peroxide Catalyzed by Titanium Silicalite. *J. Catal.* **1991**, *129*, 159–167.
- (27) Clerici, M. G.; Ingallina, P. Epoxidation of lower olefins with Hydrogen-Peroxide and Titanium Silicalite. *J. Catal.* **1993**, *140*, 71–83.
- (28) <http://corporate.evonik.com/en/media/archive/pages/news-details.aspx?newsid=15734> (accessed Jan 2013).
- (29) Short, P. L. BASF, Dow Open Novel Propylene Oxide Plant. *Chem. Eng. News* **2009**, *87* (11), 21.
- (30) EPA, The Presidential Green Chemistry Challenge Awards Program: Summary of 2010 Award Entries and Recipients. <http://www.epa.gov/greenchemistry> (accessed Jan 2013).
- (31) <http://corporate.evonik.com/en/media/search/Pages/news-details.aspx?newsid=26719> (accessed Jan 2013).
- (32) <http://www.dow.com/polyurethane/news/2012/20120104a.htm> (accessed Jan 2013).
- (33) *Nexant Chemsystems PERP Program; Propylene Oxide, Process Technology*; 2009; PFRP07/08-6.
- (34) <http://www.ihs.com/products/chemical/planning/ceh/propylene-oxide.aspx> (accessed Jan 2013).
- (35) Shin, S. B.; Chadwick, D. Kinetics of Heterogeneous Catalytic Epoxidation of Propene with Hydrogen Peroxide over Titanium Silicalite (TS-1). *Ind. Eng. Chem. Res.* **2010**, *49*, 8125–8134.
- (36) Wang, Q.; Wang, L.; Chen, J.; Wu, Y.; Mi, Z. Deactivation and regeneration of titanium silicalite catalyst for epoxidation of propylene. *J. Mol. Catal. A: Chem.* **2007**, *273*, 73–80.
- (37) To, J.; Sherwood, P.; Sokol, A. A.; Bush, I. J.; Richard, C.; Catlow, A.; van Dam, H. J. J.; French, S. A.; Guest, M. F. QM/MM modelling of the TS-1 catalyst using HPCx. *J. Mater. Chem.* **2006**, *16*, 1919–1926.
- (38) Bordiga, S.; Coluccia, S.; Lamberti, C.; Marchese, L.; Zecchina, A.; Boschérini, F.; Buffa, F.; Genoni, F.; Leofanti, G.; Petrini, G.; Vlaic, G. XAFS Study of Ti-Silicalite: Structure of Framework Ti(IV) in the Presence and Absence of Reactive Molecules (H₂O, NH₃) and Comparison with Ultraviolet-Visible and IR Results. *Phys. Chem.* **1994**, *98* (15), 4125–4132.
- (39) Neri, C.; Anfossi, B.; Esposito, A.; Buonomo, F. Process for the epoxidation of olefinic compounds. US 4833260, ANIC S.p.A.; 1989.
- (40) Van der Pol, A. J. H. P.; Van Hooff, J. H. C. Parameters Affecting the Synthesis of Titanium Silicalite-1. *Appl. Catal. A: Gen.* **1992**, *92* (2), 93–111.
- (41) Van der Pol, A. J. H. P.; Verduyn, A. J.; Van Hooff, J. H. C. Why Are Some Titanium Silicalite-1 Samples Active and Others Not. *Appl. Catal. A: Gen.* **1992**, *92* (2), 113–130.
- (42) Tatsumi, T.; Nakamura, M.; Yuasa, K.; Iominaga, H. Shape selectivity as a function of pore size in epoxidation of alkenes with supported titanium catalysts. *Catal. Lett.* **1991**, *10*, 259–262.
- (43) Perego, C.; Carati, A.; Ingallina, P.; Mantegaza, M. A.; Bellussi, G. Production of titanium containing molecular sieves and their application in catalysis. *Appl. Catal. A: Gen.* **2001**, *221*, 63–72.
- (44) Carati, A.; Flego, C.; Berti, D.; Millini, R.; Stocchi, B.; Perego, G. Influence of synthesis media on the TS-1 Characteristics. *Stud. Surf. Sci. Catal.* **1999**, *125*, 45–52.
- (45) Millini, R.; Previde Massara, E.; Perego, G.; Bellussi, G. Framework composition of titanium silicalite-1. *J. Catal.* **1992**, *137*, 497–503.
- (46) Scarano, D.; Zecchina, A.; Bordiga, S.; Geobaldo, F.; Spoto, G.; Petrini, G.; Leofanti, G.; Padovan, M.; Tozzola, G. Fourier-transform infrared and Raman spectra of pure and Al-, B-, Ti- and Fe-substituted silicalites: stretching-mode region. *J. Chem. Soc., Faraday Trans.* **1993**, *89*, 4123.
- (47) Geobaldo, F.; Bordiga, S.; Zecchina, A.; Giamello, E.; Leofanti, G.; Petrini, G. DRS UV-Vis and EPR spectroscopy of hydroperoxo and superoxo complexes in titanium silicalite. *Catal. Lett.* **1992**, *16*, 109–115.
- (48) Park, S.; Cho, K. M.; Youn, M. H.; Seo, J. G.; Jung, J. C.; Baek, S. H.; Kim, T. J.; Chung, Y. M.; Oh, S. H.; Song, I. K. Direct Epoxidation of Propylene with Hydrogen Peroxide over TS-1 Catalysts: Effect of Hydrophobicity of the Catalysts. *Catal. Commun.* **2008**, *9* (15), 2485–2488.
- (49) Fan, W. B.; Duan, R. G.; Yokoi, T.; Wu, P.; Kubota, Y.; Tatsumi, T. Synthesis, Crystallization Mechanism, and Catalytic Properties of Titanium-Rich TS-1 Free of Extraframework Titanium Species. *J. Am. Chem. Soc.* **2008**, *130* (31), 10150–10164.
- (50) Bellussi, G.; Buonomo, F.; Esposito, A.; Clerici, M. G.; Romano, U.; Notari, B. Catalyst of silicon and titanium having high mechanical strength and a process for its preparation. US 4701428, 1987.
- (51) Li, G.; Wang, X.; Yan, H.; Liu, Y.; Liu, X. Epoxidation of propylene using supported titanium silicalite catalyst. *Appl. Catal. A: Gen.* **2002**, *236*, 1–7.
- (52) Clerici, M. G. Oxidation of saturated-hydrocarbons with Hydrogen-Peroxide, catalyzed by Titanium Silicalite. *Appl. Catal.* **1991**, *68*, 249–261.
- (53) Clerici, M. G. The role of the solvent in TS-1 chemistry: active or passive? An early study revisited. *Top. Catal.* **2001**, *15*, 257–263.
- (54) Maspero, F.; Romano, U. Oxidation of alcohols with H₂O₂ catalyzed by Titanium Silicalite-1. *J. Catal.* **1994**, *146*, 476–482.
- (55) Clerici, M. G.; Ingallina, P.; Millini, R. Titanium Silicalite-1 Peroxides. *Proceedings of 9th International Zeolite Conference*, Montreal, 1992; Butterworth-Heinemann: Boston, 1993, p 445.
- (56) Papparato, G.; Forlin, A.; De Alberti, G.; D'Alòsio, R.; Tegon, P. Integrated process for the preparation of epoxides. US 6541648 B1, Polimeri Europa S.r.l.; 2003.
- (57) Santacesaria, E.; Tesser, R.; Di Serio, M.; Russo, V.; Turco, R. A New Simple Microchannel Device To Test Process Intensification. *Ind. Eng. Chem. Res.* **2011**, *50* (5), 2569–2575.
- (58) Teles, J. II.; Rehfinger, A.; Bassler, P.; Wenzel, A. Method for the production of propylene oxide. US 6756503 B2, BASF Aktiengesellschaft; 2004.
- (59) Thiele, G. F.; Roland, E. Propylene epoxidation with hydrogen peroxide and titanium silicalite catalyst: Activity, deactivation and regeneration of the catalyst. *J. Mol. Catal. A* **1997**, *117*, 351.
- (60) Crocco, G. L.; Zajacek, J. G. Regeneration of a titanium-containing molecular sieve. US 5741749, Arco Chemical Technology, L.P.; 1998.
- (61) Catina, J. P.; Strebelle, M. *Process for regeneration of catalysts of titanium silicalite type*. US 6169050, Solvay; 2001.
- (62) Mantegazza, M. A.; Balducci, L.; Rivetti, L. Process for the regeneration of zeolitic catalysts containing titanium. US 6403514, Enichem S.p.A.; 2002.
- (63) Sun, B.; Wu, W.; Wang, E.; Li, Y.; Zhang, S.; Hu, L. Process for regenerating titanium-containing catalysts. US 2003/0228970, China Petroleum & Chemical Corporation, Research Institute of Petroleum Processing Sinopec; 2003.
- (64) Han, H. Z.; Carrol, K. M. Heterogeneous catalyst regeneration. US 6872679, 2005. Arco Chemical Technology, L.P.
- (65) Müller, U.; Teles, J. H.; Wenzel, A.; Harder, W.; Rudolf, P.; Rehfinger, A.; Reiber, N. Method for regenerating a zeolite catalyst. US 6790969, BASF Aktiengesellschaft; 2004.
- (66) Grosh, G. H.; Müller, U.; Walch, Q.; Reiber, N.; Harder, W. Method for regenerating a zeolitic catalyst. US 6710002, BASF Aktiengesellschaft; 2004.

- (67) Thiele, G. Method for the regeneration of a catalyst. US 5620935, Degussa Aktiengesellschaft; 1997.
- (68) Gilbeau, P. Method for regenerating catalysts. WO 9818555, Solvay; 1998.
- (69) Zuo, Y.; Wang, M.; Song, W.; Wang, X.; Guo, X. Characterization and Catalytic Performance of Deactivated and Regenerated TS-1 Extrudates in a Pilot Plant of Propene Epoxidation. *Ind. Eng. Chem. Res.* **2012**, *51* (32), 10586–10594.
- (70) Carrol, K. M.; Morales, H. E.; Han, Y. Z. Heterogeneous catalyst regeneration. US 5916835, Arco Chemical Technology, L.P.; 1999.
- (71) Chang, T. Process for epoxidation of propylene. WO 9901445, Lyondell Chemical Technology; 1999.
- (72) Chang, T. Process for regenerating epoxidation catalysts. EP 1190770, Lyondell Chemical Technology; 2002.
- (73) Thiele, G. Process for the production of epoxides from olefins. US 5675026, Degussa Aktiengesellschaft; 1997.
- (74) Neurock, M.; Manzer, L. E. Theoretical insights on the mechanism of alkene epoxidation by H₂O₂ with titanium silicalite. *Chem. Commun.* **1996**, 1133–1134.
- (75) Sinclair, P. E.; Catlow, C. R. A. Computational and EXAFS study of the nature of the Ti(IV) active sites in mesoporous titanosilicate catalysts. *J. Phys. Chem. B* **1997**, *101* (21), 4232–4237.
- (76) Liang, X.; Mi, Z.; Wu, Y.; Wang, L.; Xing, E. Kinetics of epoxidation of propylene over TS-1 in isopropanol. *React. Kinet. Catal. Lett.* **2003**, *80* (2), 207–215.
- (77) Haas, T.; Hofen, W.; Sauer, J.; Thiele, G. Process for the epoxidation of olefins. US 6600055 B2, Degussa AG, Uhde GmbH; 2003.
- (78) Haas, T.; Hofen, W.; Pilz, S.; Thiele, G.; Woell, W. Process for the epoxidation of olefins. WO 02/085874 A1, Degussa AG, Uhde GmbH; 2002.
- (79) Hofen, W.; Thiele, G. Process for the epoxidation of olefins. WO 03/016296 A2, Degussa AG, Uhde GmbH; 2003.
- (80) Haas, T.; Hofen, W.; Thiele, G.; Pilz, S.; Woell, W. Process for the epoxidation of olefins. US 6608219 B2, Degussa AG, Uhde GmbH; 2003.
- (81) Corma, A.; Esteve, P.; Martinez, A. Solvent effects during the oxidation of olefins and alcohols with hydrogen peroxide on Ti-beta catalyst: The influence of the hydrophilicity-hydrophobicity of the zeolite. *J. Catal.* **1996**, *161* (1), 11–19.
- (82) Van der Wall, J. C.; Van Bekkum, H. Zeolite titanium beta: A versatile epoxidation catalyst. Solvent effects. *J. Mol. Catal. A* **1997**, *124*, 137.
- (83) Liu, X. W.; Wang, X. S.; Guo, X. W.; Li, G. Effect of solvent on propylene epoxidation over TS-1 catalyst. *Catal. Today* **2004**, *93*, 505.
- (84) Jappar, N.; Xia, Q. H.; Tatsumi, T. Oxidation activity of Ti-beta synthesized by a dry-gel conversion method. *J. Catal.* **1998**, *180*, 132.
- (85) Miyano, Y.; Fukuchi, K. Henry's Constants of Propane, Propene, Trans-2-butene and 1,3-Butadiene in Methanol at 255–320 K. *Fluid Phase Equilib.* **2004**, *226*, 183–187.
- (86) Perry, R. H.; Green, D. W. *Perry's Chemical Engineers' Handbook*; McGraw-Hill: New York, 2007.
- (87) Crocco, G. L.; Zajacek, J. G. Process for titanium silicalite-catalyzed epoxidation. US 5646314, ARCO Chemical Technology, L.P.; 1997.
- (88) Grey, R. A. Epoxidation process. US 6037484, Arco Chemical Technology, L.P.; 2000.
- (89) Thiele, G. Process for the preparation of epoxides from olefins. US 6372924 B2, Degussa-Huls AG; 2002.
- (90) Haas, T.; Brasse, C.; Stochniol, G.; Hofen, W.; Wöll, W.; Thiele, G. US 6838572 B2, Degussa AG, Uhde GmbH; 2005.
- (91) Haas, T.; Hofen, W.; Wöll, W.; Brasse, C.; Stochniol, G.; Ullrich, N. Process for the epoxidation of olefins. US 7169945 B2, Degussa AG, Uhde GmbH; 2007.
- (92) Paparatto, G.; Forlin, A.; De Alberti, G.; D'Alosio, R.; Tegov, P. Integrated process for the preparation of olefin oxides. US 6888013 B2, Polimeri Europa S.p.A.; 2005.
- (93) Arca, V.; Buzzoni, R.; Furlan, P. Process for the preparation of olefinic epoxides. EP0930308 B1, Dow Global Technologies Inc; 1998.
- (94) Clerici, M. G.; Romano, U. Process for the epoxidation of olefinic compounds and catalysts used therein. US4824976, Eniricerche, S.p.A., Enichem Sintesi, S.p.A.; 1988.
- (95) Clerici, M. G.; Ingallina, P. Process for producing olefin oxides. US5221795, Eniricerche, S.p.A., Enichem Sintesi, S.p.A.; 1993.
- (96) Clerici, M. G.; Ingallina, P. Process for oxidizing organic compounds. US5252758, Eniricerche, S.p.A., Enichem Sintesi, S.p.A.; 1992.
- (97) Crocco, G. L.; Zajacek, J. G. Regeneration of a titanium-containing molecular sieve. US5753576, ARCO Chemical Technology, L.P.; 1995.
- (98) Catinat, J. P.; Strebelle, M. Method for making an oxirane. US6380407, Solvay; 2002.
- (99) Paparatto, G.; D'Aloisio, R.; De Alberti, G.; Furlan, P.; Arca, V.; Buzzoni, R.; Meda, L. Catalyst, process for the production of hydrogen peroxide and its use in oxidation processes. US6284213, Enichem S.p.A.; 1999.
- (100) Muller, U.; Brocker, F. J.; Grosch, G. H.; Putter, H.; Schulz, M.; Rieber, N.; Harder, W. Gauze catalyst based on titanium or vanadium zeolites and inert gauze fabrics for accelerating oxidation reactions. US6106797, BASF Aktiengesellschaft; 2000.
- (101) Bassler, P.; Harder, W.; Resch, P.; Rieber, N.; Ruppel, W.; Teles, J. H.; Walch, A.; Wenzel, A.; Zehner, P. Method for reacting an organic compound with a hydroperoxide. US6479680, BASF Aktiengesellschaft; 2002.
- (102) Grosch, G. H.; Müller, U.; Walch, A.; Rieber, N.; Fischer, M.; Quaiser, S.; Harder, W.; Eller, K.; Bassler, P.; Wenzel, A.; Kaibel, G.; Stammer, A.; Henkelmann, J.; Battcher, A.; Teles, J. H.; Schulz, M.; Treiber, G. Method for oxidizing an organic compound containing at least one C-C double bond. US6518441, BASF Aktiengesellschaft; 2003.
- (103) Schindler, G. P.; Walsdorff, C.; Korner, R.; Gobbel, H. G. Process for producing propylene oxide. US 2007/0004926 A1, BASF Aktiengesellschaft, The Dow Chemical Company; 2007.
- (104) Haas, T.; Hofen, W.; Thiele, G.; Pilz, S.; Woell, W. Process for the epoxidation of olefins. US6608219, Degussa AG, Uhde GmbH; 2002.
- (105) Catinat, J. P.; Strebelle, M. Method for making an oxirane. US6429322, Solvay; 2002.
- (106) Strebelle, M. Process for manufacturing an oxirane. US2008/0132718, Solvay; 2008.
- (107) Catinat, J. P.; Strebelle, M. Process for manufacturing an oxirane. US7323578, Solvay; 2008.
- (108) Strickler, G. R.; Quarader, G. J., Jr.; Lindner, J. P. Process of preparing an olefin oxide from olefin and organic hydroperoxide. US 7273941 B2, Dow Global Technologies Inc.; 2007.
- (109) Jubin, J. C., Jr. Catalytic converter and method for highly exothermic reactions. US 5466836, ARCO Chemical Technology, L.P.; 1995.
- (110) *Ullmann's Encyclopedia of Industrial Chemistry*, 5th ed.; Wiley-VCH: New York, 1999; Vol. 13, 447–456.
- (111) Samanta, C. Direct synthesis of hydrogen peroxide from hydrogen and oxygen: An overview of recent developments in the process. *Appl. Catal. A: Gen.* **2008**, *350*, 133–149.
- (112) Santacesaria, E.; Di Serio, M.; Russo, A.; Leone, U.; Velotti, R. Kinetic and catalytic aspects in the hydrogen peroxide production via anthraquinone. *Chem. Eng. Sci.* **1999**, *54*, 2799–2806.
- (113) <http://www.chemicals-technology.com/projects/basf-hppo/> (accessed Jan 2013).
- (114) Clerici, M. G.; Ingallina, P. Oxidation reactions with in-situ generated oxidants. *Catal. Today* **1998**, *41*, 351–364.
- (115) Muller, U.; Lingelbach, P.; Bassler, P.; Harder, W.; Eller, K.; Kohl, W.; Kohl, V.; Dembowski, J.; Rieber, N.; Fischer, M. Oxidation catalyst, its preparation and oxidation using the oxidation catalyst. US 5859265, BASF Aktiengesellschaft; 1999.
- (116) Bowman, G. R.; Womack, L. J.; Clark, W. H. Process for the direct oxidation of olefins to olefin oxides. WO 98/00413 A1, The Dow Chemical Company; 1998.

(117) Kaminsky, M. P.; Grey, R. A. Direct epoxidation process using a mixed catalyst system. US 7671222, Lyondell Chemical Technology, L. P.; 2010.

(118) Romano, U.; Occhiello, E.; Paludetto, R. Integrated Process for the production of olefin oxides. WO 02/085875 A1, Polimeri Europa S.p.A.; 2002.

(119) Gobbel, H. G.; Bassler, P.; Teles, J. H.; Rudolf, P.; Müller, U.; Forlin, A.; Schultz, M.; Weidenbach, M. A process for epoxidizing propene. WO 2007/074101 A1, BASF SE, The DOW Chemical Company; 2007.

(120) Gobbel, H. G.; Schultz, H.; Schultz, P.; Petrascu, R.; Schultz, M.; Weidenbach, M. Separation of propylene oxide from a mixture comprising propylene oxide and methanol. US 2006/0009648 A1, BASF Aktiengesellschaft, The Dow Chemical Company; 2006.

(121) <http://www.knak.jp/big/evonik-hppo.htm> (accessed Jan 2013).

(122) http://www.uhde.eu/fileadmin/documents/brochures/uhde_brochures_pdf_en_10000032.pdf (accessed Jan 2013).

Kinetics of Propene Oxide Production via Hydrogen Peroxide with TS-1

V. Russo, R. Tesser, E. Santacesaria, M. Di Serio*

University of Naples "Federico II". Department of Chemical Sciences, via Cintia 80126 Napoli, Italy

Abstract – Propene oxide is a building block of the modern chemical industry. The research related to the development of convenient and greener processes has led to the development of the HPPO (Hydrogen Peroxide Propene Oxide) process, where propene is oxidized by hydrogen peroxide in the presence of methanol as solvent and titanium silicalite (TS-1) as catalyst. Even if the first industrial plants based on this technology are already running, only few information have been published till now about the kinetics of the process, in particular regarding the side reactions that lower the yields and increase the cost of propene oxide purification. This paper is devoted to the kinetic investigation of both main and side reactions, with the aim to find general kinetic expressions, and related parameters.

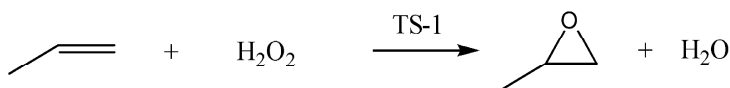
Key-words: Propene oxide, HPPO process, hydrogen peroxide, TS-1, kinetics.

* Corresponding author : diserio@unina.it

1. Introduction

Propene oxide (PO) is a highly reactive chemical used as an intermediate for the production of numerous commercial materials such as polyether polyols (polyglycol ethers), propene glycols and propene glycol ethers^{1,2}. Nowadays, several routes to produce PO are possible and chemical plants based on these technologies are already running^{1,3}; among them, the emerging one is the direct epoxidation of propene with hydrogen peroxide (HPPO - Hydrogen Peroxide Propene Oxide)^{1,4} in the presence of titanium silicalite-1 as catalyst (TS-1)⁵⁻⁹ and methanol as solvent.

TS-1 is a crystalline zeolite material in which tetrahedral [TiO₄] and [SiO₄] units are arranged in a MFI structure¹⁰. The chemical nature of Ti species in TS-1 catalyst is made by “close” Ti(OSi)₄ tetrahedral sites and defective “open” Ti(OSi)₃(OH) sites^{5-7,11}. Owing to this structure TS-1 shows a three-dimensional system of channels having molecular dimension of 5.1-5.6 Å and which constitutes the micropores of the zeolitic material. By using this catalyst, the reaction is normally carried out under mild conditions (40-50 °C and 20-30 bar), and theoretically, only water is generated as byproduct (see scheme 1).



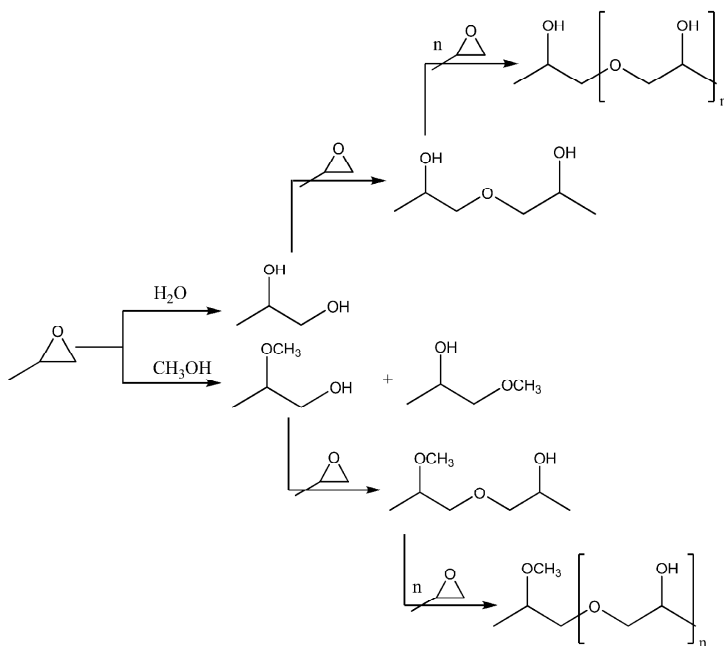
Scheme 1 – Epoxidation of propene

In 2008, after about 25 years from the first ENI patent, Evonik (former Degussa) and SKC have launched the first commercial-scale propene oxide plant, based on the HPPO technology¹, with a capacity of 100 ktons/year. The next year BASF and DOW Chemical started with a new plant based on a similar technology, with a 300 ktons/year capacity^{1,3}. After that, some new plants have been put on stream or are under construction^{1, 12-15}.

By considering the scientific literature, a lot of effort has been made by considering the catalyst synthesis and the investigation on the reaction mechanism^{4,5,8,9,16-18}. The most accredited mechanism on the basis of spectroscopic evidences is the Eley-Redeal one⁴. It is important to point out that only three papers have been published till now concerning the HPPO kinetics¹⁹⁻²¹, and these papers are all mainly focused on the main reaction investigation. Moreover, two of the mentioned papers^{20,21} report kinetic runs performed by using isopropanol as solvent, while only one¹⁹ has used methanol, that is, the solvent most commonly employed in the industrial plants. However, there are discrepancy about the reaction kinetic law, as a matter of fact two of these

paper^{20,21} confirm the Eley-Redeal mechanism, while another found that the best mechanism, in terms of statistical analysis, would be a dual-site Langmuir-Hinshelwood¹⁹. More experimental work is, therefore, necessary to individuate the correct kinetics in the presence of methanol as solvent and determine the related parameters.

As before mentioned, the cited paper is focused only on the main reaction, giving no kinetic information related to the side-reactions that reduce the yield of the process and increase the costs of PO purification. As a matter of fact after the PO formation, PO can continue to react giving places to different by-products, as it can be seen in scheme 2²²⁻²⁵.



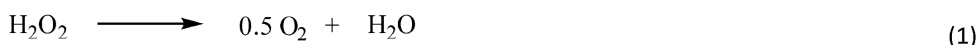
Scheme 2 – Epoxide ring opening reactions.

All the reactions reported in scheme 2 are related to the ring opening reactions, and are clearly responsible of lowering the PO selectivity. PO can react either with water or methanol, giving place to respectively propene glycol and 1 and 2-methoxy propanol. Then, the reaction proceeds, because PO reacts with either methoxy propanol or glycol, giving dimers that can react further forming different oligomerization products^{8,19}. It must be pointed out that the formation of oligomers is detrimental for the catalytic activity^{8,19,26}. For what concerns the mechanism of the mentioned reactions, only one hint is reported by Thiele et al.²⁷. The authors have reported that the by-products formation, in the absence of hydrogen peroxide, is mainly due to acid sites. These sites would be, for example, silanol groups, in correspondence of crystal defects, but these sites

are not catalytic sites, while, titanium hydroperoxide specie, formed as a consequence of the contact between TS-1 and hydrogen peroxide, is acid too and can promote, therefore, both the main reaction from propene to propene oxide and the ring opening side reactions with two different mechanisms.

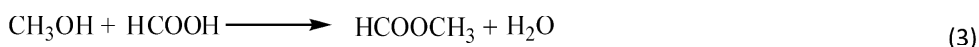
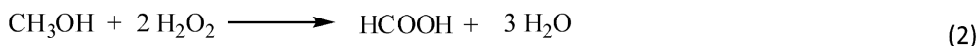
In conclusion, the adsorption of hydrogen peroxide on TS-1 leads to the formation of titanium hydroperoxide specie, acid sites that are responsible of the desired reaction but also increase the ring opening reaction rate¹⁶⁻¹⁸. Clearly, this aspect needs to be carefully considered by studying the kinetics of the ring opening reactions.

Moreover, mainly at high temperatures, the hydrogen peroxide decomposition reaction has to be taken into account, too²⁸.



This reaction is very important for two reasons: (i) the cost of hydrogen peroxide is one of the main factor for the economy of the process, (ii) the hydrogen peroxide decomposition gives place to molecular oxygen that can lead to explosive mixtures with propene.

The possibility of methanol oxidation to formic acid, that can then further react with methanol to give methyl formate, has also been reported²⁹.



Methyl formate has a boiling point similar respect to PO, therefore, its presence in the reaction mixture is a serious problem in PO purification.

In this paper, a detailed investigation on the kinetics of all the mentioned reactions has been performed to overcome the mentioned lack of information by obtaining, for any reaction, the corresponding kinetic law and related kinetic parameters.

2. Experimental section

2.1. Reagents

Propene has been supplied by SIAD with a purity of 99.5 % (0.5 % propane), methanol has been supplied by Clean Consult at 99.8% purity, hydrogen peroxide (60 wt.%) has been supplied by Mythen s.r.l. . All the other reagents employed have been supplied by Aldrich at the highest level of purity available and have been used as received without further purification. TS-1 catalyst has been supplied by Conser S.p.A. in microspheres form obtained by spray-drying technique. The microspheres, characterized by an average diameter of 35 μm , are composed by crystalline TS-1 (Ti content of 3 wt.% and average size of crystallites of 30 nm) and silica as binder in a ratio 1:1 g/g.

2.2. Analytical methods

The products distribution and the PO conversion have been analytically determined by gas-chromatographic analysis, using a gas chromatograph (HP 6890), equipped with a flame ionization detector (FID), a split-splitless column injector, and employing a Restek RT-Q-Bond Plot column (30 m x 0.32 mm I. D., 0.1 μm film). The temperature ramp has been set as it follows: 100°C for 1 minute, heating to 220°C with a rate of 20°C/min followed by a heating step to 270°C at 30°C/min; temperature is kept at the final value for 10 minutes. Before the analysis, 100 μL of ethyl acetate have been added to 5 cm^3 of sample, as internal standard. The residual hydrogen peroxide concentration has been analytically determined by a iodometric titration³⁰.

2.3. Apparatus

Two reactors have been used in order to perform all the kinetic runs. The runs made for studying the side-reactions have been performed in a 300 cm^3 hastelloy cylindrical autoclave. The hastelloy reactor has been supplied by Parr Instrument and allows to work at a maximum of 55 bars. Both temperature and pressure have been acquired trough a built-in data acquisition system. Temperature have been controlled by a PID system always provided by Parr Instrument. The sketch of this reactor is reported in Figure 1 A.

The epoxidation tests have been performed in a 1000 cm^3 AISI 316 stainless steel jacketed cylindrical. This reactor has been equipped with a gaseous effect stirrer in order to favor the propene mass transfer from the gas to the liquid phase. Reactor's temperature has been regulated by circulating water in the reactor's jacket through a ultracryostat, in order to keep the system

isothermal. For each run, the system has been previously washed with nitrogen, in order to avoid contact between propene and air, then propene is fed to the reactor at constant pressure, reading propene flow through a mass flow-meter opportunely calibrated. In this ways, propene flow can be measured on-line and information about the gas-liquid mass transfer are collected. Both temperature, pressure and propene flow have been acquired trough a built-in data acquisition system. The sketch of this reactor is reported in Figure 1 B.

Being the reaction system composed of three phases (gas-liquid-solid), the reactor has been fluid-dynamically characterized in order to define the mass transfer parameters.

For each kinetic tests, samples of 2 cm³ have been withdrawn in vials, using a pin valve, connected to a tube that reaches the bottom of the reactor. At the end of this tube, a sintered AISI 316 filter, of 10 µm mesh, has been mounted in order to avoid any catalyst drainage.

2.4. Methods

Different sets of experimental runs have been performed in order to deeply investigate the kinetics of all the previously described reactions together with the involved mass transfer phenomena. In particular, the hydrogen peroxide decomposition and the methyl formate/formic acid formation, have been studied simultaneously. A 180g of solution of about 9 wt.% H_2O_2 /10wt.% H_2O /80wt.% CH_3OH is loaded to the reactor, adding the desired amount of catalyst. The reactor is pressurized with nitrogen at 5 bar and the stirrer speed has been fixed at 300 rpm. All the performed runs, with the adopted reaction conditions for both the study of hydrogen peroxide decomposition and methyl formate formation, are listed in Table 1.

The ring opening reaction kinetics have been investigated by following three different modalities: (i) considering PO degradation in the presence of methanol; (ii) studying the ring opening in the presence of both water and methanol; (iii) considering the effect of hydrogen peroxide on the PO degradation reaction rate in the presence of both water and methanol. In all cases, in the reactor 180 g of mixture has been pressurized with nitrogen at 5 bars in order to keep all reagents in the liquid phase. The effect of temperature and catalyst concentration has been studied for all the different modalities. All the performed runs related to the ring opening reactions kinetic investigation, with the adopted reaction conditions, are listed in Table 2.

The propene oxide production runs have been carried out by changing the temperature, the catalyst concentration, the propene partial pressure and the methanol/water ratio. All the tests have been performed using charging the reactor with 300 g of reaction mixture, at a total pressure of 3.75 bars and a mixing rate of 500 rpm. The reactor has been first pressurized with nitrogen, set to the desired temperature and finally propene is sent to the reactor. All the adopted reaction conditions are reported in Table 3. A fluid-dynamic characterization of the system has been performed by charging the vessel with 300 g of a solution of methanol/water (14 g/g) and stimulating the system with a step-wise tests. In particular, the methanol/water solution has been pressurized with nitrogen at a desired temperature and propene has been added step-wise to the reactor. The evolution of the propene consumption along the time has been monitored through a mass-flowmeter connected to a data acquisition system, while the pressure has been kept constant along all the experiment. All the experimental conditions adopted in the characterization tests are reported in Table 4.

3. Results and discussion

3.1. Fluid dynamic characterization.

Fluid dynamic characterizations tests have been carried out in order to determine the influence of the stirring rate on the mass transfer parameters. Examples of experimental runs are reported in Figure 2 A, where the evolution with time of the propene absorption for different stirring rates are reported. As it can be seen, by increasing the stirring rate the system reaches more fastly the propene solution saturation (the plateau of the absorption curve).

The solubility of the propene ($[C_3H_6]^*$) is a function of the pressure and temperature and can be calculated using the following relation.

$$[C_3H_6]^* = H_{C_3H_6} \cdot P_{C_3H_6} \quad (4)$$

The measured solubility is congruent with the data reported in the literature. For example, at $T=40^\circ C$ we obtained a solubility constant $H=0.25 \text{ mol}/(\text{L}\cdot\text{atm})$ that is very near to the value reported in the literature ($H=0.26 \text{ mol}/(\text{L}\cdot\text{atm})$)³¹.

From the collected experimental data the following relation for the solubility of propene in the reaction mixture as a function of temperature can be derived.

$$H_{C_3H_6} = -0.0046 \cdot (T - 273.15) + 0.4393 \quad (5)$$

All the collected experimental data have then been subjected to mathematical regression analysis for evaluating the global mass transfer coefficient (β) from the following mass balances equations (6-7).

$$\frac{dN_{C_3H_6}^{GAS}}{dt} = F_{C_3H_6} - J_{C_3H_6} = F_{C_3H_6} - k_L \cdot a_L \cdot ([C_3H_6]^* - [C_3H_6]) \cdot V = F_{C_3H_6} - \beta \cdot ([C_3H_6]^* - [C_3H_6]) \cdot V \quad (6)$$

$$\frac{dN_{C_3H_6}^{LIQ}}{dt} = J_{C_3H_6} \cdot V = k_L \cdot a_L \cdot ([C_3H_6]^* - [C_3H_6]) \cdot V = \beta \cdot ([C_3H_6]^* - [C_3H_6]) \cdot V \quad (7)$$

$F_{C_3H_6}$, the inlet propene feed rate, depends on the global pressure as in reported in the literature³², equation (8).

$$F_{C_3H_6} = k_v \cdot (P^{SET} - P^{Actual}) \quad (8)$$

Being P^{SET} the set pressure, P^{Actual} the pressure of the system varying with the time and k_v a parameter related with the Cv of the adopted inlet valve. This value has been estimated on the basis of the valve characteristics, obtaining a value of 20.

A list of the estimated parameters together with the relative confidence interval is reported in Table 4. The agreement between the experimental and calculated propene absorption can be appreciated in Figure 2 A. The trend of the evaluated global mass transfer coefficient (β) as a function of the stirring rate is reported in Figure 2 B. As can be seen it is quite linear in the range 10-700 rpm. With this preliminary investigation we are now confident on the gas-liquid mass transfer phenomena that occurs in the adopted experimental device. By considering that the epoxidation of propene occurs in a gas-liquid-solid system, an effort has to be made in order to estimate the liquid-solid mass transfer coefficient, too. By applying the correlations published by Sano et al.³³ we have estimated a liquid-solid mass transfer coefficient of about $k_s=6.0$ cm/min. By considering that the TS-1 adopted catalyst is characterized by a very high specific area ($1.7E+03$ cm²/cm³), we obtain a very high value for $k_s \cdot a_s$. For this reason, by considering that the gas-liquid resistance to the mass transfer is much greater than the liquid-solid one, that is $1/(k_L \cdot a_L) \gg 1/(k_s \cdot a_s)$, we have considered negligible the second contribution.

3.2. *H₂O₂ decomposition and methyl formate/formic acid formation.*

First of all, in order to exclude any limitation due to the external mass transfer, some kinetic runs have been performed at different stirring rate, finding no difference when working at 300 or 600 rpm. The first reaction (Run D0 of Table 1) has been performed at 70 °C without catalyst (blank run). Only a very small hydrogen peroxide decomposition and methyl formate formation has been observed, in this case, even for a long reaction time (5 h).

Then, some kinetic runs (Runs D1-D4 of Table 1) have been performed at fixed catalyst concentration (2.22 wt.% TS-1) varying the reaction temperature (40-70°C) in order to verify the effect of the temperature on the reaction rate (see Table 1 and Figure 3) . As it can be seen, by

increasing the temperature, a strong increase in the hydrogen peroxide conversion is observed. Moreover, starting from a nitrogen pressure of 5 bars, the global pressure of the system increases as a consequence of the hydrogen peroxide decomposition and the consequent oxygen formation. Therefore, the maximum pressures reached different values (see Table 1). Two set of runs have been performed in order to investigate the catalyst concentration effect at a fixed temperature. At this purpose, some experimental runs have been performed at both 40 (Runs D4, D7 and D8 of Table 1) and 60°C (Runs D2, D5 and D6 of Table 1), observing an increase in hydrogen peroxide decomposition with the increase of catalyst concentration (see Figure 4 A and B).

The kinetics of hydrogen peroxide decomposition has been investigated by submitting all the experimental data of Table 1 to mathematical regression analysis by solving the following mass balance equations.

$$\frac{dN_{H_2O_2}}{dt} = -r_d \cdot V \quad (9)$$

$$\frac{dN_{H_2O}}{dt} = r_d \cdot V \quad (10)$$

Considering that the decomposition is favored by increasing the amount of catalyst, we have assumed as first approximation, the following second order kinetic law that is linearly dependent on the TS-1 concentration, in agreement with the behavior of catalyzed hydrogen peroxide decomposition observed for other catalytic system³⁴.

$$r_d = k_d \cdot [TS - 1] \cdot [H_2O_2] \quad (11)$$

A modified Arrhenius equation has been adopted in order to express the dependence between the kinetic constant and the temperature (12).

$$k_d = k_d^{ref} \cdot \exp\left(\frac{E_d}{R} \cdot \left(\frac{1}{T^{ref}} - \frac{1}{T}\right)\right) \quad (12)$$

All the collected experimental data have been submitted to a simultaneous mathematical regression analysis, by adopting a 4th order Runge-Kutta algorithm for the integration of the differential equations (9-10). The good agreements between the experimental data and the simulation obtained with the kinetic parameters reported in Table 5 can be appreciated in Figures

3-4. The average difference between the experimental data and the corresponding calculated values is of about 3%.

The rate of formation of formic acid and methyl formate is very low. In Table 1, the concentrations of these products, after 5 h of reaction, are reported. At low catalyst concentration and low temperature, the formation of formic acid and methyl formate was not appreciable. The formation rate of these products increases by increasing the catalyst concentration but strongly increases with the increase of the reaction temperature. In the case of formic acid and methyl formate formation a detailed kinetic analysis was not possible, because, the few available experimental data obtained. However, we can conclude that in the industrial plants the choice of the reaction conditions is fundamental, because both the hydrogen peroxide decomposition and the formation of both methyl formate and formic acid are favored by the high concentration of the catalyst and by the possible presence of hot spot along the reactor: care must be made on controlling these two variables.

3.3. Propene oxide ring opening reaction: defective sites effect

In order to correctly investigate the ring opening reaction, a number of experimental runs, that covers the panorama shown in the introduction section, has been performed.

To investigate separately the effect of reaction environment on the propene oxide ring opening reaction, runs have been done in the presence of only methanol, of both methanol and water, of methanol, water and hydrogen peroxide.

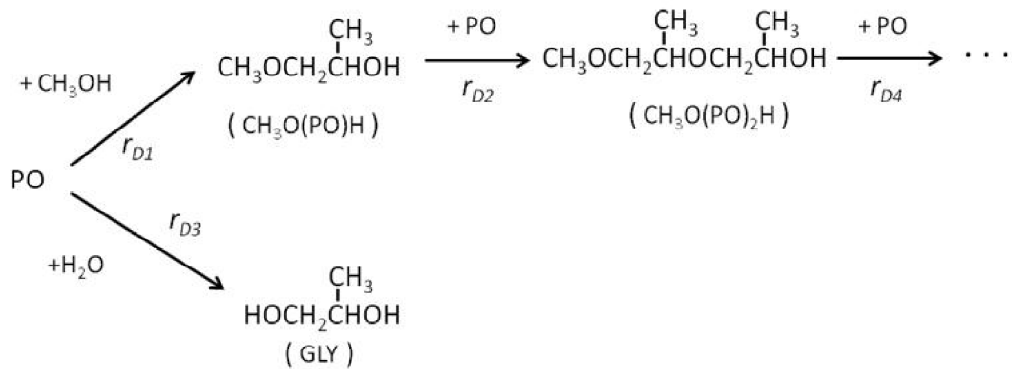
First of all, the influence of the defective sites and/or silanols on the ring opening reaction has been investigated, performing experimental runs by varying both temperature and catalyst concentration in the absence of hydrogen peroxide.

Run AA0a of Table 2 has been performed without catalyst (blank runs), and no PO decomposition has been observed. Clearly, the presence of TS-1 catalyzes the propene oxide ring opening reaction. As an example, by fixing the temperature at 40°C (Runs AA1,AA4-AA6 of Table 2), the increase of the catalyst concentration leads to an increase of the ring opening reaction rate (see Figure 5 A). The formation of methoxypropanol and its oligomers has been observed in all cases (see Figure 6 A). Moreover, the presence of water causes also the formation of propene glycol but the main product is always methoxypropanol (see Figure 6 B). This fact is due to the much greater

concentration of methanol with respect to water. As a consequence no oligomers of propene glycols have been observed.

To investigate the effect of the temperature on the ring opening reactions, different runs (Runs AA1-3 and AA7-AA9 of Table 2) have been performed by fixing the catalyst concentration. In Figure 5 B, it is possible to see that by increasing the temperature, the PO conversion (X_{PO}) increases accordingly.

In order to interpret the collected experimental data we have considered the following reaction scheme (scheme 3).



Scheme 3 – Reaction scheme of epoxide ring opening.

The experimental data of the runs reported in Table 2 (Runs AA1-AA13) have been simulated solving the following mass balances equations (13-18).

$$\frac{dN_{\text{CH}_3\text{OH}}}{dt} = -r_{D1} \cdot V \quad (13)$$

$$\frac{dN_{\text{PO}}}{dt} = -(+r_{D1} + r_{D2} + r_{D3} + r_{D4}) \cdot V \quad (14)$$

$$\frac{dN_{\text{CH}_3\text{O}(\text{PO})\text{H}}}{dt} = (+r_{D1} - r_{D2}) \cdot V \quad (15)$$

$$\frac{dN_{\text{Gly}}}{dt} = +r_{D3} \cdot V \quad (16)$$

$$\frac{dN_{H_2O}}{dt} = -r_{D3} \cdot V \quad (17)$$

$$\frac{dN_{Olig}}{dt} = +r_{D4} \cdot V \quad (18)$$

All the reaction rates in equations (19-22) have been considered linearly dependent from catalyst and reagent concentrations.

$$r_{D1} = k_{D1} \cdot [TS - 1] \cdot [PO] \cdot [CH_3OH] \quad (19)$$

$$r_{D2} = k_{D2} \cdot [TS - 1] \cdot [PO] \cdot [CH_3O(PO)H] \quad (20)$$

$$r_{D3} = k_{D3} \cdot [TS - 1] \cdot [PO] \cdot [H_2O] \quad (21)$$

$$r_{D4} = k_{D2} \cdot [TS - 1] \cdot [PO] \cdot [Oligom] \quad [Oligom] = \sum_{i=2, \dots} [CH_3O(PO)_i H] \quad (22)$$

The kinetic constant of the kinetic law (20) and (22) can be assumed the same for both the reaction of PO with methoxy propanol and its oligomers, independently on their molecular weight, because, all these side reactions (reaction to methoxy propanol and to oligomers) occur according to the same mechanism, where PO reacts with an alcoholic group³⁵. All the collected experimental data have been submitted to a simultaneous mathematical regression analysis, by adopting a 4th order Runge-Kutta algorithm, obtaining the activation energies and the kinetic constant at the reference temperature of 313 K reported in Table 6, In Figures 5-6, it is possible to appreciate the obtained agreement between experimental and calculated data. As it can be seen, the achieved agreement is very satisfactory for both PO conversions (average difference between experimental data and calculated value of 4%) and by-products distribution (average difference between experimental data and calculated value of 6%).

The previous good results indicate that the assumption done can be considered acceptable.

3.4. Ring opening reaction in the presence of hydrogen peroxide

Run AA0b of Table 2 has been performed at 30 °C without catalyst (blank runs) and also in presence of hydrogen peroxide and no PO decomposition has been observed.

By performing the ring opening experimental tests, in the presence of both hydrogen peroxide and catalyst, a higher PO degradation occurs in comparison with the runs performed in the absence of hydrogen peroxide. By increasing the hydrogen peroxide concentration, fixing both temperature and catalyst concentration, an increase of the initial reaction rate is observed (see Figure 7, Runs AA13, AA15 and AA18-AA21 of Table 2). In Figure 8, the byproduct distribution at 4 hours reaction time is reported (Runs AA14-AA21 of Table 2).

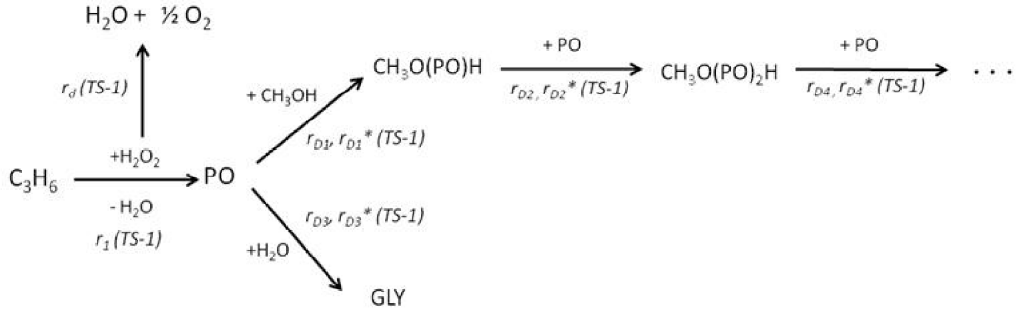
As for the previous case we have observed a linear dependence of the catalyst concentration for the ring opening reaction occurring in the presence of hydrogen peroxide, while from the data of Figure 7 it is clear that the effect of hydrogen peroxide concentration is complicated, presenting a sharp increase at very low hydrogen peroxide concentration. For higher concentrations a rough linear trend of the ring opening reaction rate with the hydrogen peroxide concentration can be observed. Probably, two different mechanisms are operative both involving acid sites that are present on the catalyst surface, that are, silanols, on the correspondence of crystal defects, and the Ti-OOH specie formed as a consequence of the interaction between the catalyst and hydrogen peroxide. However, the first type of catalytic sites are not active in producing PO but can decompose it, while, the second type of sites can promote both the PO synthesis and the successive decomposition. Therefore, by considering that the ring opening reaction in the presence of hydrogen peroxide is in series and parallel with the propene oxide synthesis and involves the same catalytic site (Ti-OOH), we have decided to elaborate simultaneously both the sets of runs. For this reason all the details of the runs interpretation are reported in paragraph 3.5.

3.5. Propene oxide synthesis

Propene oxide synthesis experimental conditions have been carefully chosen in order to avoid hydrogen peroxide decomposition, so by considering that hydrogen peroxide decomposition is promoted both at high temperature and catalyst concentration, we have performed these studies far from risky situations (see Table 3 for details). What it can be observed from Figure 9 (Runs PO1-PO3 and PO7 of Table 3) is that by increasing the catalyst concentration an increase in hydrogen peroxide conversion can be obtained. This can be considered acceptable because it corresponds to an increase in the concentration of active sites. Of course, by increasing the amount of loaded TS-1, also the side reactions get fastened and the by-products amount increases accordingly. Moreover, the by-products concentration is always very low being the reaction time small and the propene oxide concentration lower than the one adopted in the ring opening reactions. An interesting effect comes out by interpreting the data reported in Figure 10 (Runs PO1, PO4 and PO5 of Table 3), where the experimental runs plotted have been performed by increasing the propene partial pressure. By increasing the propene partial pressure a linear increase of the propene concentration in the liquid phase is expected (see equation 4), but a not linear increase on the reaction rate has been observed. By increasing the temperature we observed a higher hydrogen peroxide conversion but, being the side reactions promoted by the temperature, the amount of the two main by-products is increased (see Figure 11).

Finally, by increasing the water content (see Figure 12), the reaction rate get lowered by two possible reasons: (i) lower propene concentration in the liquid phase, (ii) water competition on the active sites, although by working at high water content the glycol concentration keeps always low, being the rate of this side reaction very low.

The complete reaction scheme that we have to consider to interpret the runs reported in Table 3 is the following (scheme 4).



Scheme 4 – Propene oxide overall reaction scheme.

All, the experimental data of the runs reported in Table 3 can be simulated solving the following mass balances equations (23-31).

$$\frac{dN_{C_3H_6}^{GAS}}{dt} = F_{C_3H_6} - J_{C_3H_6} \cdot V \quad (23)$$

$$\frac{dN_{C_3H_6}^{LIQUID}}{dt} = (+J_{C_3H_6} - r_1) \cdot V \quad (24)$$

$$\frac{dN_{H_2O_2}}{dt} = (-r_1 - r_d) \cdot V \quad (25)$$

$$\frac{dN_{PO}}{dt} = (+r_1 - r_{D1} - r_{D2} - r_{D3} - r_{D4} - r_{D1}^* - r_{D2}^* - r_{D2}^* - r_{D4}^*) \cdot V \quad (26)$$

$$\frac{dN_{CH_3OH}}{dt} = -(+r_{D1} + r_{D1}^*) \cdot V \quad (27)$$

$$\frac{dN_{CH_3O(PO)H}}{dt} = (+r_{D1} + r_{D1}^* - r_{D2} - r_{D2}^*) \cdot V \quad (28)$$

$$\frac{dN_{GLY}}{dt} = (+r_{D3} + r_{D3}^*) \cdot V \quad (29)$$

$$\frac{dN_{H_2O}}{dt} = (-r_{D3} - r_{D3}^* + r_d) \cdot V \quad (30)$$

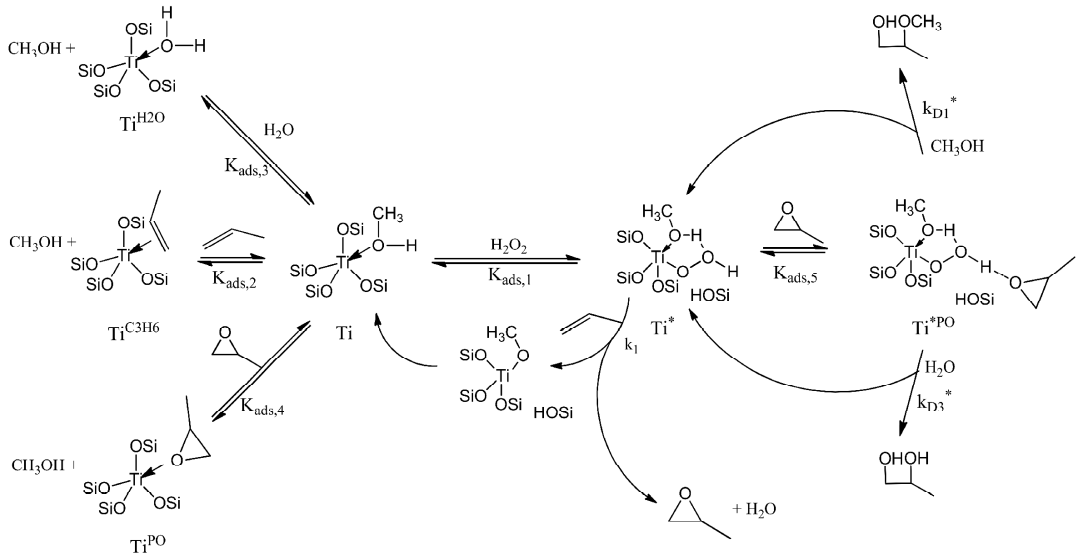
$$\frac{dN_{O_{1g}}}{dt} = (+r_{D4} + r_{D4}^*) \cdot V \quad (31)$$

Of course, both the hydrogen peroxide decomposition and the ring opening reaction kinetics in the absence of hydrogen peroxide has been considered too, so the previously find kinetic rate laws and related parameters have been used in the calculations. In particular, r_d , r_{D1} , r_{D2} , r_{D3} , r_{D4} can be calculated using the equations (11,19-22) introducing the kinetic parameters of Table 5-6. In this way, we have verified that the developed kinetic models predicts no hydrogen peroxide decomposition and well describes the observed experimental phenomena.

However, we have to define also the kinetic laws for r_{1} , r_{D1^*} , r_{D2^*} , r_{D3^*} , r_{D4^*} and evaluate the related kinetic parameters. We will try to derive these kinetic laws from the reaction mechanism.

Clerici et al.⁴, and papers within, have reported that the key factor of the propene epoxidation mechanism is the reversible splitting of a Ti-O-Si (Ti) bond by H₂O₂ leading to a Ti-OOH (Ti*) specie and the coadsorption of one alcohol or water molecule stabilizing the hydroperoxide through a five-membered ring, as it is reported in scheme 5 (Ti*). Then, the epoxidation step occurs, where the peroxy oxygen vicinal to Ti is transferred to the double bond, with the contemporary formation of a Ti-alkoxide specie, a molecule of water, and a molecule of propene oxide. Finally, Ti-OR quickly reforms the initial Ti-O-Si bond completing the catalytic cycle (see scheme 5). The formation of Ti-OOH specie is favored by the coordination on Ti-O-Si site of methanol⁴, however other species can coordinate the Ti-O-Si sites. (see scheme 5). These equilibria reduce the concentration of active sites and, as a consequence, the reaction rate.

Moreover the Ti* specie can catalyze also the secondary reaction interacting with the epoxide, forming the activate specie Ti^{*PO} (see scheme 5).



Scheme 5 - Propene oxide formation mechanism.

From the previous described mechanism it is possible to write:

$$r_1 = k_1^0 \cdot [Ti^*] \cdot [C_3H_6] \quad (32)$$

$$r_{D1}^* = k_{D1}^{0*} \cdot [Ti^{*PO}] \cdot [CH_3OH] \quad (33)$$

$$r_{D2}^* = k_{D2}^{0*} \cdot [Ti^{*PO}] \cdot [CH_3O(PO)H] \quad (34)$$

$$r_{D3}^* = k_{D3}^{0*} \cdot [Ti^{*PO}] \cdot [H_2O] \quad (35)$$

$$r_{D4}^* = k_{D2}^{0*} \cdot [Ti^{*PO}] [Oligom] \quad [Oligom] = \sum_{i=2, \dots} [CH_3O(PO)_i H] \quad (36)$$

So, an Eley-Rideal mechanism is operative for both the propylene oxide formation and the ring opening reactions. The concentration of the active specie can be derived solving the mass balance on Titanium species reported in (37).

$$[Ti] + [Ti^*] + [Ti^{*H_2O}] + [Ti^{*C_3H_6}] + [Ti^{*PO}] = [Ti - Si] f_{Ti} \quad (37)$$

Where f_{Ti} is the titanium total site concentration of TS-1. Considering the equilibria reported in the scheme 5, it is possible to write the following equilibrium constants.

$$\frac{[Ti^*]}{[Ti][H_2O_2]} = K_{ads1} \quad (38)$$

$$\frac{[Ti^{C^3H_6}][CH_3OH]}{[Ti][C_3H_6]} = K_{ads2} \quad (39)$$

$$\frac{[Ti^W][CH_3OH]}{[Ti][H_2O]} = K_{ads3} \quad (40)$$

$$\frac{[Ti^{PO}][CH_3OH]}{[Ti][PO]} = K_{ads4} \quad (41)$$

$$\frac{[Ti^{*PO}]}{[Ti^*][PO]} = K_{ads5} \quad (42)$$

As a first approximation the concentration of the specie $[Ti^{*PO}]$ has been considered lower with respect to the other ones. Moreover, being the methanol concentration always very high, it is possible to assume it constant and include it in the adsorption constants. Starting from this assumptions, it is possible to write the analytical solution for $[Ti^*]$ as in equation (43).

$$\frac{[Ti^*]}{f_{Ti}} = \frac{K_{ads1} \cdot [H_2O_2][TS-1]}{1 + K_{ads1} \cdot [H_2O_2] + K_{ads2} \cdot [C_3H_6] + K_{ads3} \cdot [H_2O] + K_{ads4} [PO]} \quad (43)$$

In this way, it is possible to substitute equation (43) in the kinetic rate laws reported in (32)-(36), obtaining the following equations.

$$r_1 = k_1^{0*} f_{Ti} \frac{[Ti^*]}{f_{Ti}} [C_3H_6] = k_1 [TS-1] \frac{K_{ads1} \cdot [H_2O_2][C_3H_6]}{1 + K_{ads1} \cdot [H_2O_2] + K_{ads2} \cdot [C_3H_6] + K_{ads3} \cdot [H_2O] + K_{ads4} [PO]} \quad (44)$$

$$\begin{aligned} r_{D1}^* &= k_{D1}^{0*} K_{ads5} [Ti^*][PO][CH_3OH] = k_{D1}^{0*} K_{ads5} f_{Ti} \frac{[Ti^*]}{f_{Ti}} [PO][CH_3OH] = k_{D1}^* \frac{[Ti^*]}{f_{Ti}} [PO][CH_3OH] = \\ &= k_{D1}^* [TS-1] \frac{K_{ads1} \cdot [H_2O_2][PO][CH_3OH]}{1 + K_{ads1} \cdot [H_2O_2] + K_{ads2} \cdot [C_3H_6] + K_{ads3} \cdot [H_2O] + K_{ads4} [PO]} \end{aligned} \quad (45)$$

$$\begin{aligned}
r_{D2}^* &= k_{D2}^{0*} K_{ads5} [Ti^*] [PO] [CH_3O(PO)H] = k_{D2}^{0*} K_{ads5} f_{Ti} \frac{[Ti^*]}{f_{Ti}} [PO] [CH_3O(PO)H] = k_{D2}^* \frac{[Ti^*]}{f_{Ti}} [PO] [CH_3O(PO)H] = \\
&- k_{D2}^* [TS-1] \frac{K_{ads1} \cdot [H_2O_2] [PO] [CH_3O(PO)H]}{1 + K_{ads1} \cdot [H_2O_2] + K_{ads2} \cdot [C_3H_6] + K_{ads3} \cdot [H_2O] + K_{ads4} [PO]}
\end{aligned} \tag{46}$$

$$\begin{aligned}
r_{D3}^* &= k_{D3}^{0*} K_{ads5} [Ti^*] [PO] [H_2O] = k_{D3}^{0*} K_{ads5} f_{Ti} \frac{[Ti^*]}{f_{Ti}} [PO] [H_2O] = k_{D3}^* \frac{[Ti^*]}{f_{Ti}} [PO] [H_2O] = \\
&= k_{D3}^* [TS-1] \frac{K_{ads1} \cdot [H_2O_2] [PO] [H_2O]}{1 + K_{ads1} \cdot [H_2O_2] + K_{ads2} \cdot [C_3H_6] + K_{ads3} \cdot [H_2O] + K_{ads4} [PO]}
\end{aligned} \tag{47}$$

$$\begin{aligned}
r_{D4}^* &= k_{D4}^{0*} K_{ads5} [Ti^*] [PO] [Oligom] = k_{D4}^{0*} K_{ads5} f_{Ti} \frac{[Ti^*]}{f_{Ti}} [PO] [Oligom] = k_{D4}^* \frac{[Ti^*]}{f_{Ti}} [PO] [Oligom] = \\
&= k_{D4}^* [TS-1] \frac{K_{ads1} \cdot [H_2O_2] [PO] [Oligom]}{1 + K_{ads1} \cdot [H_2O_2] + K_{ads2} \cdot [C_3H_6] + K_{ads3} \cdot [H_2O] + K_{ads4} [PO]}
\end{aligned} \tag{48}$$

As for the ring opening reaction in the absence of hydrogen peroxide, also when hydrogen peroxide is present we have considered that in the kinetic laws (34) and (36), the kinetic constants are the same for both the reaction of PO with methoxy propanol and its oligomers, independently on their molecular weight.

Being the catalyst a solid particle, attention must be paid to the absence of internal diffusion limitation. At this purpose, by applying the Weisz-Prater correlation³⁶ to the initial reaction rates estimated from the slopes of the hydrogen peroxide concentration profiles, we have found in all cases an effectiveness factor always near to the unity. Therefore, we can conclude that the chemical regime is operative and the kinetic expressions found are reliable.

All the collected experimental data have been submitted to a simultaneous mathematical regression analysis, by adopting a 4th order Runge-Kutta algorithm, obtaining the activation energies and the kinetic constant at the reference temperature of 313 K reported in Table 7, together with all the statistical information. An important observation that rises up is that the two biggest equilibrium constants that are K_{ads2} and K_{ads4} respectively related to propene and propene oxide. This means that these two species are competitive in the adsorption on the catalytic sites.

This phenomena could be explained by considering that the physisorption of propene and propene oxide is favored on the hydrophobic surface of TS-1 catalyst^{37,38}.

As a consequence an increase of the propene concentration does not give a linear increase of the reaction rate (as experimentally observed). Moreover, high propene oxide concentration in the system slow down the reaction. Both these aspects must be taken into account in designing a continuous plant. An idea, for example, could be to separate propene oxide at the end of a continuous reactor and feed the resulting part of the mixture to another reactor.

In Figures 9-12, it is possible to appreciate the obtained agreement between experimental and calculated data. As it can be seen, the achieved agreement can be considered satisfactory for both PO conversions and by-products distribution. In this case an average error of about 5% is obtained for all the runs.

4. Conclusions

In this paper, a detailed kinetic investigation on all the reactions occurring in the HPPO process has been performed. In particular, a detailed study has been made on both the hydrogen peroxide decomposition kinetics, the ring opening reactions and the epoxidation reaction, also considering the mass transfer phenomena involved in the process. The kinetic law expressions for describing the mentioned reactions have been proposed and the corresponding parameters determined. This could be useful for the design of the HPPO reactor and for optimizing the yield to PO. A semi-quantitative approach has been applied also to the methanol oxidation reactions in order to define all the possible products. In particular we observed that only at high temperature and catalyst concentration methyl formate and formic acid are formed in appreciable amount. This fact can lead to problems in the PO purification, being methyl formate boiling point very similar to that of PO. Moreover, we have demonstrated that the temperature is a key factor also for the hydrogen peroxide decomposition, observing that at temperature below than 40 °C, the corresponding reaction rate can be considered negligible but, at higher temperatures, the reaction rate becomes faster and faster, and a strong oxygen development has been observed, with a strong increase of the overall pressure. This observation is very helpful, because, for safety reasons in HPPO reactor it is opportune to work at temperatures not higher than 40-50°C in order

to reduce the oxygen concentration in the system and the consequent risk of explosion due to the interaction with propene.

By considering the PO ring opening reactions, we have observed that, the key factors are both temperature, catalyst concentration and hydrogen peroxide concentration. So, even if by increasing the TS-1 amount in the HPPO system the propene conversion gets higher, in the meantime, the selectivity to PO slows down as a consequence of the ring opening reaction. For this reason, it is necessary to choose a good compromise for optimizing the activity and selectivity of the HPPO process. Moreover, it is important to consider that during the propene oxidation, propene oxide selectivity changes with the hydrogen peroxide concentration.

Finally, concerning the main reaction, we have underlined that catalyst concentration is the really key factor of the system, and that reaction rate is not linear dependent on propene concentration. All these information have been translated in general kinetic laws, able to describe all the collected experimental data. These expressions, and the related parameters, can be useful to maximize the HPPO process in terms of safety (hydrogen peroxide decomposition) and productivity.

Acknowledgments

Acknowledgments are due to CONSER S.p.A. that funded this study.

List of symbols

$[C_3H_6]^*$	Solubility concentration [mol/L]
$H_{C_3H_6}$	Henry constant [mol/(L·bar)]
P	Pressure [bar]
p^{MAX}	Maximum reached pressure [bar]
N_J^k	Moles of the J component in the phase k [mol]
F_J	Molar flow-rate of the J component [mol/min]
$J_{C_3H_6}$	Propene mass transfer velocity [mol/min]
k_L	Gas-liquid mass transfer coefficient [cm/min]
a_L	Gas-liquid interfacial area [cm ² /cm ³]
β	Mass transfer coefficient [min ⁻¹]
V	Liquid volume [L]
k_v	Valve opening constant [mol/(min·bar)]
[J]	Concentration of the J component [mol/L]
k_s	Liquid-solid mass transfer coefficient [cm/min]
a_s	Catalyst specific area [cm ² /cm ³]
[TS-1]	Catalyst concentration [g/L]
r_n	Reaction rate of the reaction n [mol/(L·min)]
k_n	Kinetic constant of the reaction n. Units depend on the reaction.
k_n^{ref}	Kinetic constant of the reaction n at a reference temperature. Units depend on the reaction.
E_n	Activation energy of the reaction n [Kcal/mol]
R	Ideal gas constant [Kcal/(K·mol)]
T^{ref}	Reference temperature [K]
T	Temperature [K]
PO	Propene oxide
MetOX	Methoxy propanol
Gly	Propene glycol
Oligom	Polimerization oligomer of the stage n
K_{adsn}	Equilibrium constant (n=1,5) [L/mol]
g_{TS-1}	Catalyst mass [g]
f_{Ti}	Titanium total site concentration on TS-1 [molTi/g _{TS-1}]

Ti^α

α site on titanium

Cited Literature

- (1) Russo, V.; Tesser, R.; Santacesaria, E.; Di Serio, M. Chemical and Technical Aspects of Propene Oxide Production via Hydrogen Peroxide (HPPO Process). *Ind. Eng. Chem. Res.* **2013**, *52*, 1168–1178.
- (2) Nijhuis, T. A.; Makkee, M.; Moulijn, J. A.; Weckhuysen, B. M. The Production of Propene Oxide: Catalytic Processes and Recent Developments. *Ind. Eng. Chem. Res.* **2006**, *45* (10), 3447–3459.
- (3) Bassler, P.; Weidenbach, M.; Goebbel, H. The new HPPO Process for Propylene Oxide: From Joint Development to worldscale Production. *Chemical Engineering Transactions* **2010**, *21*, 571-576.
- (4) Clerici, M. G. TS-1 and Propylene Oxide, 20 Years Later; *Erdöl, Erdgas, Kohle* **2006**, *122* (6), OG77-OG82.
- (5) Taramasso, M.; Perego, G.; Notari, B. Preparation of porous crystalline synthetic material comprised of silicon and titanium oxides. US 4410501, 1983.
- (6) Neri, C.; Anfossi, B.; Esposito, A. ; Buonomo, F. Process for the epoxidation of olefinic compounds. IT 22608, 1982.
- (7) Neri, C.; Anfossi, B.; Esposito, A.; Buonomo, F. Process for the epoxidation of olefinic compounds. EP 100119, 1986.
- (8) Clerici, M. G.; Bellussi, G.; Romano, U. Synthesis of Propylene Oxide from Propylene and Hydrogen Peroxide Catalyzed by Titanium Silicalite. *J. Catal.* **1991**, *129*, 159-167.
- (9) Clerici, M. G.; Ingallina, P. Epoxidation of lower olefins with Hydrogen-Peroxide and Titanium Silicalite. *J. Catal.* **1993**, *140*, 71-83.
- (10) To, J.; Sherwood, P.; Sokol, A. A.; Bush, I. J.; Richard, C.; Catlow, A.; van Dam, H. J. J.; French, S. A.; Guest, M. F. QM/MM modelling of the TS-1 catalyst using HPCx. *J. Mater. Chem.* **2006**, *16*, 1919–1926.
- (11) Bordiga, S.; Coluccia, S.; Lamberti, C.; Marchese, L.; Zecchina, A; Boscherini, F.; Buffa, F.; Genoni, F.; Leofanti, G.; Petrini, G.; Vlais, G. XAFS Study of Ti-Silicalite: Structure of Framework Ti(IV) in the Presence and Absence of Reactive Molecules (H₂O, NH₃) and Comparison with Ultraviolet-Visible and IR Results. *Phys. Chem.* **1994**, *98* (15), 4125–4132.
- (12) Short, P. L. BASF, Dow Open Novel Propylene Oxide Plant. *Chem.Eng. News* **2009**, *87* (11), 21.
- (13) <http://www.knak.jp/big/evonik-hppo.htm> (accessed Mar 20, 2014).
- (14) <http://corporate.evonik.com/en/media/search/Pages/news-details.aspx?newsid=26719> (accessed Mar 20, 2014).

- (15) <http://www.dow.com/polyurethane/news/2012/20120104a.htm> (accessed Mar 20, 2014).
- (16) Bellussi, G.; Carati, A.; Clerici, M. G.; Maddinelli, G.; Millini, R. Reactions of titanium silicalite with protic molecules and hydrogen peroxide. *J. Catal.* **1992**, *133*, 220-230.
- (17) Khouw, C. B.; Dartt, C. B.; Labinger, J. A.; Davis, M. E. Studies on the Catalytic-Oxidation of Alkanes and Alkenes by Titanium Silicates. *J. Catal.* **1994**, *149* (1), 195–205.
- (18) Bonino, F.; Damin, A.; Ricchiardi, G.; Ricci, M.; Spanò, G.; D'Aloisio, R.; Zecchina, A.; Lamberti, C.; Prestipino, C.; Bordiga, S. Ti-Peroxo Species in the TS-1/H₂O₂/H₂O System. *J. Phys. Chem. B* **2004**, *108*, 3573-3583.
- (19) Shin, S. B.; Chadwick, D. Kinetics of Heterogeneous Catalytic Epoxidation of Propene with Hydrogen Peroxide over Titanium Silicalite (TS-1). *Ind. Eng. Chem. Res.* **2010**, *49*, 8125–8134.
- (20) Liang, X.; Mi, Z.; Wu, Y.; Wang, L.; Xing, E. Kinetics of epoxidation of propylene over TS-1 in isopropanol. *React. Kinet. Catal. Lett.* **2003**, *80* (2), 207-215.
- (21) Danov, S. M.; Sulimov, A. V.; Kolesnikov, V. A.; Ovcharov, A. A. Kinetics of Propylene Epoxidation with Hydrogen Peroxide. *Kinetics and Catalysis* **2013**, *2*, 193-198.
- (22) Clerici, M. G. Oxidation of saturated-hydrocarbons with Hydrogen-Peroxide, catalyzed by Titanium Silicalite. *Appl. Catal.* **1991**, *68*, 249-261.
- (23) Clerici, M. G. The role of the solvent in TS-1 chemistry: active or passive? An early study revisited. *Topics Catal.* **2001**, *15*, 257-263.
- (24) Maspero, F.; Romano, U. Oxidation of alcohols with H₂O₂ catalyzed by Titanium Silicalite-1. *J. Catal.* **1994**, *146*, 476-482.
- (25) Clerici, M. G.; Ingallina, P.; Millini, R. Titanium Silicalite-1 Peroxides. *Proceedings of 9th International Zeolite Conference, Montreal 1992*. Butterworth-Heinemann: Boston, 1993, 445.
- (26) Zuo, Y.; Wang, M.; Song, W.; Wang, X.; Guo, X.. Characterization and Catalytic Performance of Deactivated and Regenerated TS-1 Extrudates in a Pilot Plant of Propene Epoxidation. *Ind. Eng. Chem. Res.* **2012**, *51*, 10586–10594.
- (27) Thiele, G.F.; Roland, E. Propylene epoxidation with hydrogen peroxide and titanium silicalite catalyst: Activity, deactivation and regeneration of the catalyst. *Journal of Molecular Catalysis A: Chemical* **1997**, *117*, 351-356.
- (28) Santacesaria, E.; Tesser, R.; Di Serio, M.; Russo, V.; Turco, R. A New Simple Microchannel Device To Test Process Intensification. *Ind. Eng. Chem. Res.* **2011**, *50* (5), 2569–2575.
- (29) Teles, J. H.; Rehfinger, A.; Bassler, P.; Wenzel, A. Method for the production of propylene oxide. US 6756503 B2, 2004.

- (30) Kolthoff, I. M.; Sandell, E. B.; Meehan, E. J. *Treatise Analytical Chemistry, Vol. 2*. Wiley: New York, 1978.
- (31) Perry, H.; Green, D. W. *Perry's Chemical Engineers' Handbook*, 7th edition; McGraw Hill: New York, 1999.
- (32) Tesser, R.; Di Serio, M.; Vitiello, R.; Russo, V.; Ranieri, E.; Speranza, E.; Santacesaria, E. Glycerol Chlorination in Gas-Liquid Semibatch Reactor: An Alternative Route for Chlorohydrins Productions. *Ind. Eng. Chem. Res.* **2012**, *51* (26), 8768-8776.
- (33) Sano, Y.; Yamaguchi, N.; Adachi, T. J. Mass transfer coefficients for suspended particles in agitated vessels and bubble columns. *Chem. Eng. Jpn.* **1974**, *7*, 255-261.
- (34) Russo, V.; Protasova, L.; Turco, R.; De Croon, M. H. J. M.; Hessel, V.; Santacesaria, E. Hydrogen Peroxide Decomposition on Manganese Oxide Supported Catalyst: From Batch Reactor to Continuous Microreactor. *Ind. Eng. Chem. Res.* **2013**, *52*, 7668-7676.
- (35) Di Serio, M.; Tesser, R.; Dimiccoli, A.; Santacesaria, E. Kinetics of Ethoxylation and Propoxylation of Ethylene Glycol Catalyzed by KOH. *Ind. Eng. Chem. Res.* **2002**, *41*, 6772.
- (36) Weisz, P. B.; Prater, C. D. Interpretation of Measurements in Experimental Catalysis. *Advances in Catalysis* **1954**, *6*, 143-196.
- (37) Weitkamp, J.; Ernst, S.; Roland, E.; Thiele, G.F. The modified hydrophobicity index as a novel method for characterizing the surface properties of titanium silicalites. *Studies in Surface Science and Catalysis* **1997**, *105*, 763-770.
- (38) Perego, C.; Carati, A.; Ingallina, P.; Mantegazza, M.A.; Bellussi, G. Production of titanium containing molecular sieves and their application in catalysis. *Applied Catalysis A: General* **2001**, *221*, 63-72.

List of Tables

Table 1 – List of the performed runs for the study of hydrogen peroxide decomposition and methyl formate formation, with related experimental conditions. Hydrogen peroxide conversion ($X_{H_2O_2}$), maximum reached pressure (P^{MAX}), methyl formate and formic acid concentrations data are related to 5 hours of reaction time. D0: blank run; D1-D8: runs performed in different operative conditions.

Run	T [°C]	H ₂ O ₂ ⁰ [wt.%]	TS-1 [wt.%]	X _{H₂O₂} [%]	P ^{MAX} [bar]	Methyl formate [mmol/dm ³]	Formic acid [mmol/dm ³]
D0	70	9.37	-	6.44	5	0.0	0.0
D1	70	9.10	2.22	95.13	>30	90.8	46.9
D2	60	9.14	2.22	62.51	18	5.6	0.0
D3	50	9.10	2.22	27.00	10	0.0	0.0
D4	40	9.10	2.22	8.41	7	0.0	0
D5	60	8.45	4.46	90.38	>20	36.6	28.2
D6	60	8.44	3.34	71.89	20	10.2	13.2
D7	40	9.62	4.43	28.74	10	0	0
D8	40	9.15	6.60	35.14	12	0	0

Table 2 – List of the performed runs for the study of the ring opening reactions. AA0a, AA0b: blank runs; AA1-AA6: runs performed in the presence of only methanol; AA7-AA13: runs performed in the presence of both water and methanol; AA14-AA21: runs performed in the presence of methanol, water and hydrogen peroxide.

Run	T [°C]	C ₃ H ₆ O [wt.%]	CH ₃ OH [wt.%]	H ₂ O [wt.%]	H ₂ O ₂ [wt.%]	TS-1 [wt.%]	P _{N₂} [bar]	P _{C₃H₆} [bar]
AA0a	70	5.84	94.16	-	-	-	5.0	-
AA0b	30	5.51	88.70	2.38	3.40	-	5.0	-
AA1	40	5.84	94.16	-	-	4.00	5.0	-
AA2	50	5.84	94.16	-	-	4.00	5.0	-
AA3	60	5.84	94.16	-	-	4.00	5.0	-
AA4	40	5.84	94.16	-	-	5.00	5.0	-
AA5	40	5.84	94.16	-	-	3.00	5.0	-
AA6	40	5.84	94.16	-	-	1.10	5.0	-
AA7	40	5.56	89.48	4.96	-	4.00	5.0	-
AA8	50	5.56	89.48	4.96	-	4.00	5.0	-
AA9	30	5.56	89.48	4.96	-	4.00	5.0	-
AA10	40	5.56	89.48	4.96	-	5.00	5.0	-
AA11	40	5.56	89.48	4.96	-	3.00	5.0	-
AA12	40	5.56	89.48	4.96	-	2.00	5.0	-
AA13	30	5.56	89.46	4.98	-	2.00	5.0	-
AA14	36	5.51	88.70	2.44	3.35	4.00	5.0	-
AA15	30	5.51	88.70	2.39	3.40	2.00	5.0	-
AA16	30	5.51	88.70	2.34	3.45	1.00	5.0	-
AA17	40	5.56	89.45	3.28	1.71	2.00	5.0	-
AA18	30	5.56	89.46	3.21	1.77	2.00	5.0	-
AA19	30	5.56	89.46	4.10	0.88	2.00	5.0	-
AA20	30	5.56	89.46	4.57	0.41	2.00	5.0	-
AA21	30	5.56	89.46	4.97	0.01	2.00	5.0	-

Table 3 – List of the performed runs for the propene oxide synthesis reaction.

Run	T [°C]	CH ₃ OH [wt.%]	H ₂ O [wt.%]	H ₂ O ₂ [wt.%]	TS-1 [wt.%]	P _{N₂} [bar]	P _{C₃H₆} [bar]
PO1	40	93.20	3.20	3.60	0.40	3.02	0.73
PO2	40	93.20	3.20	3.60	1.00	3.02	0.73
PO3	40	93.20	3.20	3.60	2.00	3.02	0.73
PO4	40	93.20	3.20	3.60	0.40	2.33	1.42
PO5	40	93.20	3.20	3.60	0.40	0.64	3.11
PO6	30	93.20	3.20	3.60	0.40	3.02	0.73
PO7	40	93.20	3.20	3.60	0.70	3.02	0.73
PO8	40	60.00	36.40	3.60	0.40	3.02	0.73

Table 4 – Summary of the performed mass transfer experimental runs.

Run	Temperature [°C]	Stirring rate [rpm]	P _{N2} [bar]	P _{C3H6} [bar]	β [min ⁻¹]
F1	40	300	3.02	0.73	0.222 ± 0.02
F2	40	500	3.02	0.73	0.323 ± 0.04
F3	40	700	3.02	0.73	0.367 ± 0.02
F4	40	10	3.02	0.73	0.086 ± 0.03
F5	40	500	2.33	1.42	0.323 ± 0.03
F6	40	500	0.64	3.11	0.328 ± 0.06
F7	50	500	3.02	0.73	0.323 ± 0.04
F8	30	500	3.02	0.73	0.324 ± 0.06

Table 5 – List of the kinetic parameters obtained by mathematical regression analysis on the hydrogen peroxide decomposition tests (kinetic constants at the reference temperature of 313 K), with related statistical information.

Parameter	Optimal Estimate	Confidence Intervals			Standard Deviation
		90%	95%	99%	
E_d [Kcal/mol]	1.95E+01	2.84E-02	3.40E-02	4.54E-02	1.69E-02
k_d^{ref} [L/(g _{TS-1} ·min)]	2.45E-05	6.82E-08	8.15E-08	1.09E-07	2.43E-06

Table 6 – List of the kinetic parameters obtained by mathematical regression analysis on the propene oxide decomposition tests performed in the presence of methanol alone or of both methanol and water (kinetic constants at the reference temperature of 313 K), with related statistical information.

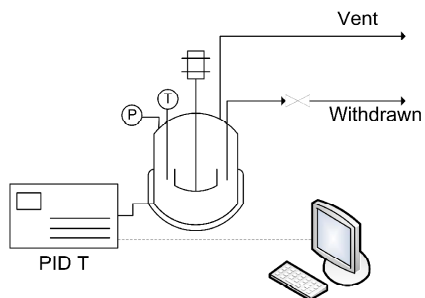
Parameter	Optimal Estimate	Confidence Intervals			Standard Deviation	
		90%	95%	99%		
E_{D1}	[Kcal/mol]	1.07E+01	1.17E+00	1.39E+00	1.84E+00	7.07E-01
E_{D2}	[Kcal/mol]	3.40E+01	1.28E+01	1.53E+01	2.02E+01	7.78E+00
E_{D3}	[Kcal/mol]	1.60E+01	5.78E+00	6.90E+00	9.09E+00	3.50E+00
$k_{D1,ref}$	[L ² /(g _{TS-1} ·mol·min)]	9.48E-06	2.94E-07	3.51E-07	4.63E-07	1.78E-07
$k_{D2,ref}$	[L ² /(g _{TS-1} ·mol·min)]	6.07E-06	7.28E-06	8.69E-06	1.15E-05	4.41E-06
$k_{D3,ref}$	[L ² /(g _{TS-1} ·mol·min)]	1.14E-05	2.20E-06	2.62E-06	3.46E-06	1.33E-06

Table 7 – List of the kinetic parameters obtained by mathematical regression analysis on the propene oxide synthesis tests (kinetic constants at the reference temperature of 313 K), with related statistical information.

Parameter	Optimal Estimate	Confidence Intervals			Standard Deviation
		90%	95%	99%	
E_1^* [Kcal/mol]	1.09E+01	4.66E-02	5.56E-02	7.34E-02	2.82E-02
E_{D1}^* [Kcal/mol]	2.54E+01	1.28E+00	1.37E+00	1.97E+00	7.05E-01
E_{D2}^* [Kcal/mol]	3.02E+01	1.32E+01	1.15E+01	1.98E+01	7.75E+00
E_{D3}^* [Kcal/mol]	3.51E+01	5.62E+00	6.84E+00	9.12E+00	3.45E+00
k_1^{ref} [L/(g _{TS-1} ·min)]	2.98E+01	1.32E+00	1.57E+00	2.08E+00	7.96E-01
$k_{D1}^{*,ref}$ [L ² /(g _{TS-1} ·mol·min)]	1.18E-01	2.87E-02	3.56E-02	4.54E-02	1.45E-06
$k_{D2}^{*,ref}$ [L ² /(g _{TS-1} ·mol·min)]	3.11E-04	7.32E-05	8.73E-05	1.23E-05	4.38E-05
$k_{D3}^{*,ref}$ [L ² /(g _{TS-1} ·mol·min)]	4.40E-02	2.23E-03	2.58E-03	3.34E-03	1.57E-05
K_{ads1} [L/mol]	3.47E-03	2.73E-06	3.25E-06	4.30E-06	1.65E-06
K_{ads2} [L/mol]	8.28E+00	4.93E-02	5.89E-02	7.77E-02	2.98E-02
K_{ads3} [L/mol]	4.54E-01	2.21E-03	2.63E-03	3.48E-03	1.33E-03
K_{ads4} [L/mol]	7.58E+00	1.01E-01	1.21E-01	1.59E-01	6.10E-02

List of Figures

A



B

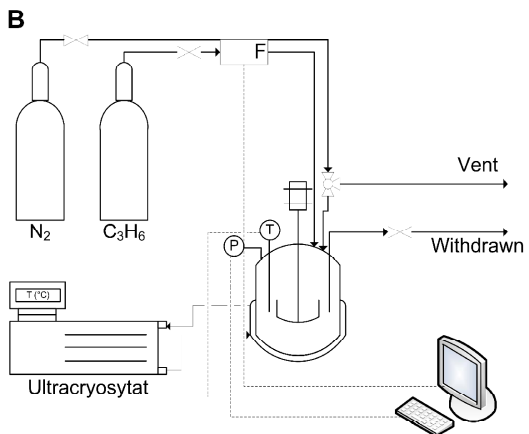


Figure 1 – Sketch, with related pictures, of the reactors used for the HPPO kinetics investigation. A. Side reaction investigation reactor; B. Main reaction investigation reactor: the details are related to the data acquisition system and the gaseous stirrer effect.

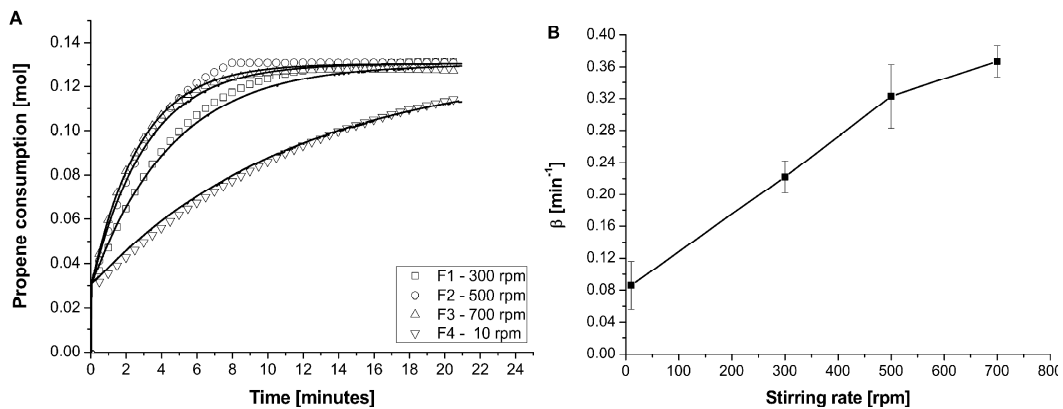


Figure 2 – A. Fluid-dynamic characterization tests performed at different stirring rates. B. Trend of the mass transfer coefficient with the stirring rate.

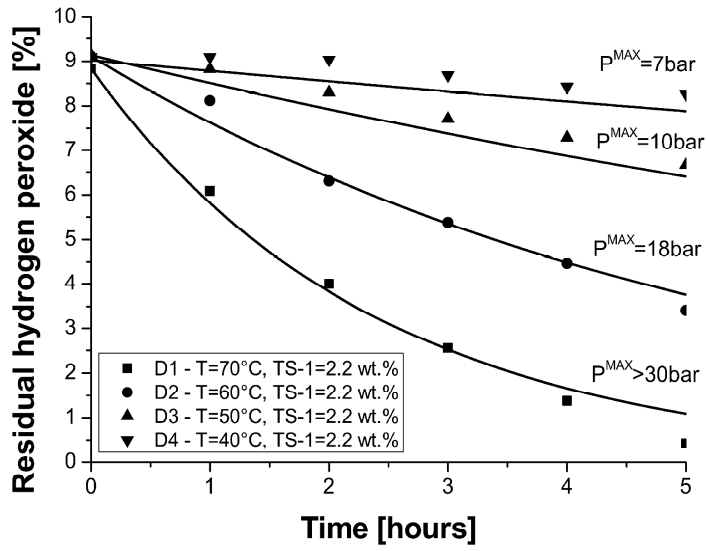


Figure 3 – Temperature effect on hydrogen peroxide decomposition and related simulations. Experimental conditions reported in Table 1.

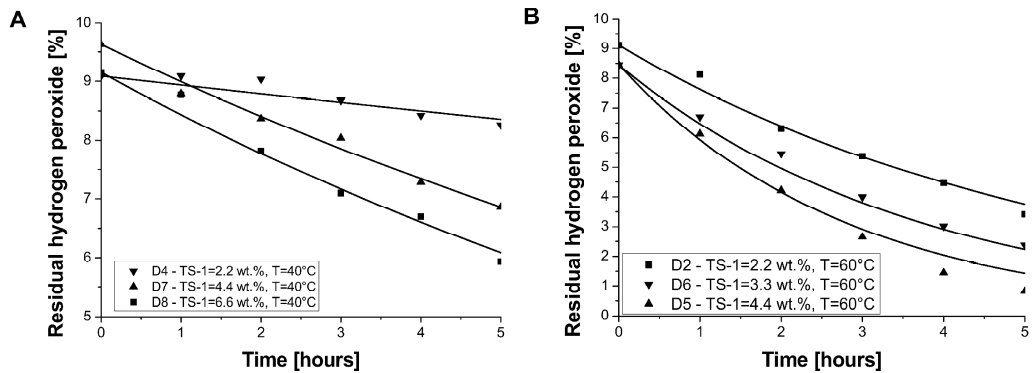


Figure 4 – Catalyst concentration effect on hydrogen peroxide decomposition and related simulations for: A. Runs in Table 1, performed at 40°C . B. Runs in Table 1, performed at 60°C.

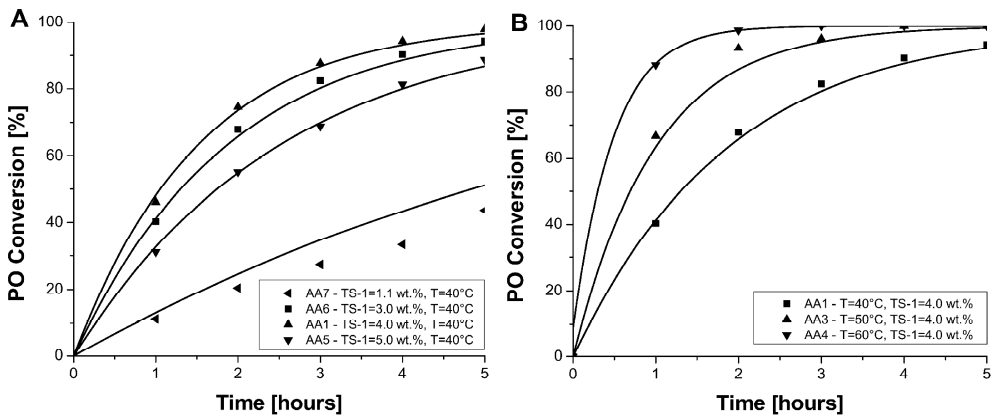


Figure 5 – A. Effect of catalyst concentration on the propene oxide degradation in the presence of methanol and related simulations. B. Effect of temperature on the propene oxide degradation in the presence of methanol and related simulations. X_{PO} stands for propene oxide conversion.

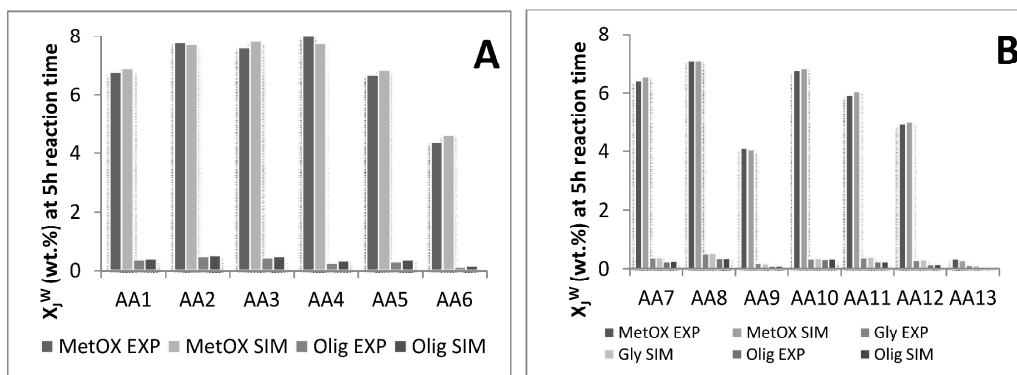


Figure 6 – By-products distribution at 5 hours of ring opening reaction time, for: A. Runs AA1-AA6 of Table 2, B. Runs AA7-AA13 of Table 2.

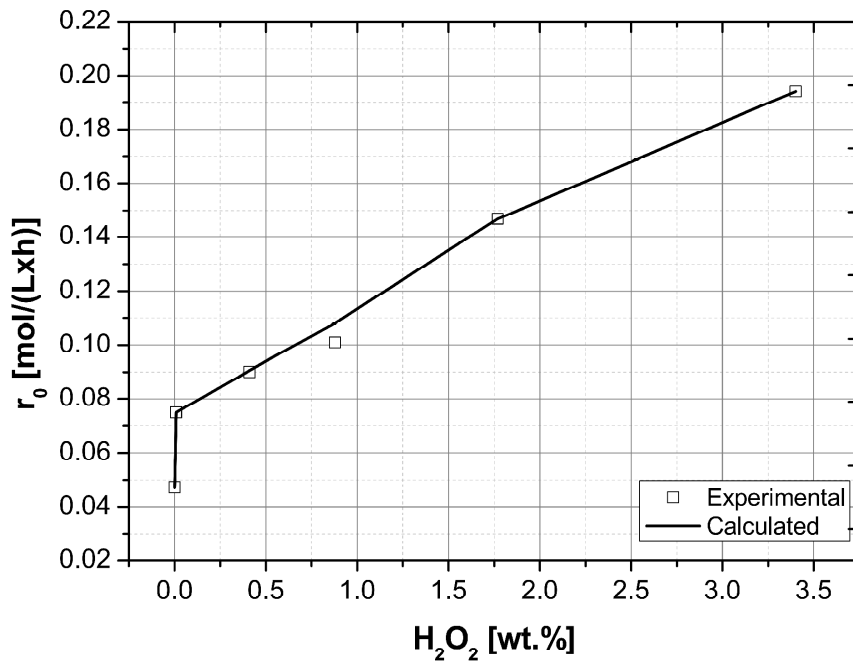


Figure 7 – Initial reaction rate trend for the ring opening reactions as a function of the hydrogen peroxide conversion (Runs AA13, AA15 and AA18-AA21 of Table 2).

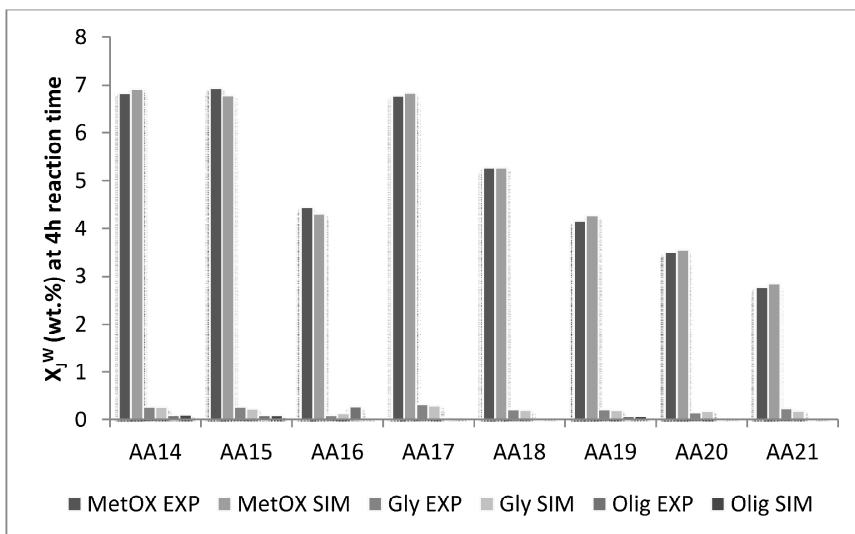


Figure 8 – By-products distribution at 4 hours of ring opening reaction time, for Runs AA14-AA21 of Table 2.

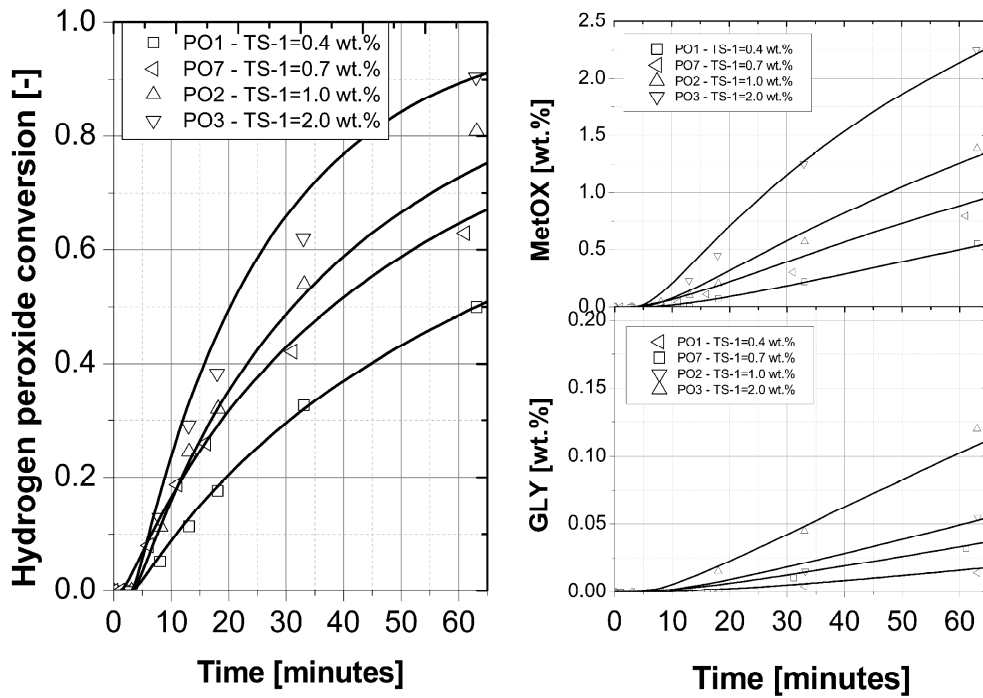


Figure 9 – Hydrogen peroxide conversion and by-product distribution for different catalyst concentration (Runs PO1-PO3 and PO7 of Table 3).

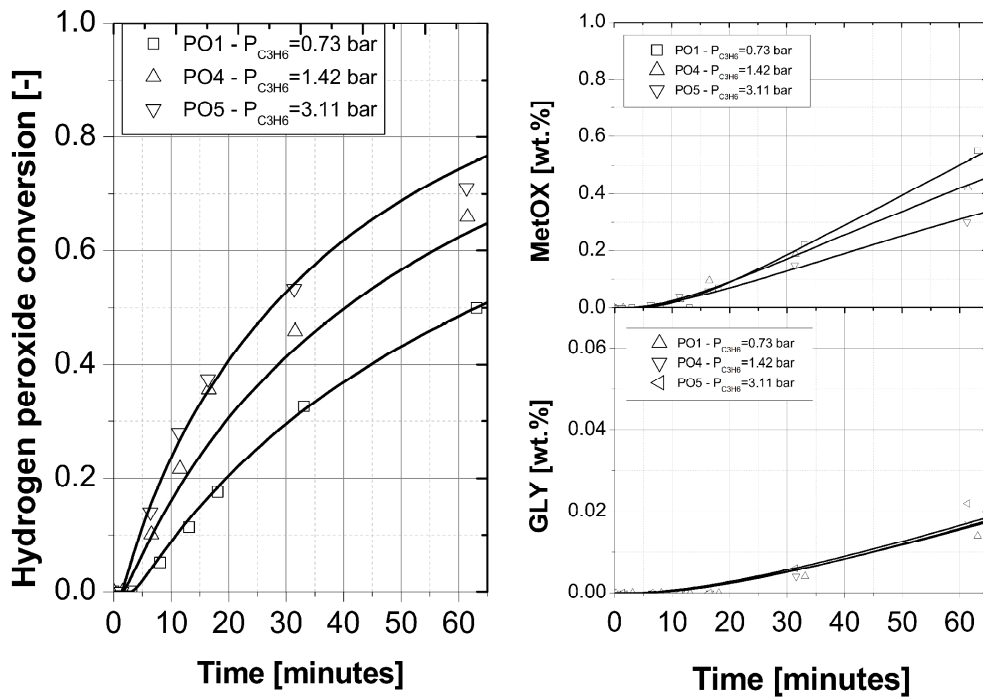


Figure 10 – Hydrogen peroxide conversion and by-product distribution for different propene partial pressure (Runs PO1, PO4 and PO5 of Table 3).

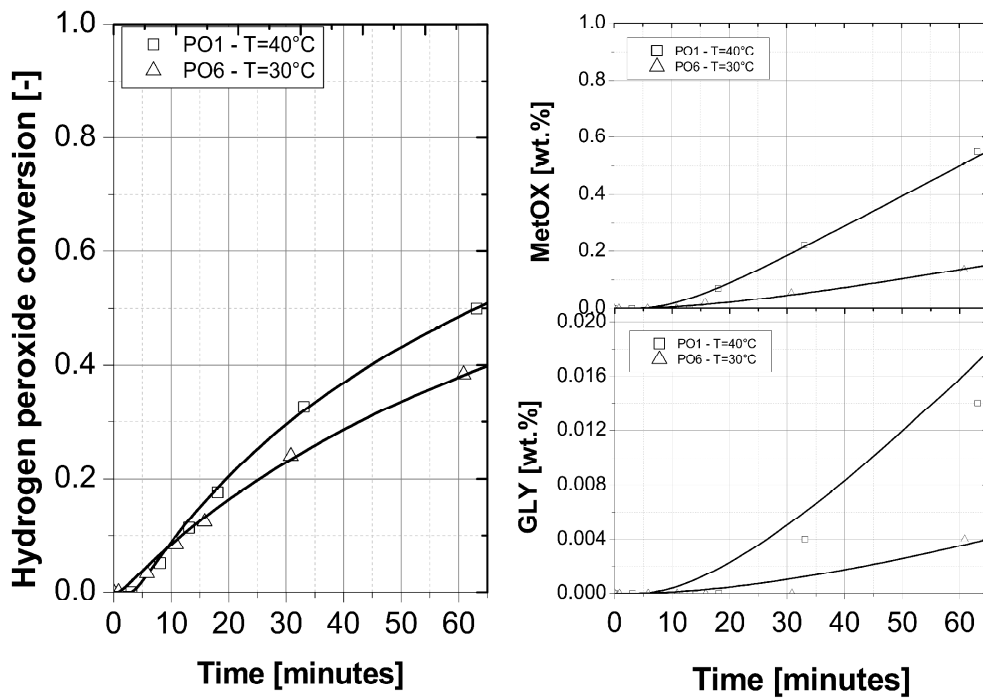


Figure 11 – Hydrogen peroxide conversion and by-product distribution for different temperatures (Runs PO1 and PO6 of Table 3).

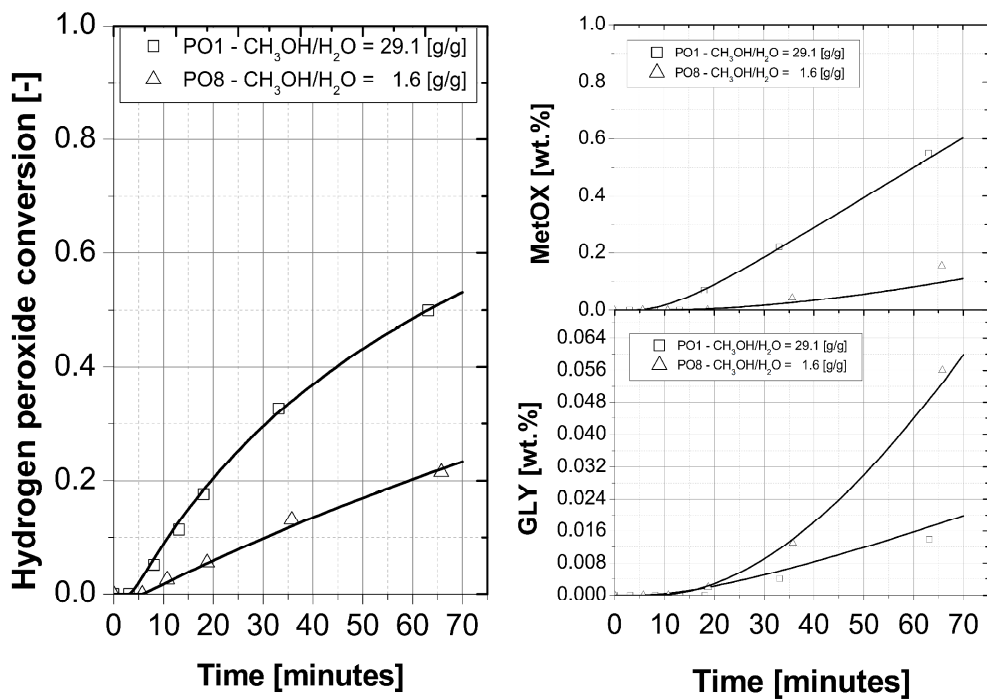


Figure 12 – Hydrogen peroxide conversion and by-product distribution for different methanol/water ratio (Runs PO1 and PO8 of Table 3).

Hydrogen Peroxide Decomposition on Manganese Oxide Supported Catalyst: From Batch Reactor to Continuous Microreactor

V. Russo,[†] L. Protasova,^{‡,§} R. Turco,[†] M. H. J. M. de Croon,^{||} V. Hessel,[‡] and E. Santacesaria^{*,†}

[†]Dipartimento di Scienze Chimiche, University of Naples Federico II, Naples Industrial Chemistry Laboratory (NICL), Complesso di Monte Sant'Angelo, Via Cintia, 80126 Napoli, Italy

[‡]Micro Flow Chemistry and Process Technology Group and ^{||}Laboratory of Chemical Reactor Engineering, Eindhoven University of Technology, P.O. Box 513, 5600 MB Eindhoven, The Netherlands

ABSTRACT: The decomposition of hydrogen peroxide, promoted by a manganese oxide catalyst supported on γ -alumina, has been studied in three different reactors. A batch reactor was used for catalyst screening and for studying the reaction kinetics, whereas a tubular continuous reactor was used for catalyst life testing and manganese loading optimization. In fact, a progressive deactivation was observed passing from 80% to 30% conversion. The final value of conversion remained unchanged for a long time. The deactivation was due to partial manganese dissolution. On the contrary, a residual activity was observed, because the undissolved manganese oxide was more strongly bonded to the alumina surface. Therefore, by reducing the amount of loaded manganese from 5 to 2 wt %, a stable catalyst was obtained. Then, catalysts containing different amounts of manganese oxide (up to 2 wt %) were prepared and tested in a kinetic study. The same catalysts were deposited as catalytic coatings on the channels wall of microchanneled stainless steel plates and tested for coating stability. Finally, the best catalyst was also deposited on the walls of a microreactor to verify the possibility of process intensification. The kinetic law derived from the batch runs was successfully used to simulate the performance of the microreactor.

1. INTRODUCTION

Some industrial processes are based on the use of hydrogen peroxide as an oxidant. Significant examples include the reactions of double-bond epoxidation for the production of propene oxide from propene¹ and epoxidized soybean oil.² In both cases, as well as in other industrial processes, an excess of hydrogen peroxide is normally used to increase, as much as possible, the reagent conversion. Therefore, at the end of the reaction, some unreacted hydrogen peroxide needs to be eliminated before the effluents can be discharged into the environment. It is possible to eliminate hydrogen peroxide simply by creating a strong basic environment by adding NaOH to the residual hydrogen peroxide solution. Under these conditions, hydrogen peroxide spontaneously and promptly decomposes to water and oxygen. This is a common practice in industry, because of its simplicity; however, it has many serious drawbacks. The decomposition of hydrogen peroxide is a strongly exothermic reaction ($\Delta H = -98$ kJ/mol), and the decomposition rate must be strictly controlled, although this is often difficult to achieve. In particular, in soybean oil epoxidation, an alkaline environment gives rise to a partial hydrolysis with the formation of free fatty acids that are undesired contaminants of the final product. Moreover, the basic environment created to decompose hydrogen peroxide requires a subsequent neutralization step that is detrimental for the environment. Finally, this operation is not simple to realize in the case of a continuous plant. A valuable alternative is to use a heterogeneous catalyst that promotes hydrogen peroxide decomposition.³ It is known, for example, that stainless steel promotes the decomposition of hydrogen peroxide under neutral or moderately acid conditions.³ Many heterogeneous catalysts have been suggested in the literature to be very active

in promoting hydrogen peroxide decomposition. In particular, a list of these catalysts includes different metals such as platinum, silver, cobalt, palladium, and manganese,^{4–8} as well as different oxides and salts.^{9,10} Manganese oxides, in particular, have shown the greatest activity in promoting this reaction.^{11–13} As mentioned before, the use of a heterogeneous catalyst is particularly favorable for continuous operations. Moreover, this operation could be advantageously intensified by using microreactors with a catalytic coating deposited on their walls.^{14–19} The two dominant methods of embedding a heterogeneous catalyst in a microflow reactors is by coating the walls [with wash-coating being the most prominent technique,²⁰ although physical vapor deposition (PVD),^{21,22} chemical vapor deposition (CVD),^{21,23} sol–gel processing,^{21,24–26} and others are also used] and by forming small, preferably uniform, beads or grains into a tight assembly, which constitutes a mini-fixed reactor²⁷ with open voids whose internal dimensions are commonly in the micrometer range and form a three-dimensional channel network. These concepts represent generically different ways to overcome heat- and mass-transfer limitations and to cope with pressure loss and residence time distributions, and the manufacture of such catalysts, on an industrial scale, is also projected to have very different costs. As a result, the manufacturing costs of the catalysts (including their embedding in the microreactor) is a decisive factor in the total costs of the combined process intensification approach with flow processing or joint flow–

Received: December 20, 2012

Revised: March 22, 2013

Accepted: May 21, 2013

Published: May 21, 2013

microwave processing. The choice of a catalyst (its activity, stability, and manufacturing costs) ultimately determines whether a flow process will be economical (i.e., result in positive cash flow), as shown in refs 28 and 29.

In this work, we used manganese oxide, supported on γ -alumina (powder and pellets), as a catalyst and evaluated its kinetic behavior in both batch and continuous reactors. The objectives of this research were to determine the best operating conditions, catalyst stability, kinetic law equation, and related kinetic parameters. Then, after the best catalyst recipe had been identified, we deposited a catalytic coating of the same composition on microchanneled stainless steel plates by the wash-coating technique.^{14–19} The obtained coating was characterized in depth to evaluate its consistency and resistance.^{14–19} Finally, the walls of a microreactor, appropriately designed to favor local mixing, were coated with the best catalyst and tested in a continuous run of hydrogen peroxide decomposition. The kinetic law, derived from batch runs, was successfully used to simulate the performance of the microreactor by operating under a moderate pressure (0.4–0.5 MPa) and reduce the volume of oxygen developed inside the reactor.

2. EXPERIMENTAL SECTION

2.1. Reagents. Boehmite (Pural SB-1) was obtained from Sasol, γ - Al_2O_3 from Fluka and Alfa Aesar, urea from Merck and H_2O_2 from Solvay Italia. All other reagents were supplied by Sigma-Aldrich at the highest level of purity available and were used as received without further purification.

2.2. Analytical Methods. The residual hydrogen peroxide concentration was determined analytically by iodometric titration.³⁰ The developed oxygen flow rate was determined by gas-volumetric analysis as described elsewhere.³ The Brunauer–Emmett–Teller (BET) surface areas, pore sizes, and pore volumes of the powders were determined with a Micromeritics ASAP 2400 instrument using nitrogen adsorption at 77 K. The scanning electron microscopy (SEM) was performed with a Quanta 3D FEG microscope at 30 kV with a resolution of 1.2 nm. XRD spectra were recorded on a Rigaku Geigerflex device with Cu $K\alpha$ radiation (40 kV, 40 mA) by continuous scan (1.5°/min).

In coating resistance tests, adherence was determined in terms of the weight loss of the coated plates after a drop test in which the plates were placed in a holder and dropped from a distance of 65 cm; the procedure was repeated five times. Weight loss was calculated as

$$x = \frac{(m_{cp1} - m_p) - (m_{cp2} - m_p)}{(m_{cp1} - m_p)} \times 100\% \quad (1)$$

where m_{cp1} is the weight of the coated plate before the drop test, m_{cp2} is the weight of the coated plate after the drop test, and m_p is the weight of the uncoated plate.

2.3. Apparatus. Three different types of reactors were used to perform the experimental runs described in this work. In particular, a glass-jacketed batch reactor with a volume of 100 cm^3 was used for both the catalytic screenings and the kinetic study of the powdered catalysts. The evolution with time of the hydrogen peroxide decomposition rate was monitored by gas-volumetric analysis in terms of the volume of oxygen produced, as described elsewhere.³

Continuous runs were performed in two different reactors. A packed-bed tubular reactor (length, 20 cm; inner diameter, 1 cm) was used to study the stability on stream of the manganese

oxide catalyst. The reactor was packed with 3 g of catalyst in spherical pellets of 2.5-mm diameter containing 5 wt % manganese. The catalyst was diluted along the bed with 17 g of glass spheres of 2.5-mm diameter.

Another continuous reactor (a disk-shaped single-plate microreactor with a void volume of 1.78 cm^3) is shown in Figure 1. The internal geometry of the reactor favors local

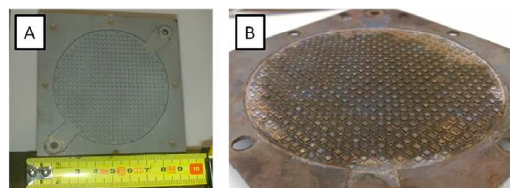


Figure 1. (A) Disk-shaped single-plate microreactor. (B) Coated-plate microreactor.

micromixing. The metallic walls of the reactor were coated with 50 mg of a catalyst whose composition was optimized by means of the runs performed in the previously described reactors. The metallic plate was covered with a polytetrafluoroethylene (PTFE) sheet held in place with another metallic plate.

The reactor was designed to have channels with a width of 0.4 mm. The continuous setup was arranged to operate between 0.1 and 0.5 MPa, to allow for the investigation of the effect of pressure on the decomposition of hydrogen peroxide. This point is very important for fluid dynamics, because the decomposition of hydrogen peroxide releases a great volume of gaseous oxygen, as indicated by the stoichiometry of the reaction



In fact, increasing the conversion of hydrogen peroxide increases the amount of oxygen released. Therefore, when operating at low pressure, the liquid hold-up is strongly reduced by the evolved oxygen, and the interpretation of the kinetic data becomes complicated. Clearly, by increasing the pressure in the reactor, the gas hold-up can be reduced linearly, so that, at 5 bar, the conversion is less affected by the presence of a gas phase and the kinetic data can be more easily interpreted.

As can be seen from Figure 1, the static mixer elements were designed as small cubes with one of the edges orthogonal to the liquid flux direction. This means that, when the flux encounters one cube, it is split in two different portions, with an angle of 90°, each of which encounters the flows coming from the adjacent cubes. This provides very active local micromixing. This phenomenon is enhanced by the disk-shaped geometry, because, when the flowing liquid reaches the disk border, it is reflected toward the center through the microchannels, thereby increasing the back-mixing effect. The described reactor is similar to the multimicropillar reactor recently introduced by de Loos et al.,³¹ although the microchannels are larger in our case.

2.4. Methods. **2.4.1. Catalyst Preparation and Screening.** A preliminary screening of catalysts was performed by testing different catalysts, including ZnO , Fe_2O_3 , Fe_3O_4 , Ni , and MnO_x . Only the MnO_x catalysts were prepared in this work; the other catalysts were purchased from Sigma-Aldrich. As MnO_x was confirmed to be the best catalyst, further investigations focused on only this catalyst. In particular,

manganese was supported on γ - Al_2O_3 (in both powder and pellet form) by the dry impregnation technique, using a solution of $\text{Mn}(\text{CH}_3\text{COO})_2 \cdot 4\text{H}_2\text{O}$ in water as the precursor. The alumina pellets were spheres of 2.5-mm diameter. Depending on the amount of Mn to be loaded, solutions of the precursor with different concentrations were used.

The catalytic coatings of Mn-doped alumina were prepared by two methods (see the details at the end of this section): impregnation of alumina coatings with Mn precursor solution [$\text{Mn}(\text{CH}_3\text{COO})_2 \cdot 4\text{H}_2\text{O}$ in water] and deposition of Mn-containing alumina sol. In the first case (see Table 1, entries A),

Table 1. Mn-Doped Alumina Coatings

Mn catalyst ^a	Mn content (calculated) (wt %)	Al_2O_3 recipe	Al_2O_3 BET surface area (m^2/g)	preparation
Mn(0.5)-2-A	0.5	2	78	A
Mn(0.5)-3-A	0.5	3	214	A
Mn(2)-2-A	2	2	78	A
Mn(2)-3-A	2	3	214	A
Mn(5)-2-A	5	2	78	A
Mn(0.5)-1-B	0.5	1	320	B
Mn(2)-1-C	2	1	320	C

^aNotation: Mn(weight percentage)- Al_2O_3 recipe-preparation mode.

the alumina coatings (ca. 55 mg each) were impregnated with 120 μL of Mn-containing solution, composed of 52, 208, or 520 mg of $\text{Mn}(\text{CH}_3\text{COO})_2 \cdot 4\text{H}_2\text{O}$ in 5 cm^3 of H_2O to obtain coatings of 0.5, 2, and 5 wt % Mn, respectively, on alumina. In the second case, two compositions were employed: in situ preparation with 22 mg of $\text{Mn}(\text{CH}_3\text{COO})_2 \cdot 4\text{H}_2\text{O}$ and 4.7 g of Al_2O_3 (see Table 1, entry B) and in situ preparation with 88 mg of $\text{Mn}(\text{CH}_3\text{COO})_2 \cdot 4\text{H}_2\text{O}$ and 4.7 g of Al_2O_3 (see Table 1, entry C).

The alumina sols were prepared according to three different recipes as indicated in Table 1 (column 3). The details of these recipes are as follows:

Recipe 1. For recipe 1, 5 g of boehmite was mixed with 2.5 g of urea and 12.4 g of 0.3 mol/L HNO_3 solution in water, and the sol was stirred at room temperature for 24 h. Then, the sol was deposited into the microchannels.

Recipe 2. For recipe 2, 5 g of poly(vinyl alcohol) (PVA) was mixed with 75 g of deionized water and 1 g of glacial acetic acid, and then 20 g of γ - Al_2O_3 powder was added. The suspension was stirred for 3 days at room temperature until a homogeneous solution was obtained. Then, the suspension was deposited into the microchannels.

Recipe 3. For recipe 3, 5 g of PVA was mixed with 1 g of glacial acetic acid and 125 cm^3 of deionized water, and then 20 g of boehmite was added. The suspension was stirred for 1 day at room temperature until a homogeneous solution was obtained. Then, the suspension was deposited into the microchannels.

The loadings of Mn in weight percentages and the corresponding specific surface areas of the alumina coatings are reported in Table 1.

The sols were applied to stainless steel plates ($50 \times 35 \times 1$ mm) with a channel depth of 400 μm and a channel diameter of 600 μm (Figure 2). The plates were pretreated before the deposition of the coating by being cleaned with 2-propanol in an ultrasonic bath for 15 min, dried at room temperature, and calcined at 800 $^\circ\text{C}$ for 2 h. The coatings were deposited by the

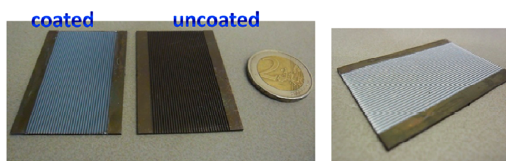
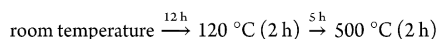


Figure 2. Microchanneled plates: (left) uncoated and coated with manganese alumina catalyst, (right) coated with γ -alumina.

wash-coating technique whereby the suspension was deposited on the substrate and the excess was then wiped off. The samples were then calcined in air according to the following program



The microreactor (Figure 1) was coated with Mn(2)-3-A coating and calcined under the same conditions.

As previously mentioned, different powdered catalysts were prepared according to different recipes with the objective of using these recipes to coat stainless steel plates and optimize the coating procedure. Then, powders prepared with the same recipes were independently tested for their kinetic behavior to evaluate the most active and stable composition. As will be explained, long-term continuous runs showed that the catalysts had to be prepared with less than 2 wt % manganese to avoid Mn leaching.

The XRD patterns of different manganese alumina powder catalysts calcined at 500 $^\circ\text{C}$ are shown in Figure 3. The peak

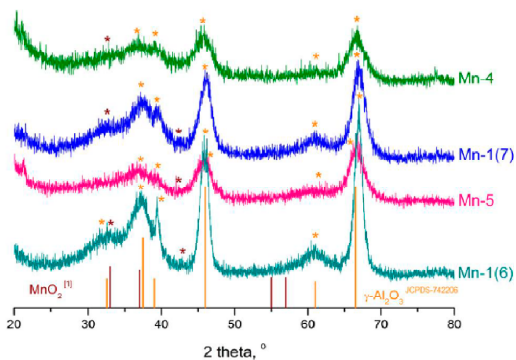


Figure 3. XRD patterns of manganese alumina powders.

positions are in a good agreement with the literature data for γ - Al_2O_3 . Some small peaks corresponding to the MnO_2 phase (dark stars, Figure 3) are also present, although the peaks are not clearly pronounced and some of them probably overlap alumina peaks. These results are in agreement with the literature reporting that mainly the MnO_2 phase is formed after calcination of Mn-doped Al_2O_3 at about 700 K.^{32,35}

As mentioned previously, some stainless steel plates were coated using the same recipes as used for the powder catalysts. A list of the different Mn- γ -alumina coatings and their main properties is provided in Table 2.

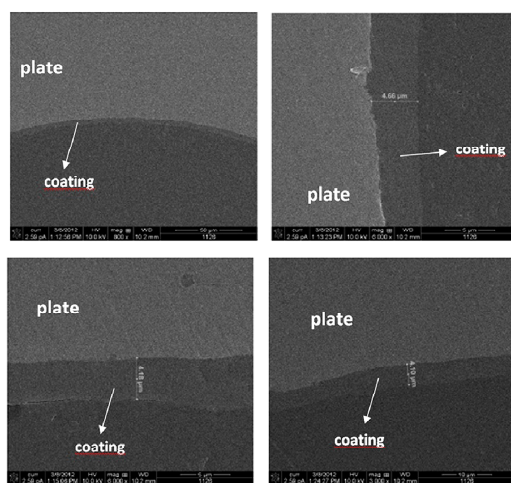
The BET surface area was mainly determined by the initial surface area of the alumina precursor (see Table 1): It decreased after Mn impregnation but was found to depend only

Table 2. Properties of Different Mn-Doped Alumina Coatings

Mn catalyst ^a	Mn content (calculated) (wt %)	drop test, weight loss (wt %)	coating thickness (μm)	BET surface area (m^2/g)	Mn content per unit surface area
Mn(0.5)-2-A	0.5	2	31 ± 3.4	65	0.008
Mn(0.5)-3-A	0.5	11	7 ± 1.4	200	0.003
Mn(2)-2-A	2	10	60 ± 10.2	97	0.021
Mn(2)-3-A	2	1	5 ± 1.0	209	0.010
Mn(0.5)-1-B	0.5	5	8 ± 1.6	276	0.002
Mn(2)-1-C	2	nd ^b	13 ± 3.3	250	0.008
Mn(5)-2-A	5	8	40 ± 3.2	95	0.053

^aNotation: Mn(weight percentage)-Al₂O₃ recipe-preparation mode.
^bnd, not determined.

slightly on Mn content. Stability tests showed that all of the coatings were reasonably adhesive (weight loss after drop tests was within 10%).³³ The coatings were uniform, as the deviation in thickness was within 20–25%. SEM cross-sectional images were recorded in different locations on the microchanneled plates. The cross-sectional SEM image of the whole plate is not shown here because of the lack of clarity of the image (low resolution). Enlarged SEM images of the Mn(2)-3-A catalytic coating are shown in Figure 4. A slightly thicker alumina layer

**Figure 4.** Cross-sectional SEM image of sample Mn(2)-3-A.

was obtained near the channel walls than in the center of the channel because of the strong surface tension of the aqueous suspension.³⁴ It is important to note that the detachment of the coatings from the substrates and the cracks in the coatings were due to the sample preparation procedure for SEM measurements (cutting, immersion in epoxy, polishing).

As a conclusion, Mn(2)-3-A was found to be the most stable coated catalyst. The synthesized catalysts were also tested for the chemical activity.

2.4.2. Batch Runs. The batch runs conducted in this work, for both catalytic screening and kinetic study, were performed in a glass-jacketed batch reactor with a volume of 100 cm³. This reactor was charged with 25 g of a 9.8 wt % hydrogen peroxide

solution in water and the desired amount of catalyst. The temperature was set at a fixed value by an ultrathermostat bath, and the solution was stirred with a magnetic stirrer. The hydrogen peroxide concentration was chosen by considering that the residual amounts of this reagent in some industrial processes can fall in the range between 2 and 10 wt %. That is, the worst industrial case was chosen. The catalytic screening was performed at a fixed temperature of 60 °C using different amounts of catalyst as specified in the following sections. In contrast, in the kinetic study, the temperature and catalyst concentration were varied appropriately.

2.4.3. Continuous Runs. A packed-bed tubular reactor was used to perform long-time runs to investigate the eventual catalyst deactivation. A high-performance liquid chromatography (HPLC) pump was used to pump a 10.0 wt % hydrogen peroxide solution to the reactor. The experimental runs were performed at atmospheric pressure, room temperature (25 °C), and a flow rate of 4 cm³/min, which allowed a relatively high hydrogen peroxide conversion to be obtained so that the eventual deactivation could be tested easily.

Some continuous runs were also performed using a coated single-plate reactor already described in a previous section. An HPLC pump was employed in this case as well to pump a 9.6 wt % hydrogen peroxide solution to the reactor. The experimental runs were performed at both atmospheric pressure and 5 bar, for which the reactor was pressurized with nitrogen.

3. RESULTS AND DISCUSSION

3.1. Catalytic Screening and Long-Life Continuous Runs on the Most Active MnO_x Catalyst. Preliminary investigations were performed to determine the most active catalyst for hydrogen peroxide decomposition, among some traditional catalysts proposed in the literature. In particular, some commercial FeO_x and Ni catalysts were tested and compared with MnO_x supported on γ -Al₂O₃ (5 wt % Mn) prepared in our laboratory. All of the catalysts were in powder form, and the related specific surface areas (a_{sp}) are reported in Table 3. A list of all performed experimental runs and hydrogen peroxide conversions, at different times, is provided in Table 3.

To correctly compare the catalyst performances, we considered the ratio between the hydrogen peroxide conversion at a fixed time (for example, 5 min), divided by the absolute surface area, which is the specific surface area multiplied by the weight of catalyst used. The obtained results are reported in Table 3.

One can see that the manganese oxide-based catalyst showed the highest activity. Therefore, before starting further investigations, we decided to evaluate the catalyst stability in long-time continuous runs performed in a tubular reactor. The catalyst for this test was prepared as explained in detail in the preceding section. The 5 wt % Mn catalyst supported on γ -Al₂O₃ spheres by dry impregnation and calcined at 500 °C was used in the first run. The long-term tests were carried out at a temperature of 25 °C and a flow rate of 4 cm³/min for more than 100 h. The obtained results are reported in Figure 5. It can be seen that a decrease of the hydrogen peroxide conversion from about 80% to 30% occurred with increasing time on stream.

The samples collected for the evaluation of the hydrogen peroxide conversion were also subjected to atomic absorption analysis to evaluate the release of Mn. The amounts released, as determined by chemical analysis, are reported in Figure 5. As

Table 3. Comparison of the Activities of Different Tested Catalysts

catalyst	H ₂ O ₂ (wt %)	T (°C)	W _{cat} (g)	X _{H₂O₂} (%)			a _{sp} (m ² /g)	X _{H₂O₂} /(a _{sp} W _{cat}) (5 min) (m ⁻²)
				5 min	15 min	1 h		
ZnO	20	60	0.564	0	0	0	nd ^a	nd ^a
Fe ₂ O ₃	20	60	2.002	24.70	—	—	240	0.051
Fe ₂ O ₃	20	60	0.500	0.91	1.83	4.43	240	0.007
Fe ₂ O ₃	20	60	1.006	8.11	19.47	—	240	0.034
Fe ₃ O ₄	20	60	0.504	0.39	0.91	3.25	240	0.003
Ni ^b	20	60	0.503	28.03	—	—	108	0.520
Ni ^b	10	60	0.108	7.24	22.23	—	108	0.618
MnO _x /Al ₂ O ₃ ^c	10	60	0.101	31.56	64.16	—	115	2.713

^and, not determined. ^bEngelhard Ni 3298 GE 3/64 in. × 3F, 60.0 wt % Ni. ^cMnO_x catalyst supported on γ-Al₂O₃, 5 wt % Mn; prepared by dry impregnation of a solution of Mn(CH₃COO)₂·4H₂O in water.

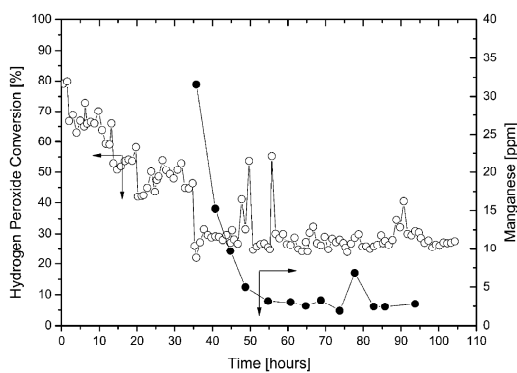


Figure 5. Hydrogen peroxide decomposition trend as a function of reaction time for a 5 wt % Mn catalyst supported on γ-Al₂O₃ and calcined at 500 °C. The run was performed at atmospheric pressure, room temperature of 25 °C, and a flow rate of 4 cm³/min in a tubular packed-bed reactor containing 3 g of catalyst in spherical pellets of 2.5-mm diameter. In the same plot is also reported the leached Mn concentration in the effluents for different times, determined by spectroscopic analysis.

can be seen, the leached amount decreased with time and stopped exactly when the conversion became constant. It can be concluded that the decrease in activity was strictly related to the manganese leaching. Because the leaching stopped when the conversion became constant, it is obvious that not all of the manganese was released. Therefore, it is possible to conclude that, after impregnation, manganese deposited on the alumina in two forms, one of which is strongly bonded to the surface and stable to leaching and another that is poorly interacting and prone to dissolve in the slightly acidic hydrogen peroxide solution. For the preparation of a more stable catalyst, it is important to load less manganese, eventually increasing the calcination temperature to favor the interaction of MnO_x with the surface support. For this purpose, two catalysts were prepared by first reducing the manganese content to 2 wt % and then calcining them at two different temperatures, namely, 500 and 800 °C. In both cases, the catalysts gained better stability, with negligible leaching of manganese. These runs were performed under the same operating conditions as those reported in Figure 5. The trend of the conversion as a function of time for the catalyst calcined at 500 °C is presented in Figure 6. The scattering of the conversion data was due not to the leaching of manganese, which was negligible, but rather to both

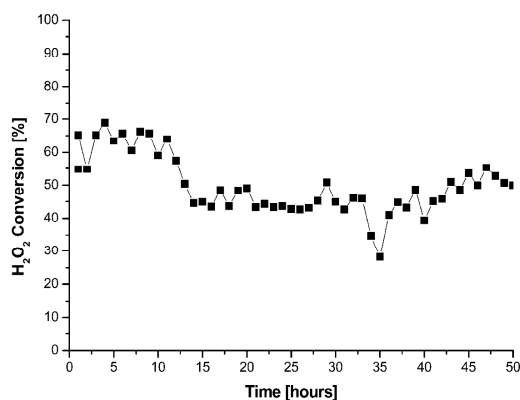


Figure 6. Hydrogen peroxide decomposition trend as a function of time on stream for a 2 wt % Mn catalyst supported on γ-Al₂O₃ calcined at 500 °C. The runs were performed at atmospheric pressure, room temperature of 25 °C, and a flow rate of 4 cm³/min in a tubular packed-bed reactor, with 3 g of catalyst in spherical pellets of 2.5-mm diameter.

temperature scattering and changes in catalyst wetting in this complex gas–liquid flow system in which a copious gas volume was produced on the surface and inside the pores, preventing the liquid access to the active sites. The calcination at 800 °C resulted in a lower conversion (ca. 30%), probably because of the decrease of the specific surface area from 170 to 123 m²/g, for the calcinations at 500 and 800 °C, respectively.

In this way, we determined the best conditions for the preparation of a stable catalyst, namely, 2 wt % manganese on γ-alumina and calcination at 500 °C. Obviously, the optimal value of manganese loading is related to the type of alumina employed. Clearly, if the alumina were changed, the optimal loading could also change.

3.2. Kinetic Runs on Powdered Catalysts. The powdered catalysts prepared as described in the previous sections were compared in terms of their activities in the decomposition of hydrogen peroxide. The operating conditions and the experimental results obtained at different times are reported in Table 4 and Figure 7.

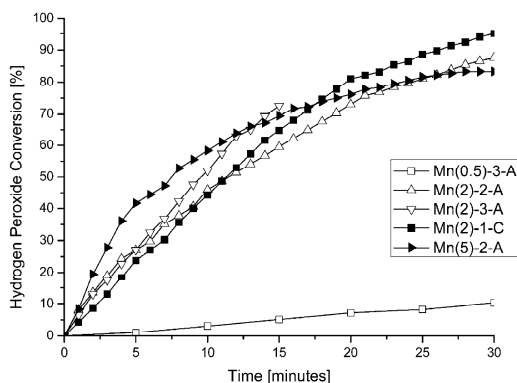
As one can see, all of the catalysts had comparable activities, with the exception of the Mn(0.5)-3-A catalyst, which exhibited a very poor activity. Because the Mn(2)-3-A catalyst showed the best stability (see the previous section) and good activity, it

Table 4. List of the Operating Conditions and the Experimental Results at Chosen Times^a

Mn catalyst ^a	T (°C)	W _{cat} (g)	X _{H₂O₂} (%)		
			5 min	10 min	15 min
Mn(0.5)-3-A	50	0.1103	1.03	3.09	5.15
Mn(2)-2-A	50	0.1014	27.06	45.99	59.52
Mn(2)-3-A	50	0.1028	27.08	51.99	72.57
Mn(2)-1-C	50	0.1040	23.78	44.32	64.86
Mn(5)-2-A	50	0.1044	41.66	58.32	69.43

^aNotation: Mn(weight percentage)-Al₂O₃ recipe-preparation mode.

^aRuns were performed by charging the reactor with 25 g of a solution of 10 wt % hydrogen peroxide in water.

**Figure 7.** Comparison of the experimental data for the performed catalytic tests. The runs were conducted in the batch reactor.

was chosen for further kinetic study in the batch reactor. The kinetic runs were performed by varying both the catalyst concentration (i.e., the catalyst weight W_{cat}) and the temperature to determine the reaction order with respect to the catalyst concentration and the kinetic parameters. A summary of the reaction conditions used is provided in Table 5.

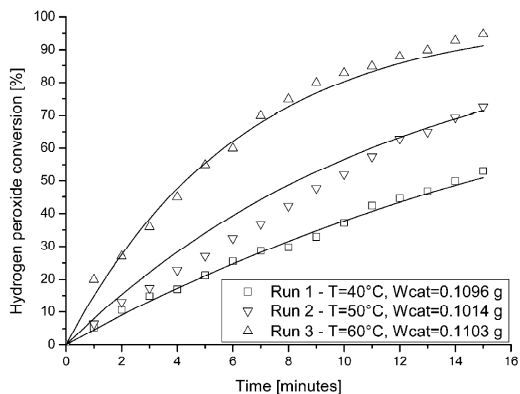
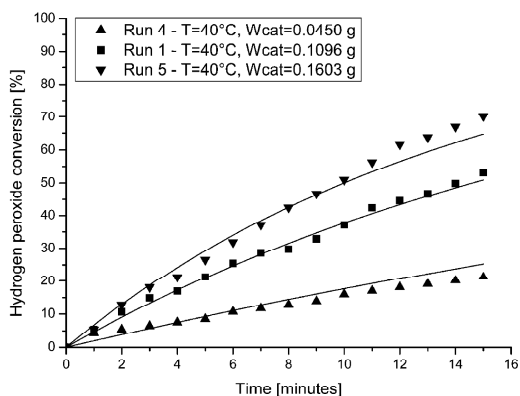
Table 5. List of Operating Conditions for the Kinetic Study^a

run	T (°C)	W _{cat} (g)
1	40	0.1096
2	50	0.1014
3	60	0.1103
4	40	0.0450
5	40	0.1603

^aRuns were performed by charging the reactor with 25 g of a solution of 10 wt % hydrogen peroxide in water.

The effect of the temperature on the reaction can be observed in Figure 8. The amount of catalyst used in three performed runs was kept roughly constant. The effect of catalyst concentration, at constant temperature (40 °C), is shown in Figure 9.

As can be seen, upon increasing both the temperature and the catalyst concentration, the reaction rate increased. To find the kinetic parameters, all of the collected experimental data were subjected to mathematical regression analysis, imposing the following reaction rate expression and mass balance equation

**Figure 8.** Hydrogen peroxide decomposition runs performed with 0.1 g of Mn(2)-3-A at different temperatures in a batch reactor. Symbols are experimental data; lines are simulated results.**Figure 9.** Hydrogen peroxide decomposition runs performed at 40 °C at different catalyst concentrations of Mn(2)-3-A in a batch reactor. Symbols are experimental data; lines are simulated results.

$$r [\text{mol}/(\text{dm}^3 \cdot \text{s})] = k[\text{catalyst}][\text{H}_2\text{O}_2] \quad (3)$$

$$\frac{dn_i}{dt} (\text{mol/s}) = \pm rV \quad (4)$$

where i represents a component and V is the liquid volume. The catalyst concentration is expressed in grams per cubic decimeter. To determine the activation energy and kinetic constant at a reference temperature (here, 40 °C), the dependence between the kinetic constant and the temperature was included through the modified Arrhenius equation

$$k [\text{dm}^3/(\text{g} \cdot \text{s})] = k^{\text{ref}} \exp \left[\frac{E_a}{R} \left(\frac{1}{T^{\text{ref}}} - \frac{1}{T} \right) \right] \quad (5)$$

where T^{ref} and T are in kelvin.

The kinetic parameters were found to be $k^{\text{ref}}(40 \text{ °C}) = (1.05 \times 10^{-2}) \pm (3.42 \times 10^{-4}) \text{ L}/(\text{g} \cdot \text{min})$ and $E_a = 12.63 \pm 0.58 \text{ kcal/mol}$, and the agreement between the experimental and calculated values can be seen in Figures 8 and 9. One can see

that the experimental data are satisfactorily fitted by the proposed model.

3.3. Continuous Runs in a MnO_x/Al₂O₃-Coated Single-Plate Microreactor. The best catalyst for both coating stability and activity, namely, Mn(2)-3-A, was coated on the walls of a stainless steel single-plate microreactor. Different continuous runs were performed under various conditions of pressure, volumetric flow rate, and temperature. A list of all of the experimental runs performed is provided in Table 6.

Table 6. List of Experimental Continuous Runs with Related Operating Conditions

run	T (°C)	P (bar)	Q (cm ³ /min)
6	25	1	0.25
7	25	1	0.50
8	25	1	0.75
9	25	1	1.00
10	35	5	0.50
11	35	5	1.00

When working at atmospheric pressure and 25 °C and varying the flow rate in the range between 0.25 and 1 cm³/min, the hydrogen peroxide conversion decreased, as can be seen in Figure 10. On the basis of kinetic eq 3 and the related

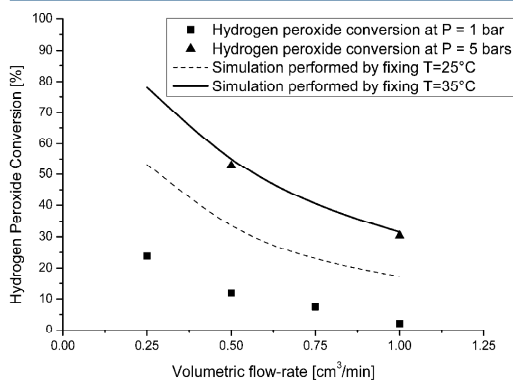


Figure 10. Hydrogen peroxide decomposition runs performed in a continuous coated-disk-shaped single-plate microreactor at different pressures and flow rates. Symbols are experimental data; lines are simulated results.

parameters determined from the batch kinetic runs, for the reactor in Figure 1, we considered a plug-flow model for interpreting the obtained results

$$\frac{dF_{\text{H}_2\text{O}_2}}{dV} \text{ (mol/L}\cdot\text{min)} = -r \quad (6)$$

This approach is rough but useful for comparison purposes. In fact, when we performed a simulation of the reactor's behavior under the previously mentioned conditions, the simulated curve was always higher than the experimental data. This fact can be explained considering that, at atmospheric pressure, the oxygen developed as a consequence of the reaction gives rise to a consistent gas hold-up in the reactor, thereby strongly reducing the liquid residence time and consequently the H₂O₂ conversion. Then, to reduce the effect

of this phenomenon, the pressure inside the reactor was increased moderately to 5 bar, thereby compressing the gas and increasing the liquid residence time and the related conversion. Under these conditions, a higher hydrogen peroxide decomposition was observed, with an increase in the temperature in the reactor from 25 to about 38 °C, because of the high exothermicity of the reaction. The temperature was measured by a thermocouple positioned at the reactor outlet. The experimental data collected at a pressure of 5 bar were fitted by assuming an average temperature of 35 °C inside the reactor, which is a reasonable value (see Figure 10). Clearly, in this way, we neglected the thermal profile. On the other hand, the thermal profile was not easily measurable because of both the geometry of the reactor and the evaluation of the heat released from the device. However, the aim was simply to evaluate the possibility of intensifying the process.

In conclusion, process intensification can be realized by identifying the optimal temperature, pressure, flow rate, and local mixing. The developed kinetic model with appropriately adjusted kinetic parameters can be used for the design of a continuous reactor for hydrogen peroxide decomposition.

4. CONCLUSIONS

First, it was confirmed that manganese oxide is one of the most active catalysts in promoting the decomposition of hydrogen peroxide in the range of pH 4.5–7. The catalyst is stable to leaching if supported on the described type of γ -Al₂O₃ in an amount of less than 2 wt % by dry impregnation. We found that the stability of this catalyst can be explained by assuming a strong interaction of manganese oxide with the alumina surface. Noninteracting manganese oxide is active but unstable, dissolving in slightly acidic hydrogen peroxide solution. Different catalysts containing less than 2% manganese oxide were then prepared using various procedures. Adhesive and uniform catalytic coatings were successfully deposited on microchanneled stainless steel plates.

The most adhesive catalyst was found to also be very active and stable; therefore, a powder having the same composition was used for a kinetic investigation in a batch reactor to examine the effects of the catalyst concentration, temperature, and hydrogen peroxide concentration. A kinetic law was observed to be able to reproduce all of the experimental data, and the related kinetic parameters were determined by subjecting all of the collected data to a mathematical regression analysis.

Finally, an attempt at process intensification was successfully made by coating the walls of a single-plate microreactor with the MnO_x/Al₂O₃ catalyst, which resulted in an adhesive, very active, and stable catalytic coating. These continuous runs were found to be strongly affected by the pressure, because oxygen released during the reaction reduced the volume available to the liquid reagent in the reactor, thereby strongly decreasing the residence time and the conversion. When the pressure was increased from 1 to 5 bar, the gas hold-up was strongly reduced, and the obtained conversions increased significantly and could be roughly predicted with the developed kinetic model.

■ AUTHOR INFORMATION

Corresponding Author

*E-mail: elio.santacesaria@unina.it.

Present Address

[§]Vlaamse Instelling voor Technologisch Onderzoek (VITO), Boeretang 200, 2400 Mol, Belgium.

Notes

The authors declare no competing financial interest.

■ ACKNOWLEDGMENTS

The EC VII Framework Program CP-IP 228853-2 COPIRIDE is gratefully acknowledged for financial support. The authors also thank Mr. C. P. M. Buijs (Eindhoven University of Technology) for his great help with SEM measurements.

■ REFERENCES

- (1) Clerici, M. G.; Bellussi, G.; Romano, U. Synthesis of Propylene Oxide from Propylene and Hydrogen Peroxide Catalyzed by Titanium Silicalite. *J. Catal.* **1991**, *129*, 159–167.
- (2) Santacesaria, E.; Renken, A.; Russo, V.; Turco, R.; Tesser, R.; Di Serio, M. Biphasic Model Describing Soybean Oil Epoxidation with H₂O₂ in Continuous Reactors. *Ind. Eng. Chem. Res.* **2012**, *51*, 8760–8767.
- (3) Santacesaria, E.; Tesser, R.; Di Serio, M.; Russo, V.; Turco, R. A New Simple Microchannel Device To Test Process Intensification. *Ind. Eng. Chem. Res.* **2011**, *50* (5), 2569–2575.
- (4) Sunglin, L. S.; Guro, D. M. Catalytic Decomposition of Hydrogen Peroxide on Iron Oxide: Kinetics, Mechanism, and Implications. *Environ. Sci. Technol.* **1998**, *32*, 1417–1423.
- (5) Salem, I. A.; El-Maazawi, M.; Zaki, A. B. Kinetics and Mechanisms of Decomposition Reaction of Hydrogen Peroxide in Presence of Metal Complexes. *Int. J. Chem. Kinet.* **2000**, *32* (11), 643–666.
- (6) Mishchuk, N. A.; Lysenko, L. L.; Zayats, O. V. Investigation of the Kinetics of Catalytic Decomposition of Hydrogen Peroxide Depending on the Solution Phase State. *Khim. Tekhnol. Vody* **2009**, *31* (2), 129–144.
- (7) Mepedović, S.; Locke, B. R. Platinum catalysed decomposition of hydrogen peroxide in aqueous-phase pulsed corona electrical discharge. *Appl. Catal. B: Environ.* **2006**, *67*, 149–159.
- (8) Hasnat, M. A.; Rahman, M. M.; Borhanuddin, S. M.; Siddiqua, A.; Bahadur, N. M.; Karim, M. R. Efficient hydrogen peroxide decomposition on bimetallic Pt–Pd surfaces. *Catal. Commun.* **2010**, *12*, 286–291.
- (9) Falcon, H.; Carbonio, R. E. Study of the heterogeneous decomposition of hydrogen peroxide: Its application to the development of catalysts for carbon-based oxygen cathodes. *J. Electroanal. Chem.* **1992**, *339*, 6943.
- (10) Allah, N.; Deraz, M. Catalytic decomposition of H₂O₂ on promoted cobaltic oxide catalysts. *Mater. Lett.* **2002**, *57*, 914–920.
- (11) Hasan, M. A.; Zaki, M. I.; Pasupulety, L.; Kumari, K. Promotion of the hydrogen peroxide decomposition activity of manganese oxide catalysts. *Appl. Catal. A: Gen.* **1999**, *181*, 171–179.
- (12) Kanugo, S. B.; Parida, K. M.; Sant, B. R. Studies on MnO₂—III. The kinetics and the mechanism for the catalytic decomposition of H₂O₂ over different crystalline modifications of MnO₂. *Electrochim. Acta* **1981**, *26* (8), 1157–1167.
- (13) Park, J. N.; Shon, J. K.; Jin, M.; Hwang, S. H.; Park, G. O.; Boo, J. H.; Han, T. H.; Kim, J. M. Highly Ordered Mesoporous α -Mn₂O₃ for Catalytic Decomposition of H₂O₂ at Low Temperatures. *Chem. Lett.* **2010**, *39*, 493495.
- (14) Zapf, R.; Becker-Willinger, C.; Berresheim, K.; Bolz, H.; Gnaser, H.; Hessel, V.; Kolb, G.; Löb, P.; Pannwitt, A. K.; Ziogas, A. Detailed Characterization of Various Porous Alumina-Based Catalyst Coatings Within Microchannels and Their Testing for Methanol Steam Reforming. *Trans. Inst. Chem. Eng. A* **2003**, *81*, 721.
- (15) Kiwi-Minsker, L.; Ruta, M.; Eslanloo Pereira, T.; Bromley, B. Structured catalytic wall microreactor for efficient performance of exothermic reactions. *Chem. Eng. Process.* **2010**, *49*, 973.
- (16) Snytnikov, P. V.; Potemkin, D. I.; Rebrov, E. V.; Sobyanyin, V. A.; Hessel, V.; Schouten, J. C. Design, scale-out, and operation of a microchannel reactor with a Cu/CeO_{2-x} catalytic coating for preferential CO oxidation. *Chem. Eng. J.* **2010**, *160*, 923.
- (17) Protasova, L. N.; Rebrov, E. V.; Skelton, H. E.; Wheatley, A. E. H.; Schouten, J. C. A kinetic study of the liquid-phase hydrogenation of citral on Au/TiO₂ and Pt-Sn/TiO₂ thin films in capillary microreactors. *Appl. Catal. A: Gen.* **2011**, *399*, 12.
- (18) Cai, W.; Wang, F.; van Veen, A.; Descorme, C.; Schuurman, Y.; Shen, W.; Mirodatos, C. Hydrogen production from ethanol steam reforming in a micro-channel reactor. *Int. J. Hydrogen Energy* **2010**, *35*, 1152.
- (19) Phan, X. K.; Bakhtyari, H. D.; Myrstad, R.; Thormann, J.; Pfeifer, P.; Venvik, H. J.; Holmen, A. Preparation and Performance of a Catalyst-Coated Stacked Foil Microreactor for the Methanol Synthesis. *Ind. Eng. Chem. Res.* **2010**, *46*, 10934.
- (20) Zapf, R.; Kolb, G.; Pennemann, H.; Hessel, V. Basic Study of Adhesion of Several Alumina-based Washcoats Deposited on Stainless Steel Microchannels. *Chem. Eng. Technol.* **2006**, *29* (12), 1509–1512.
- (21) Tigelaar, R. M.; Gardeniers, J. G. E. Silicon and glass microreactors. In *Micro Process Engineering: A Comprehensive Handbook*; Hessel, V., Renken, A., Schouten, J. C., Yoshida, J.-i., Eds.; Wiley-VCH: Weinheim, Germany, 2009; Vol. 2, pp 8–11.
- (22) Cao, E.; Gavrilidis, A.; Motherwell, W. B. Oxidative dehydrogenation of 3-methyl-2-buten-1-ol in microreactors. *Chem. Eng. Sci.* **2004**, *59*, 4803–4808.
- (23) Lin, W. C.; Yang, Y. J.; Hsieh, G. W.; Tsai, C. H.; Chen, C. C.; Liang, C. C. Selective local synthesis of nanowires on a microreactor chip. *Sens. Actuators A* **2006**, *130–131*, 625–632.
- (24) Haas-Santo, K.; Fichtner, M.; Schubert, K. Preparation of microstructure compatible porous supports by sol-gel synthesis for catalyst coatings. *Appl. Catal. A: Gen.* **2001**, *220*, 79–92.
- (25) Younes-Metzler, O.; Svagin, J.; Jensen, S.; Christensen, C. H.; Hansen, O.; Quaade, U. Microfabricated high-temperature reactor for catalytic partial oxidation of methane. *Appl. Catal.* **2005**, *284*, 5–10.
- (26) Younes-Metzler, O.; Johansen, J.; Thorsteinsson, S.; Jensen, S.; Hansen, O.; Quaade, U. Oxidation of methane over a Rh/Al₂O₃ catalyst using microfabricated reactors with integrated heating. *J. Catal.* **2006**, *241*, 74–82.
- (27) Kolb, G.; Zapf, R.; Hessel, V.; Löwe, H. Propane steam reforming in micro-channels—Results from catalyst screening and optimization. *Appl. Catal. A: Gen.* **2004**, *277*, 155–166.
- (28) Ajmera, S. K.; Losey, M. W.; Jensen, K. F.; Schmidt, M. A. Microfabricated packed-bed reactor for phosgene synthesis. *AIChE J.* **2001**, *47* (7), 1639–1647.
- (29) Benaskar, F.; Ben-Abdelmoumen, A.; Patil, N. G.; Rebrov, E. V.; Meuldijk, J.; Hulshof, L. A.; Hessel, V.; Krtschil, U.; Schouten, J. C. Cost Analysis for a Continuously Operated Fine Chemicals Production Plant at 10 kg/Day Using a Combination of Micro-processing and Microwave Heating. *J. Flow Chem.* **2011**, *2* (1), 74–89.
- (30) Kolthoff, I. M.; Sandell, E. B.; Meehan, E. J. *Treatise on Analytical Chemistry*; John Wiley & Sons: New York, 1993; Vol. 2, p 888.
- (31) de Loos, S. R. A.; van der Schaaf, J.; Tiggelaar, R. M.; Nijhuis, T. A.; de Croon, M. H. J. M.; Schouten, J. C. Gas–liquid dynamics at low Reynolds numbers in pillared rectangular micro channels. *Microfluid. Nanofluid.* **2010**, *9*, 131–144.
- (32) Kapteijn, F.; van Langeveld, A. D.; Moulijn, J. A.; Andreini, A.; Vuurman, M. A.; Turek, A. M.; Jehng, J. M.; Wachs, I. E. Alumina-Supported Manganese Oxide Catalysts: I. Characterization: Effect of Precursor and Loading. *J. Catal.* **1994**, *150*, 94–104.
- (33) Zapf, R.; Kolb, G.; Penneman, H.; Hessel, V. Basic study of the adhesion of several alumina-based washcoats deposited onto stainless steel microchannels. *Chem. Eng. Technol.* **2006**, *29* (12), 1509–1512.
- (34) Zapf, R.; Becker-Willinger, C.; Berresheim, K.; Bolz, H.; Gnaser, H.; Hessel, V.; Kolb, G.; Löb, P.; Pannwitt, A. K.; Ziogas, A. Detailed Characterization of Various Porous Alumina-Based Catalyst Coatings Within Microchannels and their Testing for Methanol Steam Reforming. *Trans. Inst. Chem. Eng. A* **2003**, *81*, 721–729.

(35) Wei, Z. D.; Huang, W. Z.; Zhang, S. T.; Tan, J. Induced effect of Mn_3O_4 on formation of MnO_2 crystals favourable to catalysis of oxygen reduction. *J. Appl. Electrochem.* **2000**, *30*, 1133–1136.



Contents lists available at ScienceDirect

Chemical Engineering and Processing: Process Intensification

journal homepage: www.elsevier.com/locate/cep

Sintered metal fibers coated with transition metal oxides as structured catalysts for hydrogen peroxide decomposition



Rosa Turco^a, Julien Haber^b, Igor Yuranov^b, Vincenzo Russo^a,
Elio Santacesaria^{a,*}, Lioubov Kiwi-Minsker^{b,**}

^a University of Naples "Federico II", Dipartimento di Scienze Chimiche, Complesso Universitario Monte S. Angelo, Via Cintia 4, IT, 80126 Naples, Italy

^b Ecole Polytechnique Fédérale de Lausanne, GGRC-EPFL, Lausanne CH-1015, Switzerland

ARTICLE INFO

Article history:

Received 8 February 2013

Received in revised form 30 June 2013

Accepted 18 August 2013

Available online 27 August 2013

Keywords:

Hydrogen peroxide decomposition

Sintered metal fibers

Manganese oxide

Structured catalyst

Process intensification

ABSTRACT

This study aimed at the development of active and stable structured catalyst for the decomposition of hydrogen peroxide under industrial conditions. Sintered metal fibers of stainless steel (SMF_{SS}) in the form of flat panels were surface coated by different catalytic metal oxides. The oxide coating has been carried out by incipient wetness impregnation of SMF_{SS} with suitable precursors followed by calcination in air at temperatures between 500 and 600 °C. The coating of SMF_{SS} renders a very thin homogeneous oxide layer of less than 1 μm covering the individual fibers and ensures an optimal accessibility of the treated H₂O₂ solution to the catalytically active phase without any mass-transfer limitations. In the decomposition of hydrogen peroxide, the 5 wt.% MnO_x/5 wt.% (Al₂O₃ + MgO)/SMF_{SS} was found to be the most active and stable catalyst in a range of pH=4–7 at 25 °C exhibiting a significant first order rate constant of 5.2 min⁻¹ at pH 7. The same catalyst was tested in the back end of the epoxidation of soybean oil process demonstrating its suitability for industrial application.

© 2013 Elsevier B.V. All rights reserved.

1. Introduction

Most oxidations carried out with hydrogen peroxide require an excess of oxidant to attain fast and complete conversion of the compound. Thereby, the excess of hydrogen peroxide must be eliminated at the end of the process to ensure a good product quality and to minimize the environmental impact. In industrial processes an alkaline solution is created by addition of sodium hydroxide to decompose hydrogen peroxide into water and oxygen. However, such a way of treating the products comes along with serious drawbacks: if the solution is not well mixed, hot spots form since the reaction is exothermic ($\Delta H_r = -98$ kJ/mol) and potentially causing a violent runaway. In addition, the alkaline solution needs to be neutralized with acid at the end of the process leading to additional costs and waste water discharge. Moreover, the alkaline environment favors the formation of soaps decreasing the quality of the final product.

The use of homogeneous and heterogeneous catalysts promoting the decomposition of hydrogen peroxide is an attractive alternative from the economic and ecological point of view [1].

The most known catalytic system used to decompose hydrogen peroxide is the Fenton reagent [2–4]. In this system, iron creates radicals which oxidize organic molecules contained in waste water. Recently, stainless steel was shown to promote the reaction [5]. However, faster decomposition is obtained with noble (platinum, silver, and palladium) and transition metals oxides such as nickel and manganese oxides [6,7]. Manganese oxide, in particular, has shown a high activity in promoting this reaction [8–10].

Important examples of industrial processes using hydrogen peroxide as reactant and needing the clean-up of the residual oxidant are the epoxidation reactions such as the propene epoxidation to propene oxide [11] and the soybean oil epoxidation to obtain epoxidized soybean oil [12]. In both cases a big excess of hydrogen peroxide is used to attain high conversion and its decomposition at the process back-end is very important.

As has been mentioned above, the use of a heterogeneous catalyst is particularly suitable for industrial applications as compared to homogeneous (like Fenton) one due to possibility of recycling. Moreover, a continuous process can be envisaged leading to process intensification (IP). IP could also be achieved by using the reactors with structured catalytic beds and/or microreactors with the catalytic phase deposited on structured fibrous supports [13–17]. As it is known, the use of microreactor is convenient in particular for exothermic reactions occurring in multi-phase system reducing mass transfer limitation.

* Corresponding author. Tel.: +39 081 674027; fax: +39 025697072.

** Corresponding author. Tel.: +41 21 693 3182.

E-mail addresses: elio.santacesaria@unina.it (E. Santacesaria),
Lioubov.kiwi-minsker@epfl.ch (L. Kiwi-Minsker).

Table 1
Characteristics of the SMF_{SS} support.

Name	Material	Composition [wt.%]	Fiber diameter [μm]	Filter thickness [mm]	Porosity
SMF _{SS}	AISI 316L (Stainless steel)	Cr 17%, Ni 12%, Mo 2%, Mn < 1%, Fe;	20	0.30	0.83

Recently, sintered metal fibers (SMF) have been successfully used as structured catalyst support in multiple reactions [14–16]. SMF are micro-fibrous metal filters consisted of uniform filaments with a diameter in the range of 10 μm . These filaments are sintered into a homogenous 3D structure and present porosities up to 80–90%, large permeability and excellent filtrating properties. The high conductivity of the metal fiber matrix provides a radial heat transfer about two-fold higher as compared to randomly packed bed, leading to a substantial reduction of temperature gradients when performing exothermic reactions. Fibers of metal alloys (stainless steel, Inconel, etc.) exhibit high mechanical strength and both chemical and thermal stability. When installed in continuous reactors, the open regular macrostructures results in reduced energy consumption due to lower pressure drops as compared to packed bed reactors. More detailed description on SMF can be found in a work published by Yuranov et al. [15].

In the present work, several SMF-based supports opportunely coated with different metal oxides have been prepared to catalyze the hydrogen peroxide decomposition. For all catalysts we have evaluated the activity and stability, controlling also the eventual leaching of active component. Finally, the performance of the most stable and active catalyst (manganese oxide supported on Al₂O₃–MgO coated SMF_{SS}) was tested for industrial application. This catalyst was also characterized via SEM, AAS and BET.

2. Experimental

In the following section, the composition of the tested SMF_{SS} support is given. Then, the catalyst preparation and characterization methods are reported in detail and the setup for activity and stability measurements in aqueous H₂O₂ is presented. Finally, the process used to test the catalysts activity and stability under realistic industrial conditions is described.

Hydrogen peroxide 60% b.w. was kindly furnished by Solvay Italia SpA, while, the other reagents were purchased by FLUKA.

2.1. Supports

The structured support used for the active phase deposition is a stainless steel sintered metal fibers, SMF_{SS}. (Southwest Screens & Filters SA, Belgium) which characteristics are summarized in Table 1.

2.2. Catalyst preparation

The catalysts that were tested in this study are listed in Table 2. A detailed description of their synthesis is reported below.

2.2.1. Preparation of the 5 wt.%(Al₂O₃ + MgO)/SMF_{SS} support

The AISI 316L stainless steel sintered metal fibers panels were washed in acetone, boiled in toluene for 30 min and air-dried at

room temperature. The filters were further oxidized in air at 450 °C (ramp of 20 °C min⁻¹) for 2 h to facilitate the adhesion of the oxide layer to the metal fiber surface.

To assure a stable coating of the supported compound and the steel surface, an oxide layer of Al₂O₃ + MgO (molar ratio 1:1) was first created and found to be stable during liquid-phase experiments [18]. Metal oxide layer deposition was performed by intrinsic wetness impregnation method. A MgO + Al₂O₃ precursor solution was prepared as following: 20 g of Al(NO₃)₃·9H₂O (Fluka) were dissolved in 70 ml of distilled water. The solution was heated up to 95 °C. 2.2 g of MgO were added slowly to the solution. Heating and stirring were maintained until MgO was completely dissolved. The solution was then cooled down to room temperature.

MgO + Al₂O₃ (molar ratio 1:1) layer deposition was performed by dipping the SMF_{SS} panel into the MgO + Al₂O₃ precursor solution followed by drying in air at room temperature (1 h) and calcination at 550 °C (2 h, temperature ramp of 10 °C min⁻¹). The dipping-drying-calcination cycle was repeated 2 times to deposit 5% wt. of MgO + Al₂O₃.

2.2.2. Preparation of the 5 wt.%(NiO + Al₂O₃ + MgO)/SMF_{SS} catalysts

The 5% wt.(NiO + Al₂O₃ + MgO)/SMF_{SS} catalysts were prepared similarly to the 5% wt.(Al₂O₃ + MgO)/SMF_{SS} support. A calculated amount of aqueous Ni(NO₃)₂ (Fluka) was directly added to the MgO + Al₂O₃ precursor solution to obtain a content of 20% or 50% of Ni oxide in the final coatings.

2.2.3. Preparation of the perovskite 5 wt.% La_{0.4}Ca_{0.6}MnO₃/SMF_{SS} catalysts

The La_{0.4}Ca_{0.6}MnO₃/SMF_{SS} was synthesized by the modified citrate gel precursor method as described by Soleymani et al. [19]. The precursor solution was prepared by dissolving the calculated amounts of calcium nitrate Tetrahydrate (Fluka 98%), Manganese (II) Nitrate Tetrahydrate (Fluka, 97%), Lanthanum Acetate hydrate (Fluka, 97%) and Citric acid (Fluka, purum) in water. The composition was prepared to have the final atomic ratio La:Ca:Mn = 0.4:0.6:1. The citric acid:total metal molar ratio was 1.2. Metal oxide layer deposition was performed by dipping the pre-treated SMF_{SS} panel into the precursor solution followed by drying in air at room temperature (1 h) and calcination at 500 °C (2 h, temperature ramp of 10 °C min⁻¹). The dipping-drying-calcination cycle was repeated 2 times to deposit 5% wt. of metal oxide leading to the catalyst "Perovskite 500 °C". The "Perovskite 600 °C" was obtained by calcination at 600 °C instead of 500 °C.

2.2.4. Preparation of the 5 wt.% MnO_x/5 wt.%(Al₂O₃ + MgO)/SMF_{SS}

Manganese (II) acetate tetrahydrate (Fluka, 99%) was used as a Mn oxide precursor. The calculated amount of the salt was dissolved in water. Mn oxide layer deposition was performed by dipping the prepared 5% wt.(Al₂O₃ + MgO)/SMF_{SS} support into the precursor solution followed by drying in air at room temperature (1 h) and calcination at 500 °C (2 h, temperature ramp of 10 °C min⁻¹). The amount of deposited Mn has been confirmed by the atomic absorption spectroscopy (AAS) analysis.

Table 2
Catalysts used for decomposition of hydrogen peroxide.

Catalyst	Detailed composition
20NiO	5 wt.%(20 wt.%NiO + Al ₂ O ₃ + MgO)/SMF _{SS}
50NiO	5 wt.%(50 wt.%NiO + Al ₂ O ₃ + MgO)/SMF _{SS}
MnO _x	5 wt.%(MnO _x /5 wt.%(Al ₂ O ₃ + MgO)/SMF _{SS}
Perovskite	5 wt.% La _{0.4} Ca _{0.6} MnO ₃ /SMF _{SS}

Table 3

Experimental conditions for the catalytic runs. W_{cat} is the overall weight of the catalyst (the active phase and the SMF_{55} support).

Run	Catalysts	$[\text{H}_2\text{O}_2]^\circ$ (mol/L)	W_{cat} (g)	T ($^\circ\text{C}$)
1	20 NiO	3.9482	1.5573	60
2	50 NiO	3.5352	1.2410	60
3	Perovskite 500 $^\circ\text{C}$	1.6461	0.3004	25
4	Perovskite 500 $^\circ\text{C}$	1.5636	0.3004	25
5	Perovskite 500 $^\circ\text{C}$	1.6461	0.3004	25
6	Perovskite 500 $^\circ\text{C}$	1.6461	0.3004	25
7	Perovskite 600 $^\circ\text{C}$	1.6461	0.3030	25
8	Perovskite 600 $^\circ\text{C}$	1.5981	0.3030	25
9	Perovskite 600 $^\circ\text{C}$	1.6607	0.3030	25
10	MnO_x	1.4097	0.3170	25
11	MnO_x	1.5857	0.3170	25
12	MnO_x	1.6374	0.3170	25
13	MnO_x^a	2.0040	0.3584	25
14	MnO_x^a	1.1850	0.3584	25
15	MnO_x^a	1.5635	0.3584	25

^a These runs were performed using the residual oxidant solution of the epoxidation reaction, discharged and then neutralized, simulating in this way the conditions close to realistic industrial process.

2.3. Catalysts characterization

The most promising catalyst, i.e. 5 wt.% $\text{MnO}_x/5$ wt.% ($\text{Al}_2\text{O}_3 + \text{MgO}$)/ SMF_{55} was characterized via BET and scanning electron microscopy (SEM).

BET area was determined using the Sorptomatic 1990 (Carlo Erba). Prior to analysis, the samples were outgassed at 523 K for 2 h under vacuum ($<5 \times 10^{-2}$ Torr). BET area and pore size distribution were obtained by nitrogen adsorption at 77 K according to the method of Dollimore and Heal [20].

Morphological features were analyzed by scanning electron microscopy (SEM) on a Philips FEI XL30-FEG equipped with an Everhart–Thornley secondary-electron (SE) detector, operated at an accelerating voltage of 15 kV and using NORAN System SIX (version 1.6) for data acquisition. Before analysis, the sample underwent a hydrocarbon decontamination treatment using a plasma-cleaner (EVACTRON).

2.4. Catalytic testing

All the experiments were conducted in a glass reactor equipped with a mechanical stirrer (stirring rate 1900 rpm) and immersed in a thermostatic water bath. The catalyst was fixed to the terminal part of the stirrer. The reactor was initially charged with water, and then for starting the run a defined amount of H_2O_2 (10–20% wt.) was added under vigorous stirring. The pH of the reacting solution under these conditions was normally in the range of 4–4.5. In some runs, the pH was adjusted to evaluate the effect of this variable on activity and/or the presence of leaching. The top of the reactor was connected to a gas volumetric measurement system consisting in two graduated cylinders filled with water, turned upside down and deep in a beaker. The oxygen released during the reaction was collected at the top of the cylinder and water is correspondingly displaced allowing the measurement of the volume of oxygen delivered as function of time. Samples of the solution were withdrawn at different times and analyzed by iodometric method for determining the residual H_2O_2 content [21]. The “blank” experiment (without a heterogeneous catalyst) has been conducted and did not show any H_2O_2 decomposition under the reaction conditions applied. The adopted experimental conditions for all the performed runs are summarized in Table 3.

2.5. Catalyst activity and stability under industrial process conditions

The model process to test the catalyst performance under relevant to industrial conditions was the epoxidation of soybean oil. The reaction was carried out using performic acid generated in situ from the reaction of H_2O_2 (60 wt.%) with formic acid (95 wt.%) in the presence of sulphuric acid (98 wt.%) as catalyst. Performic acid is an oxygen transfer molecule better than hydrogen peroxide and promptly reacts with soybean oil double bonds giving place to the epoxide rings and to formic acid that is again oxidized to performic acid. The apparatus, procedure and the occurring reactions were described in detail elsewhere [12]. For the semi-batch operation mode, a cylindrical jacketed glass reactor (500 ml) with three necks was used. It was equipped with a thermocouple, a reflux condenser and a glass dipping funnel for the addition of aqueous reactants. The reaction mixture was stirred with a magnetic bar at 750 rpm and temperature was controlled by a thermostat.

In this work, a continuous dosing rate of 0.3 cm^3/min of an oxidizing mixture of hydrogen peroxide (36.7 g) and formic acid (5.38 g) was added to 100 g of well stirred soybean oil containing sulfuric acid (0.64 g). The oil was kept at about 65 $^\circ\text{C}$, while, the oxidizing mixture was fed at room temperature. During the process, temperature rose up to 72 $^\circ\text{C}$ due to the exothermic reaction. After a neutralization step (with NaOH 2 M) followed by a settling step to separate the organic phase from the aqueous one, hydrogen peroxide decomposition experiments were carried out. The main contaminants present in the aqueous solution were on the one hand ions (HCO_3^- , HCO_2^- , HSO_4^- , SO_4^{2-} , Na^+), and on the other hand, organic molecules (epoxidized soybean oil).

3. Results and discussion

The kinetics of hydrogen peroxide decomposition over all catalysts synthesized was found to obey first order according to the following equation:

$$r = k \cdot [\text{H}_2\text{O}_2] = \text{mol} \cdot (\text{L} \cdot \text{min})^{-1} \quad (1)$$

where $[\text{H}_2\text{O}_2]$ is the concentration of hydrogen peroxide in the solution, r is the reaction rate and k is the rate constant in min^{-1} which depends on respectively: the catalyst amount (linearly), the reaction temperature and the pH of the solution [22–24]. To compare different catalysts in this study, the rate constant was calculated with the following mass balance equation:

$$\frac{d[\text{H}_2\text{O}_2]}{dt} = -r = \text{mol} \cdot (\text{L} \cdot \text{min})^{-1} \quad (2)$$

It must be pointed out that the kinetic constant is, normally, related to the amount of the catalyst used. We have not separated the terms because, with the exception of NiO, we have used in all cases comparable amounts of catalyst (see Table 3). For MnO_x , for example, we experimentally found a linear dependency of the kinetic constant with the MnO_x concentration. This linear trend confirms the absence of any internal or external diffusion limitations under the conditions used. Since the MnO_x -based SMF_{55} catalyst demonstrated the highest activity, for the other catalyst formulations we also adopted the same conclusion about the absence of mass-transfer effects on the overall kinetics.

3.1. Activity and stability of SMF_{55} based catalysts

In Fig. 1 conversion obtained with four different selected catalysts is plotted as function of time. The corresponding rate constants of the catalysts are compared in Fig. 2.

The experiments with the nickel oxide based catalyst were carried out at a temperature of 60 $^\circ\text{C}$ and a concentration of hydrogen

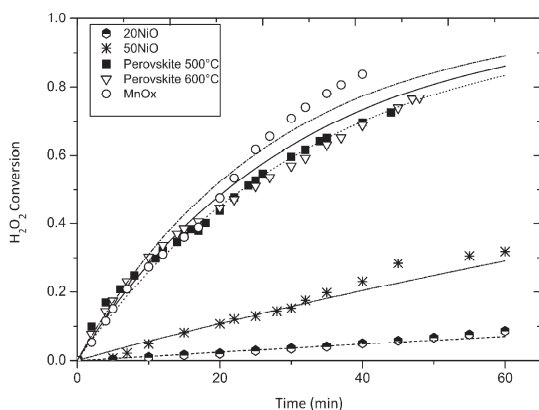


Fig. 1. Conversion as function of time for selected metals on SMF_{SS}. The runs with NiO catalysts have been performed at 60 °C, while the others at 25 °C.

peroxide of 3.5 mol/l–4 mol/l. With a 2.5-fold increase of NiO loading on the SMF, the rate constant per gram of catalyst rises from 1.2×10^{-3} to $5.7 \times 10^{-3} \text{ min}^{-1}$, that is, a ratio of 4.75. This behavior can be explained only by assuming that the lower amount of NiO corresponds to a coating of NiO strongly interacting with Al_2O_3 and less active in promoting the reaction with respect to the not interacting NiO which is more abundant in the 50 NiO sample. However, as the other catalysts showed better results, no further investigation was done on the NiO-based SMF.

The activities of the perovskite based catalysts were preliminarily tested under the same experimental conditions adopted for testing the other catalysts (see Table 3), but under these conditions a run-away produced a vigorous release of oxygen with a sudden increase of temperature in less than one minute. For this reason, the reaction conditions have been changed to keep the reaction under control (Table 3), lowering both the hydrogen peroxide concentration and the amount of loaded catalyst.

The perovskite catalysts, compared in this section, were calcinated at two different temperatures i.e. 500 °C and 600 °C, respectively, and no significant difference in activity was noted between both of them.

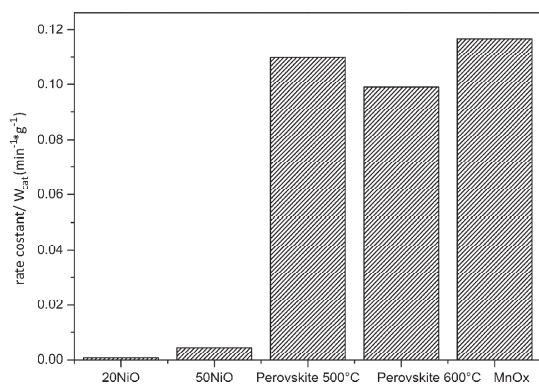


Fig. 2. First order rate constant per gram of catalysts of the selected metal oxides on SMF. Runs with NiO catalysts have been performed at 60 °C, while the others at 25 °C.

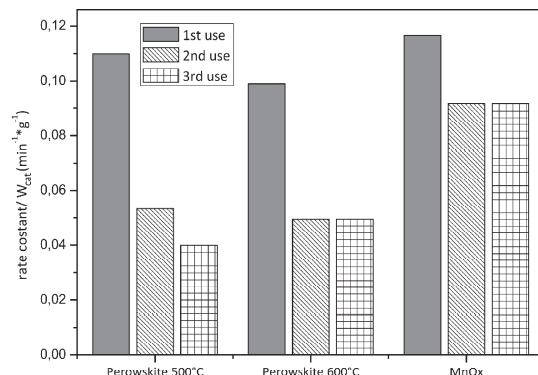


Fig. 3. Rate constant per gram of catalyst after three reuses.

Manganese oxide based structured catalyst showed activity comparable with perovskite, so, three catalysts underwent the stability tests: Perovskite 500 °C, Perovskite 600 °C and MnO_x .

The three selected catalysts were tested for stability in aqueous solutions of hydrogen peroxide by comparing the rate constant (per gram of the catalyst) in three successive runs of 1 h (Fig. 3).

The rate constant of both Perovskite catalysts diminishes in the consecutive runs of about 50%. The deactivation of Perovskite calcinated at 600 °C catalyst is observed only after the first run and maintained constant activity afterwards. On the contrary, the activity of the MnO_x -based catalyst only slightly (<20%) diminished after the first run remaining constant afterwards. The reasons of this deactivation were not studied in details since the catalyst was stable in the consecutive runs. It could be probably related to reconstruction of the active phase under reaction conditions, blockage of some active sites, or an eventual small leaching of the manganese not strongly anchored to the support. It's worth to note that we failed to quantify any MnO_x in the solution after the first run.

The catalyst found as the most active and stable in consecutive runs was the 5 wt.% MnO_x /5 wt.% ($\text{Al}_2\text{O}_3 + \text{MgO}$)/SMF_{SS} and, therefore, it was the catalyst of choice for the further study.

A slight discontinuity can be observed in the trends of temporary conversion curves reported on Fig. 1. Probably, such behavior is due to the development of gaseous oxygen inside the pores affecting the catalyst surface wetting. Considering also the high reaction enthalpy, local surface hot spots could be formed favored by the gaseous environment. All these aspects are probably responsible for the instability observed during the reaction runs.

3.2. Manganese oxide based SMF-structured catalyst for cleaning-up residual hydrogen peroxide in soybean oil epoxidation as a model for industrial application

As it has been seen, all the described catalysts have been tested in neutral pH or slightly acidic conditions (pH = 4–7). Under these conditions the contribution of homogeneous H_2O_2 decomposition is negligible [5]. When hydrogen peroxide is used for the epoxidation of soybean oil, residual hydrogen peroxide is dissolved in a strongly acidic solution containing both sulfuric and formic or acetic acids. Clearly, in these conditions all the catalysts become unstable giving place to a considerable deactivation due to leaching. Therefore, a preliminary neutralization is necessary. We observed that at the end of the epoxidation reaction an emulsion of the epoxidized oil and water comes out from the reactor. This emulsion is very stable and the separation of the two phases is strongly accelerated by the neutralization, as it can be appreciated in Fig. 4. As a matter of fact, it can be observed that if the aqueous solution is not neutralized,

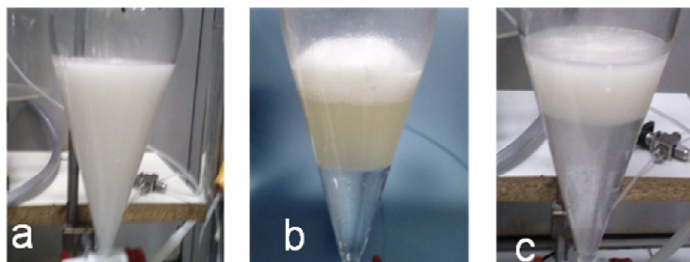


Fig. 4. Separation of mixture of the epoxidized oil and residual acid oxidant reagent (HCOOH , H_2O_2 and H_2SO_4) before ($\text{pH} = 2$) and after the neutralization ($\text{pH} = 7$): (a) Initial emulsion of epoxidized oil and water at the end of epoxidation reaction; (b) Separation after 24 h at $\text{pH} = 2$; (c) Separation after 2 h at $\text{pH} = 7$.

more than 24 h are necessary for a complete separation of the two phases. On the contrary, the neutralization to $\text{pH} = 7$ allows to separate the phases in less than 2 h. This means that neutralization is imperative for both phase separation and catalytic post treatment. It is interesting to note that neutralization is advantageous with respect to the classic method of adding an excess of NaOH producing the H_2O_2 decomposition thanks to the alkaline environment, because, at high pH saponification occurs with the formation of soaps lowering the quality of the product.

Other advantages are both economic and ecological, because, the lower amount of NaOH applied avoids a successive neutralization step and the obtained waste water is less concentrated of salts.

We have finally tested the activity for H_2O_2 decomposition of the MnO_x supported on $(\text{Al}_2\text{O}_3 + \text{MgO})/\text{SMF}_{\text{SS}}$ in the aqueous solution obtained after soybean oil epoxidation (neutralized, $\text{pH} = 7$). The obtained results are reported in Fig. 5 in which also the effect of catalyst reuse is reported (run 16–18), compared with a reference run (run 13 of Table 3) performed at $\text{pH} 4.5$.

The comparison of the three runs confirms that the selected catalyst is active for hydrogen peroxide decomposition and stable even

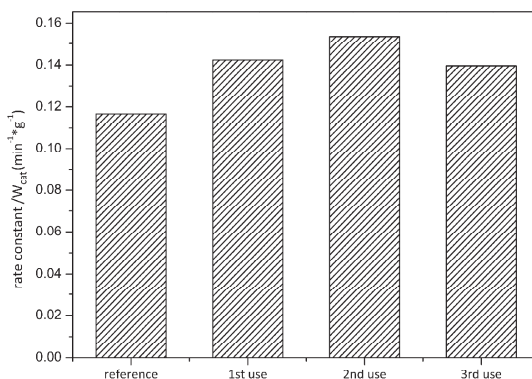


Fig. 5. The rate constant of 5% wt. $\text{MnO}_x/5$ wt. $(\text{Al}_2\text{O}_3 + \text{MgO})/\text{SMF}_{\text{SS}}$ obtained in three consecutive runs under industrial process conditions compared to a reference run in a pure aqueous solution of H_2O_2 . Reference run: $T = 25^\circ \text{C}$, $m_{\text{cat}} = 0.317 \text{ g}$, $C_{\text{H}_2\text{O}_2} = 1.59 \text{ mol/l}$, $\text{pH} = 4.5$.

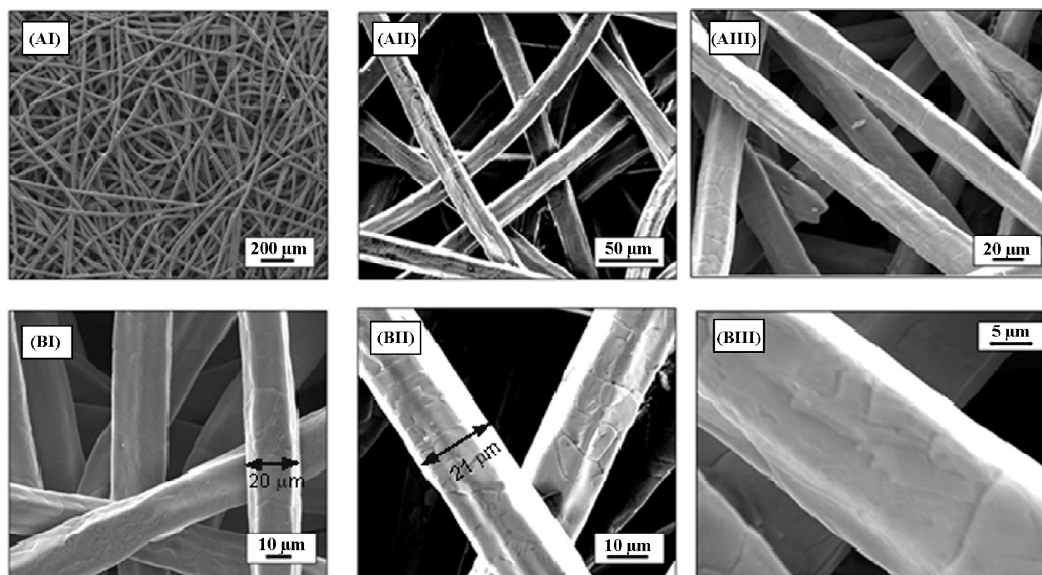


Fig. 6. Representative (A) medium and (B) high resolution SEM micrographs of stainless steel sintered metal fibers, (SMF_{SS}), pre- (I) and post- (II) covered with homogeneous 5 wt.% $(\text{Al}_2\text{O}_3 + \text{MgO})$ layer and (III) final 5 wt.% $\text{MnO}_x/5$ wt.% $(\text{Al}_2\text{O}_3 + \text{MgO})/\text{SMF}_{\text{SS}}$.

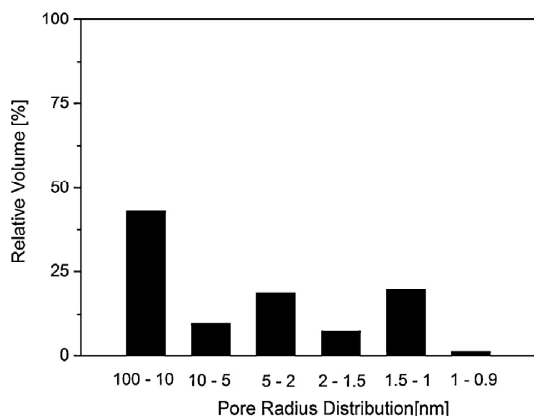


Fig. 7. Pore size distribution in Al₂O₃ + MgO.

using industrial water. Moreover, an increase of the reaction rate constant per gram of the catalyst is observed in comparison to the experiments carried out in pure solution yielding 0.12 min⁻¹ g⁻¹. This can be attributed to the change of pH from about 4.5 to 7 being in line with the other reports demonstrated that pH has a strong influence on the decomposition kinetics [10].

3.3. Characterization of 5 wt.% MnO_x/5 wt.% (Al₂O₃ + MgO)/SMF_{SS}

3.3.1. Scanning electron microscopy

Representative SEM micrographs of the treated (acetone+boiled in toluene+calcination to 723 K) sintered metal fibers SMF_{SS} before and after deposition of the oxide mixture (Al₂O₃ + MgO) layer by intrinsic wetness impregnation method are presented in Fig. 6. The metallic network shows a random distribution of fibers (Fig. 6A(I)) with high porosity. The individual filaments exhibit a tetragonal-like structure with diameters of ca. 20 μm (Fig. 6A(I)) as indicated by the data supplied by the provider (given in Table 1)). Series II shows the formation of a thin (ca. 0.5 μm thickness determined on a sample area of ca. 10 mm²) homogeneous oxide layer where the macroporosity, i.e. open structure, of the fibrous network is maintained as a result of the concomitant homogeneous deposition and low oxide loading. This structure obtained by the wetness impregnation method is maintained when the MnO_x catalyst is added to the oxide mixture to form the catalyst of choice 5 wt.% MnO_x/5 wt.% (Al₂O₃ + MgO)/SMF_{SS} (see Fig. 6A(III) B(III)). The high stability of this catalyst is ensured by this thin and uniform layer which strongly interacts with the SMF support and prevents any leaching. Moreover, the thin coating preserves the open network of SMF allowing keeping high permeability of the final catalyst.

3.3.2. Surface morphology

BET measurements were carried out with (Al₂O₃ + MgO) in powder form as the introduction of sufficient amount of SMF-based catalyst into the apparatus turned out to be not feasible. A total surface area of 83 m²/g of (Al₂O₃ + MgO) was determined. Assuming a similar structure of the oxide mixture (Al₂O₃ + MgO) on the SMF surface, a specific area of about 4 m²/(g of SMF_{SS}) can be estimated. The pore size distribution presented in Fig. 7 shows a bi-modal micro- & meso-porous material with almost half of the pore volume consisting of pores in the range of 100–10 nm. This morphology together with the thin (<1 μm) coating layer provides an effective internal mass-transfer avoiding eventual diffusion limitations and ensures an optimal availability of catalytic phase.

4. Conclusions

The results obtained during this study support the following conclusions:

- Structured catalysts for the decomposition of hydrogen peroxide have been developed consisting of manganese oxide supported on sintered metal fibers (SMF_{SS}) homogeneously coated by alumina-magnesia mixed oxides, 5 wt.% (Al₂O₃ + MgO)/SMF_{SS}. The deposition of MnO_x was carried out via intrinsic wetness impregnation. The final SMF_{SS} coating consists of a homogeneous (bi-modal: micro- & meso-porous) layer of <1 μm thickness with a specific surface area of 83 m²/g.
- The catalyst, 5 wt.% MnO_x/5 wt.% (Al₂O₃ + MgO)/SMF_{SS}, exhibited a rate constant as high as 3.7 × 10⁻² min⁻¹ at pH 4.5 and 25 °C. This was found to be considerably higher than any other catalyst used for this reaction under these conditions.
- The developed structured catalyst was tested for the decomposition of hydrogen peroxide under industrially relevant conditions (at the back end of the epoxidation of soybean oil process at neutral pH) and found stable and effective rendering a high rate constant of 5.2 × 10⁻² min⁻¹.
- The developed structured catalyst demonstrated a potential for its industrial application opening new horizons for process intensification and diminishing environmental impact.

Acknowledgments

The financial support of the EU Seventh Framework Program for Research and Technological Development (CP-IP 228853, COPIRIDE) was gratefully acknowledged.

References

- [1] www.mathworks.com; Accessed: 2013.
- [2] M.C. Ortega-Liebana, E. Sánchez-López, J. Hidalgo-Carrillo, A. Marinas, J.M. Marinas, F.J. Urbano. A comparative study of photocatalytic degradation of 3-chloropyridine under UV and solar light by homogeneous (photo-Fenton) and heterogeneous (TiO₂) photocatalysis, *Appl. Catal. B: Environ.* 127 (2012) 316–322.
- [3] D. Spuhler, J. Andrés Rengifo-Herrera, C. Pulgarin, The effect of Fe²⁺, Fe³⁺, H₂O₂ and the photo-Fenton reagent at near neutral pH on the solar disinfection (SODIS) at low temperatures of water containing *Escherichia coli* K12, *Appl. Catal. B: Environ.* 96 (2010) 126–141.
- [4] R. Andreozzi, V. Caprio, A. Insola, R. Marotta, Advanced oxidation processes (AOP) for water purification and recovery, *Catal. Today* 53 (1999) 51–59.
- [5] E. Santacesaria, R. Tesser, M.D. Serio, V. Russo, R. Turco, A new simple microchannel device to test process intensification, *Ind. Eng. Chem. Res.* 50 (2010) 2569–2575.
- [6] Y. Ono, T. Matsumura, N. Kitajima, S. Fukuzumi, Formation of superoxide ion during the decomposition of hydrogen peroxide on supported metals, *J. Phys. Chem.* 81 (1977) 1307–1311.
- [7] J. Weiss, The Free Radical Mechanism in the Reactions of Hydrogen peroxide, in: V.I.K.W.G. Frankenburg, E.K. Rideal (Eds.), *Advances in Catalysis*, Academic Press, 1952, pp. 343–365.
- [8] M.A. Hasan, M.I. Zaki, L. Pasupulety, K. Kumari, Promotion of the hydrogen peroxide decomposition activity of manganese oxide catalysts, *Appl. Catal. A: Gen.* 181 (1999) 171–179.
- [9] J.T. Kohler, R.E. Altomare, J.R. Kittrell, Catalytic decomposition of hydrogen peroxide by manganese-alumina, *Prod. Res. Dev.* 14 (1975) 36–40.
- [10] J. Mooi, P.W. Selwood, Catalytic activity of supported manganese oxides for the hydrogen peroxide decomposition, *J. Am. Chem. Soc.* 74 (1952) 1750–1754.
- [11] V. Russo, R. Tesser, E. Santacesaria, M. Di Serio, Chemical technical aspects of propene oxide production via hydrogen peroxide (HPPO Process), *Ind. Eng. Chem. Res.* 52 (2013) 1168–1178.
- [12] E. Santacesaria, R. Tesser, M. Di Serio, R. Turco, V. Russo, D. Verde, A biphasic model describing soybean oil epoxidation with H₂O₂ in a fed-batch reactor, *Chem. Eng. J.* 173 (2011) 198–209.
- [13] L. Kiwi-Minsker, A. Renken, Microstructured reactors for catalytic reactions, *Catal. Today* 110 (2005) 2–14.
- [14] K. Nikolajsen, L. Kiwi-Minsker, A. Renken, Structured fixed-bed adsorber based on zeolite/sintered metal fibre for low concentration VOC removal, *Chem. Eng. Res. Des.* 84 (2006) 562–568.
- [15] I. Yuranov, L. Kiwi-Minsker, A. Renken, Structured combustion catalysts based on sintered metal fibre filters, *Appl. Catal. B: Environ.* 43 (2003) 217–227.

- [16] N. Semagina, M. Grasemann, N. Xanthopoulos, A. Reken, L. Kiwi-Minsker, Structured catalyst of Pd/ZnO on sintered metal fibers for 2-methyl-3-butyn-2-ol selective hydrogenation, *J. Catal.* 251 (2007) 213–222.
- [17] L. Kiwi-Minsker, I. Yuranov, V. Holler, A. Renken, Supported glass fiber catalysts for novel multi-phase reactor design, *Chem. Eng. Sci.* 54 (1999) 4785–4790.
- [18] W. Bonrath, L. Kiwi-Minsker, I. Iouranov, New structured catalyst based on sintered metal fibers coated by a basic oxide layer impregnated with palladium-nanoparticles, useful for production of e.g. vitamins and carotinoids, *Dsm. Ip. Assets Bv. (Stam)* (2013) pp24.
- [19] M. Solcymani, A. Mohcb, D. Babakhani, Hydrogen peroxide decomposition over nanosized $\text{La}_{1-x}\text{Ca}_x\text{MnO}_3$ ($0 \leq x \leq 0.6$) Perovskite oxides, *Chem. Eng. Technol.* 34 (2011) 49–55.
- [20] D. Dollimore, G.R. Heal, Pore-size distribution in typical adsorbent systems, *J. Colloid Interf. Sci.* 33 (1970) 508–519.
- [21] I.M. Kolthoff, P.J. Elving, *Teatise on Analytical Chemistry*, Wiley, New York, 1978.
- [22] K. Akhtar, N. Khalid, M. Ali, Effect of pH and temperature on the catalytic properties of manganese dioxide, *J. Chem. Soc. Pak.* 34 (2012) 263–268.
- [23] S.H. Do, B. Barchelor, H.K. Lee, S.H. Kong, Hydrogen peroxide decomposition on manganese oxide (pyrolusite): kinetics, intermediates, and mechanism, *Chemosphere* 75 (2009) 8–12.
- [24] T. Rhadfi, J.Y. Piquemal, L. Sicard, F. Herbst, E. Briot, M. Benedetti, A. Atlamsani, Polyol-made Mn_2O_4 nanocrystals as efficient Fenton-like catalysts, *Appl. Catal. A: Gen.* 386 (2010) 132–139.